

MSUHEP-70410
 hep-ph/9704288
 March, 1997

Probing the Electroweak Symmetry Breaking Sector with the Top Quark[†]

F. Larios^(a,b) E. Malkawi^(c) and C.-P. Yuan^(a)

*(a) Department of Physics and Astronomy, Michigan State University
 East Lansing, Michigan 48824, USA.*

*(b) Departamento de Física, CINVESTAV,
 Apdo. Postal 14-740, 07000 México, D.F., México.*

*(c) Dept. of Physics, Jordan University of Science I& Technology,
 P.O. Box 3030-IRBID-22110, Jordan.*

Abstract

A study on the effective anomalous interactions, up to dimension 5, of the top quark with the electroweak gauge bosons is made in the non-linear Chiral Lagrangian approach. Bounds on the anomalous dimension four terms are obtained from their contribution to low energy data. Also, the potential contribution to the production of top quarks at hadron colliders (the Tevatron and the LHC) and the electron Linear Collider from both dimension 4 and 5 operators is analyzed.

PACS numbers: 14.65.Ha, 12.39.Fe, 12.60.-i

[†] Lectures given by C.-P. Yuan at the CCAST Workshop on " Physics at TeV Energy Scale ", July 15-26, 1996, Beijing, China

1 Introduction

Despite the unquestionable significance of its achievements, like that of predicting the existence of the top quark [1], there is no reason to believe that the Standard Model (SM) is the final theory. For instance, the SM contains many arbitrary parameters with no apparent connections. In addition, the SM provides no satisfactory explanation for the symmetry-breaking mechanism which takes place and gives rise to the observed mass spectrum of the gauge bosons and fermions. Because the top quark is heavy relative to other observed fundamental particles,¹ one expects that any underlying theory; to supersede the SM at some high energy scale $\Lambda \gg m_t$, will easily reveal itself at lower energies through the effective interactions of the top quark to other light particles. Also because the top quark mass ($\sim v/\sqrt{2}$) is of the order of the Fermi scale $v = (\sqrt{2}G_F)^{-1/2} = 246 \text{ GeV}$, which characterizes the electroweak symmetry-breaking scale, the top quark system could be a useful probe of the symmetry-breaking sector. Since the fermion mass generation can be closely related to the electroweak symmetry-breaking, one expects some residual effects of this breaking to appear in accordance with the mass hierarchy [2, 3, 4, 5]. This means that new effects should be more apparent in the top quark sector than in any other light sector of the theory. Therefore, it is important to study the top quark system as a direct tool to probe new physics effects [6].

Many attempts to offer alternative scenarios for the electroweak symmetry breaking mechanism are discussed in literature. A general trend among all alternatives is that new physics appear at or below the TeV scale. Examples include Supersymmetry models [7], technicolor models [8] and possibly extended technicolor sectors to account for the fermion masses [3, 4]. Other examples include top-mode condensate models [9] and a strongly interacting Higgs sector [10].

An attempt to study the nonuniversal interactions of the top quark has been carried out in Ref. [2, 5] by Peccei et al. However, in that study only the vertex $t\text{-}t\text{-}Z$ was considered based on the assumption that this is the only vertex which gains a significant modification due to a speculated dependence of the coupling strength on the fermion mass: $\kappa_{ij} \leq \mathcal{O}\left(\frac{\sqrt{m_i m_j}}{v}\right)$, where κ_{ij} parameterizes some new dimensional-four interactions among gauge bosons and fermions i and j . However, this is not the only possible pattern of interactions, *e.g.*, in some extended technicolor models [4] one finds the nonuniversal residual interactions associated with the vertices $b_L\text{-}\bar{b}_L\text{-}Z$, $t_L\text{-}\bar{t}_L\text{-}Z$, and $t_L\text{-}\bar{b}_L\text{-}W$ to be of the same order.

Because of the great diversity of models proposed for possible new physics (beyond the SM), it has become necessary to be able to study these possible new interactions

¹ As of the summer of 1996, the mass of the top quark has been measured at the Fermilab Tevatron to be $m_t = 175.6 \pm 5.7 \text{ (stat.)} \pm 7.1 \text{ (sys.) GeV}$ by the CDF group and $m_t = 169 \pm 8 \text{ (stat.)} \pm 8 \text{ (sys.) GeV}$ by the DØ group, through the detection of $t\bar{t}$ events.

in a model independent approach [11]. This approach has proved to render relevant non-trivial information about the possible deviations from the standard couplings of the heavier elementary particles (heavy scalar bosons, the bottom and the top quarks, etc.) [12]. Our study focuses on the top quark, which because of its remarkably higher mass is the best candidate (among the fermion particles) for the manifestation of these anomalous interactions at high energies [13].

A common approach to study these anomalous couplings is by considering the most general on-shell vertices (form factors) involving the bottom and the top quarks together with the interaction bosons [6]. In this work we will incorporate the effective chiral Lagrangian approach [14, 15], which is based on the principle of gauge symmetry, but the symmetry is realized in the most general (non-linear) form so as to encompass all the possible interactions consistent with the existing experimental data. The idea of using this approach is to exploit the linearly realized $U(1)_{\text{em}}$ symmetry and the non-linearly realized $SU(2)_L \times U(1)_Y$ symmetry to make a systematic characterization of all the anomalous couplings. In this way, for example, different couplings which otherwise would be considered as independent become related through the equations of motion.

We show that in general low energy data (including Z pole physics) do not impose any stringent constraints on the anomalous dimension four coefficients κ of $\mathcal{L}^{(4)}$ (see Eq. (32))². This means that low energy data do not exclude the possibility of new physics whose effects come in through the deviations from the standard interactions of the top quark, and these deviations have to be directly measured via production of top quarks at the colliders. For instance, the couplings $\kappa_{L,R}^{CC}$ can be measured from the decay of the top quarks in $t\bar{t}$ pairs produced either at hadron colliders (the Fermilab Tevatron and the CERN Large Hadron Collider (LHC)) or at the electron linear collider (LC). They can also be studied from the production of the single-top quark events via, for example, W -gluon or W -photon fusion process [42, 43, 44]. The coupling $\kappa_{L,R}^{NC}$ can only be sensitively probed at a future linear collider via the $e^+ e^- \rightarrow \gamma, Z \rightarrow t\bar{t}$ process because at hadron colliders the $t\bar{t}$ production rate is dominated by QCD interactions ($q\bar{q}, gg \rightarrow t\bar{t}$). However, at the LHC $\kappa_{L,R}^{NC}$ may also be studied via the associated production of $t\bar{t}$ with Z bosons (this requires a separate study).

Also, we will include the next higher order dimension 5 fermionic operators and then examine the precision with which the coefficients of these operators can be measured in high energy collisions. Since it is the electroweak symmetry breaking sector that we are interested in, we shall concentrate on the interaction of the top quark with the longitudinal weak gauge bosons; which are equivalent to the would-be-Goldstone bosons in the high energy limit. This equivalence is known as the

² For simplicity, we will only construct the complete set of dimension 4 and 5 effective operators for the fermions t and b , although our results can be trivially extended for the other fermion fields, e.g. flavor changing neutral interactions t - c - Z , etc.

Goldstone Equivalence Theorem [16]-[19].

Our strategy for probing these anomalous dimension 5 operators ($\mathcal{L}^{(5)}$) is to study the production of $t\bar{t}$ pairs as well as single- t or \bar{t} via the $W_L W_L$, $Z_L Z_L$ and $W_L Z_L$ (denoted in general as $V_L V_L$) processes in the TeV region. As we shall show later, based on a power counting method [20], the leading contribution of the scattering amplitudes at high energy goes as E^3 for the anomalous operators $\mathcal{L}^{(5)}$, where $E = \sqrt{s}$ is the CM energy of the WW or ZZ system (that produces $t\bar{t}$), or the WZ system (that produces $t\bar{b}$ or $b\bar{t}$). On the other hand, when the κ coefficients are set equal to zero the dimension 4 operators $\mathcal{L}^{(4)}$ can at most contribute with the first power E^1 to these scattering $V_L V_L$ processes. In other words, the high energy $V_L V_L \rightarrow f\bar{f}$ scatterings are more sensitive to $\mathcal{L}^{(5)}$ than to $\mathcal{L}^{(4)}$ (with κ 's = 0). If the κ 's are not set equal to zero, then the high energy behaviour can at most grow as E^2 as compared to E^3 for the dimension 5 operators (see Appendix B). Furthermore, the dimension 4 anomalous couplings κ 's are better measured at the scale of M_W or m_t by studying the decay or the production of the top quark at either the Tevatron and the LHC as mentioned before, or the LC at the $t\bar{t}$ threshold (for the study of Z - t - t). Since, as mentioned above, the dimension 5 operators are better measured in the TeV region, we shall assume that by the time their measurement is feasible, the κ 's will already be known. Thus, to simplify our discussion, we will take the values of the κ 's to be zero when presenting our numerical results.

We show that there are 19 independent dimension 5 operators (with only t , b and gauge boson fields) in $\mathcal{L}^{(5)}$ after imposing the equations of motion for the effective chiral lagrangian. The coefficients of these operators can be measured at either the LHC or the LC to magnitudes of order 10^{-2} or 10^{-1} after normalizing (the coefficients) with the factor³ $\frac{1}{\Lambda}$ based on the naive dimensional analysis [15]. It is expected that at the LHC or the LC there will be about a few hundreds to a few thousands of $t\bar{t}$ pairs or single- t or single- \bar{t} events produced via the $V_L V_L$ fusion process.

This work is organized as follows: In section 2 we will introduce the basic framework of the non-linearly realized chiral Lagrangian, in which the $SU(2)_L \times U(1)_Y$ gauge symmetry is nonlinearly realized. In this approach, only the $U(1)_{EM}$ symmetry remains unbroken and thus the realization under this subgroup is linear as usual. We will set up a Lagrangian with dimension 4 terms that will reproduce the couplings of the Standard Model type, as well as possible deviations. Then, in sections 3 and 4 we discuss the constraints on the dimension 4 anomalous couplings from low energy data and the strategies to directly measure these couplings at the hadron or electron colliders. In sections 5 and 6 we construct the complete set of dimension 5 couplings and discuss their effects to the production of top quarks in high energy regime via weak boson fusion processes. Finally our conclusions are given in section 7.

³ Λ is the cut-off scale of the effective theory. It could be the lowest new heavy mass scale, or something around $4\pi v \simeq 3.1$ TeV if no new resonances exist below Λ .

2 The Non-linearly Realized Electroweak Chiral Lagrangian

We consider the electroweak theories in which the gauge symmetry $G \equiv \text{SU}(2)_L \times \text{U}(1)_Y$ is spontaneously broken down to $H = \text{U}(1)_{em}$ [21, 14, 22]. There are three Goldstone bosons, ϕ^a ($a = 1, 2, 3$), generated by this breakdown of G into H , which are eventually *eaten* by the W^\pm and Z gauge bosons and become their longitudinal degrees of freedom.

In the non-linearly realized chiral Lagrangian formulation, the Goldstone bosons transform non-linearly under G but linearly under the subgroup H . A convenient way to implement this is to introduce the matrix field

$$\Sigma = \exp \left(i \frac{\phi^a \tau^a}{v_a} \right), \quad (1)$$

where τ^a , $a = 1, 2, 3$, are the Pauli matrices normalized as $\text{Tr}(\tau^a \tau^b) = 2\delta_{ab}$. The matrix field Σ transforms under G as

$$\Sigma \rightarrow \Sigma' = g_L \Sigma g_R^\dagger, \quad (2)$$

with

$$\begin{aligned} g_L &= \exp \left(i \frac{\alpha^a \tau^a}{2} \right), \\ g_R &= \exp \left(i \frac{y \tau^3}{2} \right), \end{aligned} \quad (3)$$

where $\alpha^{1,2,3}$ and y are the group parameters of G . Because of the $\text{U}(1)_{em}$ invariance, $v_1 = v_2 = v$ in Eq. (1), but they are not necessarily equal to v_3 . In the SM, v ($= 246 \text{ GeV}$) is the vacuum expectation value of the Higgs boson field, and characterizes the scale of the symmetry-breaking. Also, $v_3 = v$ arises from the approximate custodial symmetry present in the SM. It is this symmetry that is responsible for the tree-level relation

$$\rho = \frac{M_W^2}{M_Z^2 \cos^2 \theta_W} = 1 \quad (4)$$

in the SM, where θ_W is the electroweak mixing angle, M_W and M_Z are the masses of W^\pm and Z boson, respectively. In this study we assume the underlying theory guarantees that $v_1 = v_2 = v_3 = v$.

In the context of this non-linear formulation of the electroweak theory, the massive charged and neutral weak bosons can be defined by means of the *composite* field:

$$\mathcal{W}_\mu^a = -i \text{Tr}(\tau^a \Sigma^\dagger D_\mu \Sigma) \quad (5)$$

where⁴

$$D_\mu \Sigma = \left(\partial_\mu - ig \frac{\tau^a}{2} W_\mu^a \right) \Sigma . \quad (6)$$

Here, W_μ^a is the gauge boson associated with the $SU(2)_L$ group, and its transformation is the usual one (g is the gauge coupling).

$$\tau^a W_\mu^a \rightarrow \tau^a W_\mu'^a = g_L \tau^a W_\mu^a g_L^\dagger + \frac{2i}{g} g_L \partial_\mu g_L^\dagger \quad (7)$$

The $D_\mu \Sigma$ term transforms under G as

$$D_\mu \Sigma \rightarrow D_\mu \Sigma' = g_L (D_\mu \Sigma) g_R^\dagger + g_L \Sigma \partial_\mu g_R^\dagger . \quad (8)$$

Therefore, by using the commutation rules for the Pauli matrices and the fact that $Tr(AB) = Tr(BA)$ we can prove that the composite field \mathcal{W}_μ^a will transform under G in the following manner:

$$\mathcal{W}_\mu^3 \rightarrow \mathcal{W}_\mu'^3 = \mathcal{W}_\mu^3 - \partial_\mu y , \quad (9)$$

$$\mathcal{W}_\mu^\pm \rightarrow \mathcal{W}_\mu'^\pm = e^{\pm iy} \mathcal{W}_\mu^\pm , \quad (10)$$

where

$$\mathcal{W}_\mu^\pm = \frac{\mathcal{W}_\mu^1 \mp i \mathcal{W}_\mu^2}{\sqrt{2}} . \quad (11)$$

Also, it is convenient to define the field

$$\mathcal{B}_\mu = g' B_\mu , \quad (12)$$

which is really the same gauge boson field associated with the $U(1)_Y$ group. (g' is the gauge coupling.) The field \mathcal{B}_μ transforms under G as

$$\mathcal{B}_\mu \rightarrow \mathcal{B}_\mu' = \mathcal{B}_\mu + \partial_\mu y . \quad (13)$$

We now introduce the composite fields \mathcal{Z}_μ and \mathcal{A}_μ as

$$\mathcal{Z}_\mu = \mathcal{W}_\mu^3 + \mathcal{B}_\mu , \quad (14)$$

$$s_w^2 \mathcal{A}_\mu = s_w^2 \mathcal{W}_\mu^3 - c_w^2 \mathcal{B}_\mu , \quad (15)$$

where $s_w^2 \equiv \sin^2 \theta_W$, and $c_w^2 = 1 - s_w^2$. In the unitary gauge ($\Sigma = 1$)

$$\mathcal{W}_\mu^a = -g W_\mu^a , \quad (16)$$

$$\mathcal{Z}_\mu = -\frac{g}{c_w} Z_\mu , \quad (17)$$

⁴This is not the covariant derivative of Σ . The covariant derivative is $D_\mu \Sigma = \partial_\mu \Sigma - ig \frac{\tau^a}{2} W_\mu^a \Sigma + ig' \Sigma \frac{\tau^3}{2} B_\mu$.

$$\mathcal{A}_\mu = -\frac{e}{s_w^2} A_\mu , \quad (18)$$

where we have used the relations $e = g s_w = g' c_w$, $W_\mu^3 = c_w Z_\mu + s_w A_\mu$, and $B_\mu = -s_w Z_\mu + c_w A_\mu$. In general, the composite fields contain Goldstone boson fields:

$$\begin{aligned} \mathcal{Z}_\mu = & -\frac{g}{c_w} Z_\mu + \frac{2}{v} \partial_\mu \phi^3 - i \frac{2g}{v} (W_\mu^+ \phi^- - W_\mu^- \phi^+) + \\ & i \frac{2}{v^2} (\phi^- \partial_\mu \phi^+ - \phi^+ \partial_\mu \phi^-) + \dots , \end{aligned} \quad (19)$$

$$\begin{aligned} \mathcal{W}_\mu^\pm = & -g W_\mu^\pm + \frac{2}{v} \partial_\mu \phi^\pm \pm i \frac{2g}{v} (\phi^3 W_\mu^\pm - W_\mu^3 \phi^\pm) \pm \\ & i \frac{2}{v^2} (\phi^\pm \partial_\mu \phi^3 - \phi^3 \partial_\mu \phi^\pm) + \dots , \end{aligned} \quad (20)$$

where \dots denotes terms with 3 or more boson fields.

The transformations of \mathcal{Z}_μ and \mathcal{A}_μ under G are

$$\mathcal{Z}_\mu \rightarrow \mathcal{Z}'_\mu = \mathcal{Z}_\mu , \quad (21)$$

$$\mathcal{A}_\mu \rightarrow \mathcal{A}'_\mu = \mathcal{A}_\mu - \frac{1}{s_w^2} \partial_\mu y . \quad (22)$$

Hence, under G the fields \mathcal{W}_μ^\pm and \mathcal{Z}_μ transform as vector fields, but \mathcal{A}_μ transforms as a gauge boson field which plays the role of the photon field A_μ .

Using the fields defined as above, one may construct the $\text{SU}(2)_L \times \text{U}(1)_Y$ gauge invariant interaction terms in the chiral Lagrangian

$$\begin{aligned} \mathcal{L}^B = & -\frac{1}{4g^2} \mathcal{W}_{\mu\nu}^a \mathcal{W}^{a\mu\nu} - \frac{1}{4g'^2} \mathcal{B}_{\mu\nu} \mathcal{B}^{\mu\nu} \\ & + \frac{v^2}{4} \mathcal{W}_\mu^+ \mathcal{W}^{-\mu} + \frac{v^2}{8} \mathcal{Z}_\mu \mathcal{Z}^\mu + \dots , \end{aligned} \quad (23)$$

where

$$\begin{aligned} \mathcal{W}_{\mu\nu}^a &= \partial_\mu \mathcal{W}_\nu^a - \partial_\nu \mathcal{W}_\mu^a + \epsilon^{abc} \mathcal{W}_\mu^b \mathcal{W}_\nu^c , \\ \mathcal{B}_{\mu\nu} &= \partial_\mu \mathcal{B}_\nu - \partial_\nu \mathcal{B}_\mu , \end{aligned} \quad (24)$$

and where \dots denotes other possible four- or higher-dimension operators [23, 24].

It is easy to show that⁵

$$\mathcal{W}_{\mu\nu}^a \tau^a = -g \Sigma^\dagger W_{\mu\nu}^a \tau^a \Sigma \quad (25)$$

and

$$\mathcal{W}_{\mu\nu}^a \mathcal{W}^{a\mu\nu} = g^2 W_{\mu\nu}^a W^{a\mu\nu} . \quad (26)$$

⁵ Use $\mathcal{W}_\mu^a \tau^a = -2i \Sigma^\dagger D_\mu \Sigma$, and $[\tau^a, \tau^b] = 2i \epsilon^{abc} \tau^c$.

This simply reflects the fact that the kinetic term is not related to the Goldstone bosons sector, i.e., it does not originate from the symmetry-breaking sector.

The mass terms in Eq. (23) can be expanded as

$$\begin{aligned} \frac{v^2}{4} \mathcal{W}_\mu^+ \mathcal{W}^{-\mu} + \frac{v^2}{8} \mathcal{Z}_\mu \mathcal{Z}^\mu &= \partial_\mu \phi^+ \partial^\mu \phi^- + \frac{1}{2} \partial_\mu \phi^3 \partial^\mu \phi^3 \\ &+ \frac{g^2 v^2}{4} W_\mu^+ W^{\mu-} + \frac{g^2 v^2}{8 c_w^2} Z_\mu Z^\mu + \dots \end{aligned} \quad (27)$$

At the tree-level, the mass of W^\pm boson is $M_W = gv/2$ and the mass of Z boson is $M_Z = gv/2c_w$.

Fermions can be included in this context by assuming that each flavor transforms under $G = \text{SU}(2)_L \times \text{U}(1)_Y$ as [25]

$$f \rightarrow f' = e^{iyQ_f} f, \quad (28)$$

where Q_f is the electric charge of f .⁶

Out of the fermion fields f_1, f_2 (two different flavors), and the Goldstone bosons matrix field Σ , the usual linearly realized fields Ψ can be constructed. For example, the left-handed fermions [$\text{SU}(2)_L$ doublet] are

$$\Psi_L \equiv \begin{pmatrix} \psi_1 \\ \psi_2 \end{pmatrix}_L = \Sigma F_L = \Sigma \begin{pmatrix} f_1 \\ f_2 \end{pmatrix}_L \quad (29)$$

with $Q_{f_1} - Q_{f_2} = 1$. One can easily show that Ψ_L transforms linearly under G as

$$\Psi_L \rightarrow \Psi'_L = g \Psi_L, \quad (30)$$

where $g = \exp(i \frac{\alpha^a \tau^a}{2}) \exp(iy \frac{Y}{2}) \in G$, and $Y = \frac{1}{3}$ is the hypercharge of the left handed quark doublet.

In contrast, linearly realized right-handed fermions Ψ_R [$\text{SU}(2)_L$ singlet] simply coincide with F_R , i.e.,

$$\Psi_R \equiv \begin{pmatrix} \psi_1 \\ \psi_2 \end{pmatrix}_R = F_R = \begin{pmatrix} f_1 \\ f_2 \end{pmatrix}_R. \quad (31)$$

With these fields we can now construct the most general gauge invariant chiral Lagrangian that includes the electroweak couplings of the top quark up to dimension four [21].⁷

$$\mathcal{L}^{(4)} = i \bar{t} \gamma^\mu \left(\partial_\mu + i \frac{2s_w^2}{3} \mathcal{A}_\mu \right) t + i \bar{b} \gamma^\mu \left(\partial_\mu - i \frac{s_w^2}{3} \mathcal{A}_\mu \right) b$$

⁶ For instance, $Q_f = 2/3$ for the top quark.

⁷ In this study we do not include possible flavor changing neutral current couplings, e.g. t - c - Z .

$$\begin{aligned}
& - \left(\frac{1}{2} - \frac{2s_w^2}{3} + \frac{1}{2}\kappa_L^{\text{NC}} \right) \bar{t}_L \gamma^\mu t_L \mathcal{Z}_\mu - \left(\frac{-2s_w^2}{3} + \frac{1}{2}\kappa_R^{\text{NC}} \right) \bar{t}_R \gamma^\mu t_R \mathcal{Z}_\mu \\
& - \left(\frac{-1}{2} + \frac{s_w^2}{3} \right) \bar{b}_L \gamma^\mu b_L \mathcal{Z}_\mu - \frac{s_w^2}{3} \bar{b}_R \gamma^\mu b_R \mathcal{Z}_\mu \\
& - \frac{1}{\sqrt{2}} (1 + \kappa_L^{\text{CC}}) \bar{t}_L \gamma^\mu b_L \mathcal{W}_\mu^+ - \frac{1}{\sqrt{2}} (1 + \kappa_L^{\text{CC}\dagger}) b_L \gamma^\mu t_L \mathcal{W}_\mu^- \\
& - \frac{1}{\sqrt{2}} \kappa_R^{\text{CC}} \bar{t}_R \gamma^\mu b_R \mathcal{W}_\mu^+ - \frac{1}{\sqrt{2}} \kappa_R^{\text{CC}\dagger} \bar{b}_R \gamma^\mu t_R \mathcal{W}_\mu^- \\
& - m_t \bar{t} t .
\end{aligned} \tag{32}$$

In the above equation κ_L^{NC} , κ_R^{NC} , κ_L^{CC} , and κ_R^{CC} parameterize possible deviations from the SM predictions [21, 5]. In general, the charged current coefficients can be complex with the imaginary part introducing a CP odd interaction, and the neutral current coefficients are real so that the effective Lagrangian is hermitian.

3 Constraints on dimension four anomalous couplings from the low energy data

In the chiral Lagrangian $\mathcal{L}^{(4)}$ given in Eq. (32), there are two complex parameters (κ_L^{CC} and κ_R^{CC}) and two real (κ_L^{NC} and κ_R^{NC}) all independent from each other, which need to be constrained using precision data. Naturally, these parameters are not expected to be large, we assume that their absolute values are at most of order one. The imaginary parts of the charged current couplings, which give rise to CP violation at this level, do not contribute to the LEP observables of interest at the one-loop level. Hence, we will ignore imaginary parts of the κ 's. Also, at this level any contributions from the right-handed charged current coupling κ_R^{CC} are proportional to the bottom quark's mass m_b (which is much smaller than m_t), and are negligible compared to the contributions from the other three couplings. Therefore, we can only obtain bounds for κ_L^{NC} , κ_R^{NC} and κ_L^{CC} from LEP data at the one loop level. However, the coupling κ_R^{CC} can be studied independently by using the CLEO measurement of $b \rightarrow s\gamma$. For this process κ_R^{CC} becomes the significant anomalous coupling. In Ref. [26] the contribution of this parameter to the branching ratio of $b \rightarrow s\gamma$ was calculated. From the result given there, and the recent CLEO measurement $1 \times 10^{-4} < Br(b \rightarrow s\gamma) < 4.2 \times 10^{-4}$ [27], we can obtain the following bounds for κ_R^{CC} at the 95% confidence level (C.L.):

$$-0.037 < \kappa_R^{\text{CC}} < 0.0015 . \tag{33}$$

With these observations we will study how κ_L^{NC} , κ_R^{NC} and κ_L^{CC} can be constrained by LEP data.

All contributions to low energy observables, under a few general assumptions, can be parameterized by 4-independent parameters: ϵ_1 , ϵ_2 , ϵ_3 , and ϵ_b [28, 29, 30]. In our case, the general assumptions are satisfied, namely all the contributions of the non-standard couplings κ 's to low energy observables are contained in the oblique corrections, *i.e.*, the vacuum polarization functions of the gauge bosons, and the non-oblique corrections to the vertex $b\text{-}b\text{-}Z$. Therefore, it is enough to calculate the new physics contribution to the ϵ parameters in order to isolate all effects to low energy observables.

The experimental values of the ϵ parameters are derived from four basic observables, Γ_ℓ (the partial width of Z to a charged lepton pair), A_{FB}^ℓ (the forward-backward asymmetry at the Z peak for the charged lepton ℓ), M_W/M_Z , and Γ_b (the partial width of Z to a $b\bar{b}$ pair) [31].

To constrain these nonstandard couplings (κ 's) one needs to have the theoretical predictions for the ϵ 's. The SM contribution to the ϵ 's have been calculated in, for example Ref. [32]. Naturally, since we are considering the case of a spontaneous symmetry breaking scenario in which there is no Higgs boson, we have to subtract the Higgs boson contribution from these SM calculations.

Since the top quark will only contribute to the vacuum polarization functions and the vertex $b\text{-}b\text{-}Z$, we only need to consider:

$$\epsilon_1 = e_1 - e_5, \quad (34)$$

$$\epsilon_2 = e_2 - c_w^2 e_5, \quad (35)$$

$$\epsilon_3 = e_3 - c_w^2 e_5, \quad (36)$$

$$\epsilon_b = e_b, \quad (37)$$

where e_1 , e_2 , e_3 , e_5 , and e_b are defined as:

$$e_1 = \frac{A^{ZZ}(0)}{M_Z^2} - \frac{A^{WW}(0)}{M_W^2}, \quad (38)$$

$$e_2 = F^{WW}(M_W^2) - F^{33}(M_Z^2), \quad (39)$$

$$e_3 = \frac{c_w}{s_w} F^{30}(M_Z^2), \quad (40)$$

$$e_5 = M_Z^2 \frac{dF^{ZZ}}{dq^2}(M_Z^2). \quad (41)$$

The vacuum polarization functions of the gauge bosons are written in the following form

$$\Pi_{\mu\nu}^{ij}(q^2) = -ig_{\mu\nu} \left(A^{ij}(q^2) + q^2 F^{ij}(q^2) \right) + q_\mu q_\nu \text{ terms}, \quad (42)$$

where $i, j = W, Z, \gamma(\text{photon})$. Alternatively, instead of using Z and γ one can use $i, j = 3, 0$ for W^3 and B , respectively. The relation between the two cases is as follows

$$A^{33} = c_w^2 A^{ZZ} + 2s_w c_w A^{\gamma Z} + s_w^2 A^{\gamma\gamma}, \quad (43)$$

$$A^{30} = -c_w s_w A^{ZZ} + (c_w^2 - s_w^2) A^{\gamma Z} + c_w s_w A^{\gamma\gamma}, \quad (44)$$

$$A^{00} = s_w^2 A^{ZZ} - 2s_w c_w A^{\gamma Z} + c_w^2 A^{\gamma\gamma}, \quad (45)$$

and similarly for F^{ij} .

The quantity e_b is defined through the proper vertex correction

$$V_\mu(Z \rightarrow b\bar{b}) = -\frac{g}{2c_w} e_b \gamma_\mu \frac{1 - \gamma_5}{2}. \quad (46)$$

3.1 Radiative Corrections in Effective Lagrangians

Before presenting our results for the contributions of the non-standard couplings to the LEP data, we will discuss a key aspect of effective theories in general.

Non-renormalizability of the effective Lagrangian presents a major issue of how to consistently handle both the divergent and the finite pieces in loop calculations [33, 34]. Such a problem arises because one does not know the underlying theory; hence, no matching can be performed to extract the correct scheme to be used in the effective Lagrangian [35]. One approach is to associate the divergent piece in loop calculations with a physical cutoff scale Λ , the upper scale at which the effective Lagrangian is valid [25]. In the chiral Lagrangian approach this cutoff Λ is taken to be $4\pi v \sim 3 \text{ TeV}$ [35].⁸ For the finite piece no completely satisfactory approach is available [33]. We assume that there exists an underlying renormalizable "full" theory that is valid at all scales (or at least at scales much higher than Λ). In this case, Λ serves as an infrared cutoff scale under which the heavy degrees of freedom can be integrated out to give rise to the effective operators in the chiral Lagrangian. Due to the renormalizability of the full theory, and from the renormalization group invariance, one concludes that the same cutoff Λ should also serve as the associated ultraviolet cutoff of the effective Lagrangian in the calculation of the Wilson coefficients. Hence, in the dimensional regularization scheme, the ultraviolet divergent piece $1/\epsilon$ is replaced by $\ln(\Lambda^2/\mu^2)$, where $\epsilon = (4 - n)/2$ and n is the space-time dimension. Furthermore, the renormalization scale μ is set to be m_t , the heaviest mass scale in the low energy effective Lagrangian. To study the effects to low energy observables due to a heavy top quark, in addition to the SM contributions, we shall only include those non-standard contributions (from the κ 's) of the order

$$\frac{m_t^2}{16\pi^2 v^2} \ln \frac{\Lambda^2}{m_t^2}. \quad (47)$$

⁸ The scale $4\pi v \sim 3 \text{ TeV}$ is only meant to indicate the typical cutoff scale. It is equally probable to have, say, $\Lambda = 1 \text{ TeV}$.

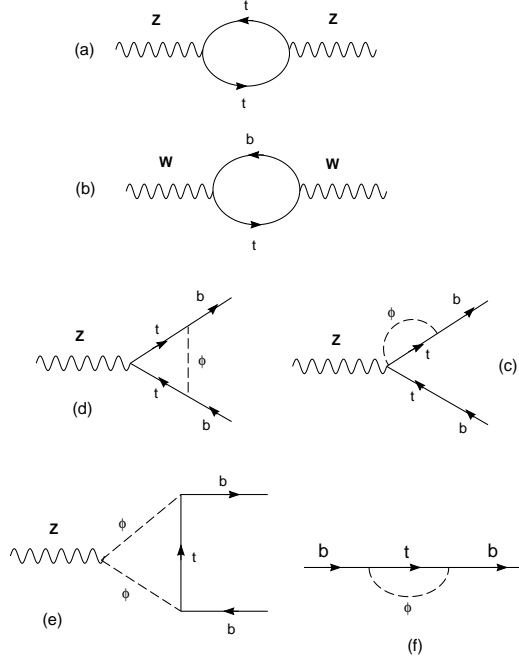


Figure 1: The relevant Feynman diagrams, for the nonstandard top quark couplings case and in the 't Hooft–Feynman gauge, which contribute to the order $\mathcal{O}(m_t^2 \ln \Lambda^2)$.

3.2 Contributions on the low energy observables

To perform calculations using the chiral Lagrangian, one should arrange the contributions in powers of $\frac{1}{4\pi v}$ and include all diagrams up to the desired power. In a general R_ξ gauge ($\Sigma \neq 1$), the couplings of the Goldstone bosons to the fermions should also be included in Feynman diagram calculations. These couplings can be easily found by expanding the operators in $\mathcal{L}^{(4)}$.

The relevant Feynman diagrams are shown in Figure 1. Calculations can be done for a general R_ξ gauge. As it turns out, the dependence on m_t for ϵ_1 (which is the deviation from $\rho = 1$) and for ϵ_b is quadratic, whereas for ϵ_2 and ϵ_3 is only logarithmic. Hence, in our effective model, the significant constraints on the parameters κ_L^{NC} , κ_R^{NC} , and κ_L^{CC} are only coming from ϵ_1 and ϵ_b .

The leading contributions (of order $m_t^2 \ln \Lambda^2$) are the following:

- For the vacuum polarization function of the Z boson (Figure 1(a)),

$$A^{ZZ}(0) = \frac{M_Z^2}{4\pi^2} \frac{3m_t^2}{v^2} \left(-\kappa_L^{NC} + \kappa_R^{NC} \right) \frac{1}{\epsilon} \quad (48)$$

- For the vacuum polarization function of the W boson (Figure 1(b)),

$$A^{WW}(0) = \frac{M_W^2}{4\pi^2} \frac{3m_t^2}{v^2} \left(-\kappa_L^{CC} \right) \frac{1}{\epsilon} \quad (49)$$

- The vertex corrections are depicted in Figs. 1(c), 1(d) and 1(e),

$$(c) \rightarrow \frac{ig}{4c_w} \frac{m_t^2}{4\pi^2 v^2} \left(-2\kappa_L^{CC} \right) \gamma_\mu (1 - \gamma_5) \frac{1}{\epsilon} \quad (50)$$

•

$$(d) \rightarrow \frac{ig}{4c_w} \frac{m_t^2}{4\pi^2 v^2} \left(-2c_w^2 \kappa_L^{CC} + \frac{1}{4} \kappa_R^{NC} - \kappa_L^{NC} \right) \gamma_\mu (1 - \gamma_5) \frac{1}{\epsilon} \quad (51)$$

•

$$(e) \rightarrow \frac{ig}{4c_w} \frac{m_t^2}{4\pi^2 v^2} \left(-c_w^2 + \frac{1}{2} \right) \kappa_L^{CC} \gamma_\mu (1 - \gamma_5) \frac{1}{\epsilon} \quad (52)$$

- Finally, the b -quark self energy (Figure 1(f)) contribution is

$$- \frac{3m_t^2}{16\pi^2 v^2} \gamma_\mu p^\mu \left(\kappa_L^{CC} \right) (1 - \gamma_5) \frac{1}{\epsilon} \quad (53)$$

Therefore, the net non-standard contributions to the ϵ parameters are

$$\delta\epsilon_1 = \frac{G_F}{2\sqrt{2}\pi^2} 3m_t^2 (-\kappa_L^{NC} + \kappa_R^{NC} + \kappa_L^{CC}) \ln \frac{\Lambda^2}{m_t^2}, \quad (54)$$

$$\delta\epsilon_b = \frac{G_F}{2\sqrt{2}\pi^2} m_t^2 \left(-\frac{1}{4} \kappa_R^{NC} + \kappa_L^{NC} \right) \ln \frac{\Lambda^2}{m_t^2}, \quad (55)$$

It is interesting to note that κ_L^{CC} does not contribute to ϵ_b up to this order ($m_t^2 \ln \Lambda^2$) which can be understood from Eq. (32). If $\kappa_L^{CC} = -1$ then there is no net t - b - W coupling in the chiral Lagrangian after including both the standard and nonstandard contributions. Hence, no dependence on the top quark mass can be generated, *i.e.*, the nonstandard κ_L^{CC} contribution to ϵ_b must cancel the SM contribution when $\kappa_L^{CC} = -1$, independently of the couplings of the neutral current. From this observation and because the SM contribution to ϵ_b is finite, we conclude that κ_L^{CC} cannot contribute to ϵ_b at the order of interest.

Given the above results we can then use the experimental values of the ϵ 's to constrain the theoretical predictions [32, 36, 37]:

$$1.95 \times 10^{-3} \leq \epsilon_1^{\text{SM}} + \delta\epsilon_1 \leq 6.65 \times 10^{-3}, \quad (56)$$

$$-10.5 \times 10^{-3} \leq \epsilon_b^{\text{SM}} + \delta\epsilon_b \leq 2.0 \times 10^{-3}, \quad (57)$$

where the minimum and maximum limits represent 1.96σ deviations from the central values of the experimental measurements [36].

For these comparisons, we have included $\epsilon_b^{\text{SM}} = (-5.3, -6.1, -7.0) \times 10^{-3}$ and $\epsilon_1^{\text{SM}} = (4.5, 6.3, 5.4) \times 10^{-3}$ for $m_t = (160, 170, 180)$ GeV, $\delta\epsilon_b$ and $\delta\epsilon_1$, where ϵ^{SM} is the SM prediction⁹ after subtracting the contributions due to a light Higgs boson (with

⁹ ϵ^{SM} includes also contributions from vertex and box diagrams.

mass $\sim M_Z$). The other term $\delta\epsilon$, is the contribution from the dimension 4 anomalous couplings given in Eqs. (54) and (55). As we can see, precision data allows for all three non-standard couplings to be different from zero. There is a three dimensional boundary region for these κ 's, which we can visualize through the three projections; on the $\kappa_L^{CC} = 0$, $\kappa_R^{NC} = 0$ and $\kappa_L^{NC} = 0$ planes, presented in Figs. 2, 3 and 4 respectively. As we can see from the three projections, the only coefficient that is constrained is κ_L^{NC} which can only vary between -0.35 and 0.35 . The other two can vary through the whole range $(-1.0 \text{ to } 1.0)$ although in a correlated manner; from Figure 4 we can say that LEP data imposes $\kappa_L^{CC} \sim -\kappa_R^{NC}$ if κ_L^{NC} is close to zero. This conclusion holds for m_t ranging from 160 GeV to 180 GeV.

In Ref. [2] a similar analysis was done, but there the anomalous charged current contribution κ_L^{CC} was not included, and only the non-standard t - t - Z couplings were considered. The allowed region they found in Ref. [2] simply corresponds, in our analysis, to the region defined by the intersection of the allowed volume (Eq. (56)) and the plane $\kappa_L^{CC} = 0$, which gives a small area confined in the vicinity of the line $\kappa_L^{NC} = \kappa_R^{NC}$ (cf. Fig. 2).

It is also interesting to consider a special case in which the underlying theory respects the global $SU(2)_L \times SU(2)_R$ custodial symmetry that is then broken in such a way as to account for a negligible deviation of the b - b - Z vertex from its standard form. This scenario will relate the non-standard terms in our effective Lagrangian $\mathcal{L}^{(4)}$ (Eq. (32)).

3.3 Underlying custodial symmetry case

The SM has an additional (accidental) symmetry called the custodial symmetry which is responsible for the tree-level relation [5, 38]

$$\rho = \frac{M_W^2}{M_Z^2 c_w^2} = 1 , \quad (58)$$

This symmetry is slightly broken at the quantum level by the $SU(2)$ doublet fermion mass splitting and the hypercharge coupling g' . Writing $\rho = 1 + \delta\rho$, $\delta\rho$ would vanish to all orders if this symmetry were exact [39]. Low energy data indicate that $\delta\rho$ is very close to zero, within about 0.1% accuracy [40].

In the chiral Lagrangian this assumption of a custodial symmetry sets $v_3 = v_2 = v_1$ (see Eq. (1)), and forces the couplings of the top quark to the gauge bosons W_μ^a to be equal after turning off the hypercharge.

Let us consider the case of an underlying global $SU(2)_L \times SU(2)_R$ symmetry that is broken in such a way as to account for a negligible deviation of the b - b - Z vertex from its standard form. Since the top quark acquires a mass much heavier than the other quarks' masses, we expect the new physics effects associated with the

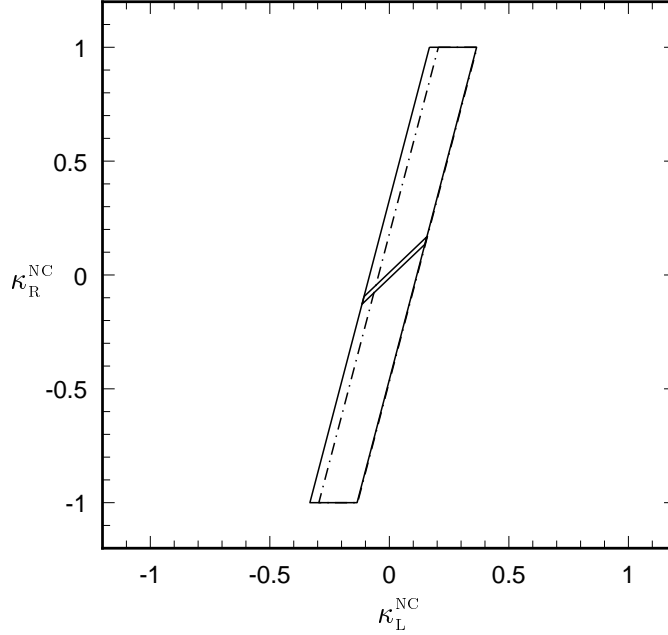


Figure 2: A two-dimensional projection in the plane of κ_L^{NC} and κ_R^{NC} , for $m_t = 160$ GeV (solid contour) and 180 GeV (dashed contour). If $\kappa_L^{CC} = 0$ the inner solid countour gives the projection for $m_t = 160$ GeV.

electroweak symmetry breaking (EWSB) sector to be substantially greater for the couplings (to the gauge bosons) of this quark than for the couplings of all the others, including the bottom quark. Therefore, it is natural to think of the initial presence of an underlying theory that respects the custodial symmetry, and then to think of the EWSB mechanism introducing an effective interaction that will explicitly break this symmetry in such a way as to favor the deviation of the couplings of the top quark more than the deviation of the other light quarks' couplings.

In the context of the chiral Lagrangian, let us think of the effective Lagrangian $\mathcal{L}^{(4)}$ (Eq. (32)) originating from two parts: one that reflects the underlying theory that respects the custodial symmetry (denoted by $\mathcal{L}^{(custodial)}$), and another part that explicitly breaks this symmetry but that keeps the coupling $b\text{-}b\text{-}Z$ essentially unmodified (denoted by $\mathcal{L}^{(EWSB)}$).

Let us find the most general form for $\mathcal{L}^{(custodial)}$. Notice that if we set $s_w = 0$ (turn off the hypercharge), then the standard $SU(2)_L$ invariant term

$$\overline{F_L} \gamma^\mu \left(i \partial_\mu - \frac{1}{2} \begin{pmatrix} \mathcal{W}_\mu^3 & \sqrt{2} \mathcal{W}_\mu^+ \\ \sqrt{2} \mathcal{W}_\mu^- & -\mathcal{W}_\mu^3 \end{pmatrix} \right) F_L, \quad (59)$$

with the left handed doublets

$$F_L = \begin{pmatrix} f_1 \\ f_2 \end{pmatrix}_L \quad (60)$$

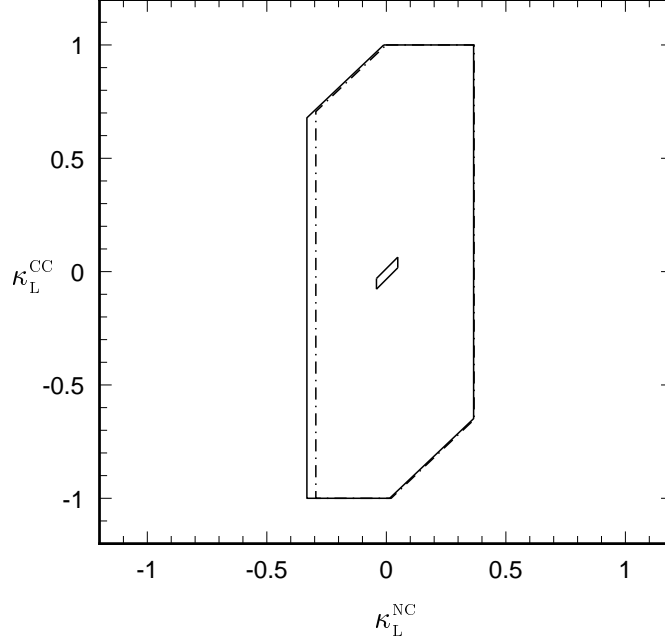


Figure 3: A two-dimensional projection in the plane of κ_L^{NC} and κ_L^{CC} , for $m_t = 160$ GeV (solid contour) and 180 GeV (dashed contour). If $\kappa_R^{NC} = 0$ the inner solid countour gives the projection for $m_t = 160$ GeV.

defined in Eq. (29), respects the global $SU(2)_L \times SU(2)_R$ symmetry¹⁰ and is the only structure that does so (the derivative term is trivial). Therefore the only way in which $\mathcal{L}^{(custodial)}$ can contain non-standard couplings is through a term proportional to the same $W^a \tau^a$ structure:

$$\mathcal{L}^{(custodial)} = \overline{F}_L \gamma^\mu \left(i \partial_\mu - \frac{1}{2} \mathcal{W}_\mu^a \tau^a \right) F_L + \kappa_1 \overline{F}_L \gamma^\mu \mathcal{W}_\mu^a \tau^a F_L. \quad (61)$$

where κ_1 is a real number (so that $\mathcal{L}^{(custodial)}$ is hermitian).

Now, for $\mathcal{L}^{(EWSB)}$ we notice that (in the context of the non-linearly realized $SU(2)_L \times U(1)_Y$ chiral Lagrangian) one can break the custodial symmetry by introducing interaction terms that involve the τ^3 matrix such as

$$\mathcal{L}^{(EWSB)} = \kappa_2 \overline{F}_L \gamma^\mu \mathcal{W}_\mu^a \tau^a \tau^3 F_L + \kappa_2^\dagger \overline{F}_L \gamma^\mu \tau^3 \mathcal{W}_\mu^a \tau^a F_L, \quad (62)$$

where κ_2 is in general a complex number.¹¹

¹⁰To verify this, we just need to use the transformation rules $\Sigma \rightarrow \Sigma' = L \Sigma R^\dagger$ and $F_L \rightarrow F'_L = R F_L$ with R and L members of global $SU(2)_L$ and $SU(2)_R$ respectively, as well as the identity $i \Sigma^\dagger D_\mu \Sigma = -\mathcal{W}_\mu^a \frac{\tau^a}{2}$.

¹¹ Another term could be $\overline{F}_L \gamma^\mu \tau^3 \mathcal{W}_\mu^a \tau^a \tau^3 F_L$, which contains two symmetry breaking factors τ^3 . We will not consider this term in our work.

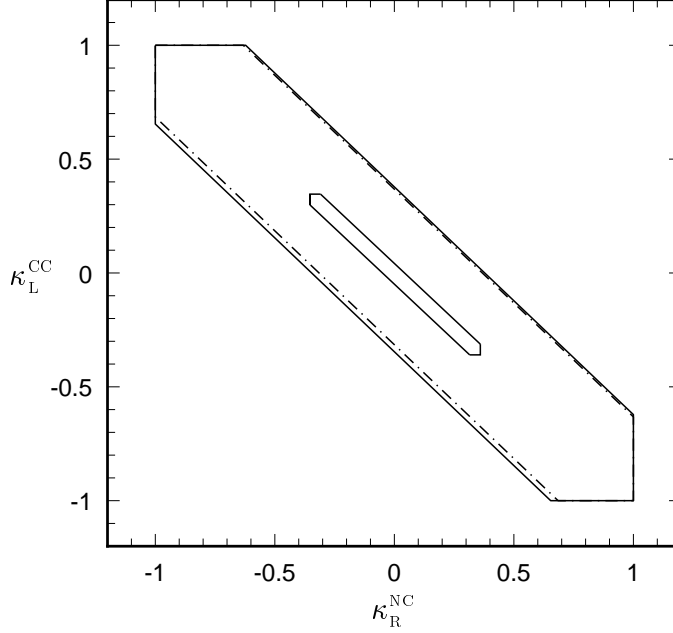


Figure 4: A two-dimensional projection in the plane of κ_R^{NC} and κ_L^{CC} , for $m_t = 160$ GeV (solid contour) and 180 GeV (dashed contour). If $\kappa_L^{NC} = 0$ the inner solid countour gives the projection for $m_t = 160$ GeV.

When we add $\mathcal{L}^{(EWSB)}$ to the non-standard part of $\mathcal{L}^{(custodial)}$ we will obtain the term:

$$\overline{F_L} \gamma^\mu \begin{pmatrix} (\kappa_1 + \kappa_2 + \kappa_2^\dagger) \mathcal{W}_\mu^3 & (\kappa_1 - \kappa_2 + \kappa_2^\dagger) \sqrt{2} \mathcal{W}_\mu^+ \\ (\kappa_1 + \kappa_2 - \kappa_2^\dagger) \sqrt{2} \mathcal{W}_\mu^- & (-\kappa_1 + \kappa_2 + \kappa_2^\dagger) \mathcal{W}_\mu^3 \end{pmatrix} F_L. \quad (63)$$

Therefore, by requiring κ_2 to be a real number, and by setting $\kappa_1 = 2\kappa_2$, the above result indeed describes the scenario in which an underlying custodial symmetric theory is being broken without modifying the coupling $b\text{-}b\text{-}Z$ from its standard value. By turning the hypercharge back on we will then see that the $\mathcal{L}^{(4)}$ Lagrangian will look like:

$$\mathcal{L}^{(4')} = \overline{F_L} \gamma^\mu \left(i\partial_\mu - \frac{1}{2} \mathcal{W}_\mu^a \tau^a \right) F_L + \overline{F_L} \gamma^\mu \kappa_1 \begin{pmatrix} 2\mathcal{Z}_\mu & \sqrt{2} \mathcal{W}_\mu^+ \\ \sqrt{2} \mathcal{W}_\mu^- & 0 \end{pmatrix} F_L. \quad (64)$$

The superscript (4') in $\mathcal{L}^{(4')}$ is just to differentiate it from the original most general Lagrangian $\mathcal{L}^{(4)}$ of Eq. (32). In conclusion, if we want to consider a special case in which an underlying custodial symmetric theory is being broken by interactions that in the end do not modify the $b\text{-}b\text{-}Z$ vertex from its standard form, we have to reproduce the matrix structure presented in Eq. (64). This is equivalent to just

requiring the relation¹²

$$\kappa_L^{NC} = 2\kappa_L^{CC} = 4\kappa_1 \equiv \kappa_L \quad (65)$$

to be satisfied in the original Lagrangian $\mathcal{L}^{(4)}$. Since for the right-handed couplings only the neutral κ_R^{NC} participates in the radiative corrections, we can simplify our notation and set $\kappa_R^{NC} \equiv \kappa_R$.

From the correlations between the effective couplings (κ 's) of the top quark to the gauge bosons, one can infer if the symmetry-breaking sector is due to a model with an approximate custodial symmetry or not, *i.e.*, we may be able to probe the symmetry-breaking mechanism in the top quark system. To illustrate this point, we can compare our results with those in Ref. [2]. Figure 5 shows the most general allowed region for the couplings κ_L^{NC} and κ_R^{NC} , *i.e.*, without imposing any "custodial symmetry" relation between κ_L^{NC} and κ_L^{CC} . This region is for a top quark mass of 170 GeV and covers the parameter space $-1.0 \leq \kappa_L^{NC}, \kappa_R^{NC} \leq 1.0$. We also show on Fig. 5 the allowed regions for our special case ($\kappa_L^{CC} = \frac{1}{2}\kappa_L^{NC}$) and the model in Ref. [2] ($\kappa_L^{CC} = 0$). One finds

$$\begin{aligned} -0.08 &\leq \kappa_L^{NC} \leq 0.13 \text{ and} \\ -0.06 &\leq \kappa_R^{NC} \leq 0.07 \text{ for } \kappa_L^{NC} = 2\kappa_L^{CC}, \end{aligned} \quad (66)$$

$$\begin{aligned} -0.09 &\leq \kappa_L^{NC} \leq 0.15 \text{ and} \\ -0.12 &\leq \kappa_R^{NC} \leq 0.18 \text{ for } \kappa_L^{CC} = 0. \end{aligned} \quad (67)$$

The two regions overlap in the vicinity of the origin (0, 0) which corresponds to the SM case. Note that for $m_t \leq 200$ GeV the allowed region of κ 's in all models of symmetry-breaking should overlap near the origin because the SM is consistent with low energy data at the 95% C.L. For $\kappa_L^{NC} \geq 0.1$, these two regions diverge and become separable. One notices that the allowed range predicted in Ref. [2] lies along the line $\kappa_L^{NC} = \kappa_R^{NC}$ whereas in our case the slope is given by the line $\kappa_L^{NC} = 2\kappa_R^{NC}$.

If we imagine that any prescribed dependence between the couplings corresponds to a symmetry-breaking scenario, then, given the present status of low energy data, it is possible to distinguish between different scenarios if κ_L^{NC} , κ_R^{NC} and κ_L^{CC} are larger than 10%. Better future measurements of ϵ 's can further discriminate between different symmetry-breaking scenarios with smaller difference in the κ 's. Next, we will discuss how the SLC precision data can contribute to the study of the nonstandard couplings.

3.4 At the SLC

The measurement of the left-right cross section asymmetry A_{LR} in Z production with a longitudinally polarized electron beam at the SLC provides a further test of the

¹²A relation like this appears in the SM after integrating out an ultra-heavy Higgs boson [5].

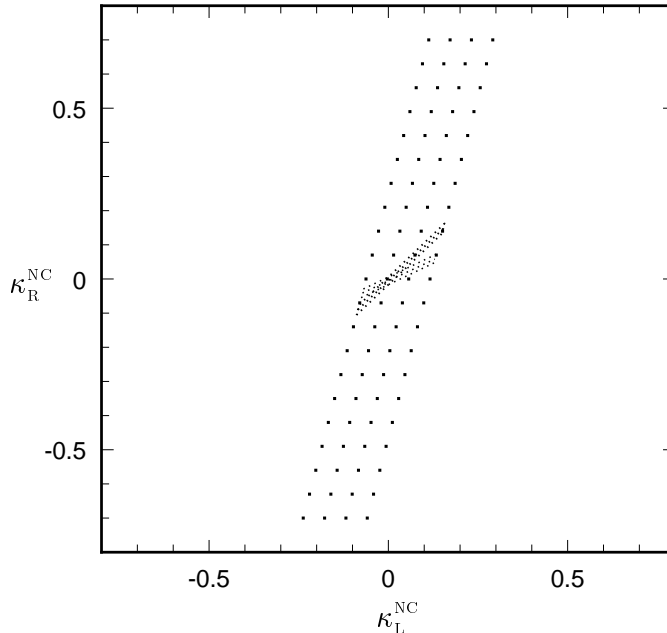


Figure 5: A comparison between our model and the model in Ref. [2]. The allowed regions in both models are shown on the plane of κ_L^{NC} and κ_R^{NC} , for $m_t = 170$ GeV.

SM and is sensitive to new physics. The reported measurement of A_{LR} [41] shows a deviation of about 2.8σ from the SM¹³ prediction. The effect of the SLC measurement of A_{LR} on possible new physics effects on the top quark couplings depends on the way one incorporates A_{LR} with LEP data. If we include and average A_{LR} with all LEP data, the anomaly in A_{LR} is almost washed away due to the large number of LEP measurements consistent with the SM. One finds that including the SLC measurement A_{LR} with all LEP data yields a slight decrease in the central value of ϵ_1 [36] while keeping the fit on ϵ_b the same. As discussed in the previous section, the nonstandard coupling κ_L^{NC} is mostly constrained by ϵ_b . Therefore, no significant change in the allowed range of κ_L^{NC} is expected. The effect of averaging the SLC and LEP data can be easily seen in the special model discussed previously ($\kappa_L^{CC} = \kappa_L^{NC}/2$). In this case, the length of the allowed area is not affected since it is controlled by ϵ_b . Since the uncertainty in $\epsilon_1^{\text{exp.}}$ remains almost the same after including the A_{LR} measurement, the width of the allowed area is also hardly modified. The only effect will be to shift the allowed area slightly downward (towards $2\kappa_R < \kappa_L$). This conclusion is simply due to the preference for a more negative new physics contribution to accommodate the smaller value of $\epsilon_1^{\text{exp.}}$.

We have seen that the precision LEP/SLC data can constrain the couplings κ_L^{NC} , κ_R^{NC} and κ_L^{CC} , without forcing them to be zero. For κ_R^{CC} (the right-handed charged

¹³With a top quark mass $m_t = 175$ GeV and a Higgs mass $m_H = 300$ GeV.

current) there is no constraint, because its contribution to the relevant radiative corrections at LEP/SLC is proportional to the bottom quark's mass. However, the nonstandard coupling κ_R^{CC} can be studied using the $b \rightarrow s\gamma$ measurement [26] [cf. Eq. (33)].

The important lesson from the above analysis is that the precision low energy data do not exclude the possibility of having anomalous top quark interactions with the gauge bosons. Also, different models for the electroweak symmetry breaking sector can induce different relations among the κ 's. These relations can in turn be used to discriminate between models by comparing their predictions with experimental data. In the next section, we examine how to improve our knowledge of these non-standard couplings by direct measurements at current and future colliders.

4 Direct measurement of dimension four anomalous couplings at colliders

In this section, we shall discuss how to measure the dimension four anomalous couplings κ_L^{NC} , κ_R^{NC} , κ_L^{CC} , and κ_R^{CC} at hadron colliders and future electron collider.

Run I at the Fermilab Tevatron (a $\bar{p}p$ collider with $\sqrt{S} = 1.8$ TeV) is now complete, and each experiment (CDF and DØ groups) has accumulated an integrated luminosity of about 110 pb^{-1} . Run II (the upgraded Tevatron with the Main Injector) will begin in 1999, with a machine energy of 2 TeV and an integrated luminosity of about 2 fb^{-1} per year. The CERN Large Hadron Collider (LHC) is a pp collider with $\sqrt{S} = 14$ TeV and an integrated luminosity of about $10 \sim 100 \text{ fb}^{-1}$ per year. A future electron Linear Collider (LC) is also proposed to run at the top quark pair threshold (via $e^-e^+ \rightarrow t\bar{t}$ process) to study the detailed properties of the top quark.

4.1 At the Tevatron and the LHC

At the Tevatron and the LHC, heavy top quarks are predominantly produced in pairs from the QCD process $gg, q\bar{q} \rightarrow t\bar{t}$. In addition, there are single-top quark events in which only a single t or \bar{t} is produced. A single-top quark signal can be produced from either the W -gluon fusion process $qg(Wg) \rightarrow t\bar{b}$ (or $q'b \rightarrow qt$ [42, 43, 44], the Drell-Yan-type W^* process $q\bar{q} \rightarrow t\bar{b}$ [45, 46, 47] and Wt production via $gb \rightarrow W^-t$ [48]. The corresponding Feynman diagrams for these single-top processes are shown in Figure 6. The approximate cross sections (in pb) for single-top quark production (including both single- t and single- \bar{t} events) at the upgraded Tevatron (and the LHC) from the above four production processes are 6.5(700), 2.0(200), 0.88(10) and 0.2(70), respectively.

The relative magnitudes between the dimension four anomalous couplings κ_L^{CC} and κ_R^{CC} can be measured from the decay of the top quark (produced from either of

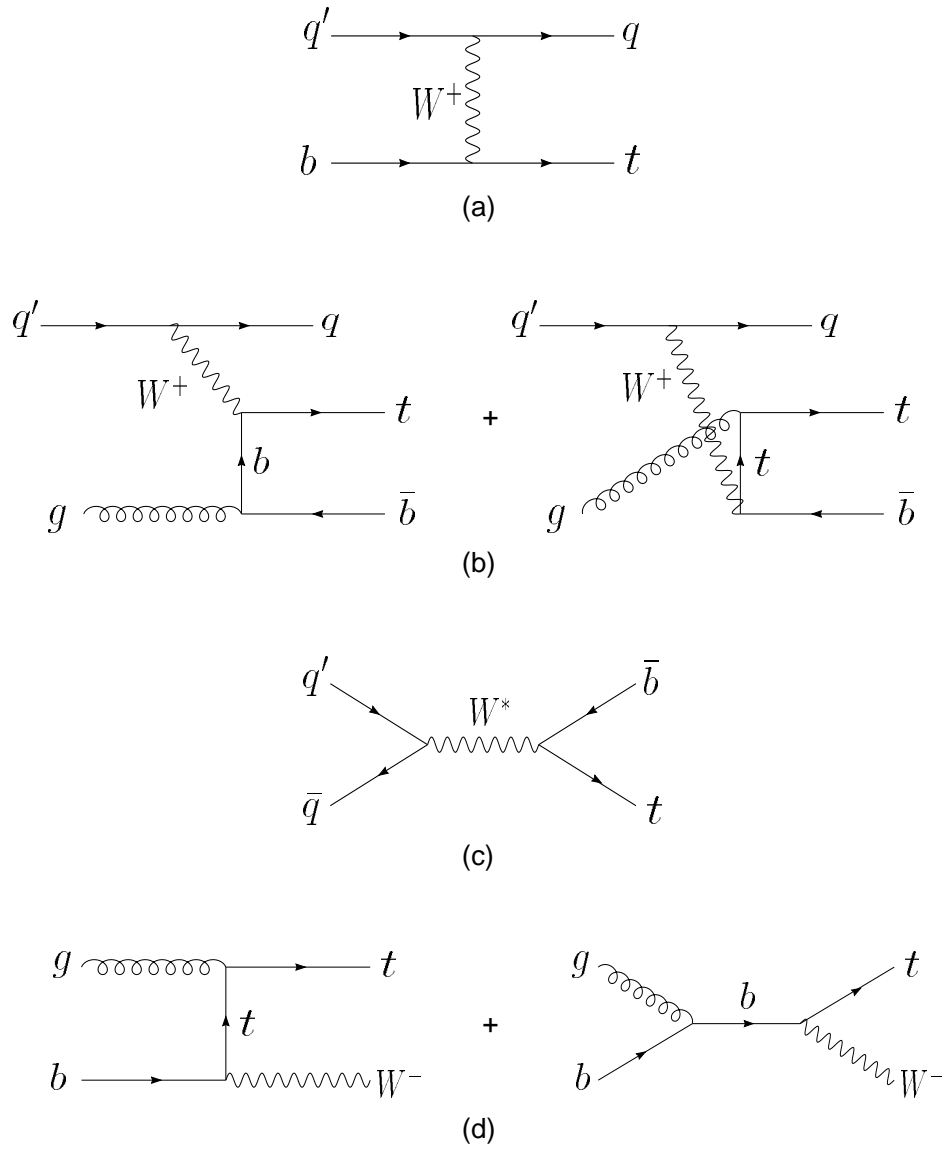


Figure 6: Diagrams for various single-top quark processes.

the above processes) to a bottom quark and a W boson. These nonstandard couplings can be furthered measured from counting the production rates of signal events with a single t or \bar{t} . More details can be found in Refs. [47], [49] and [50].

4.1.1 From the decay of top quarks

In $t\bar{t}$ events, the final state with most kinematic information is $W + 4j$, where the W is detected via its leptonic decay. These events are fully reconstructable. To reduce backgrounds, it is best to demand at least one b tag. The number of such events is about 500 per fb^{-1} [50]. Thus there will be on the order of 1000 tagged, fully reconstructed top-quark events in Run II, to be compared with the approximately 25 $W + 4j$ single-tagged top events in Run I. To probe κ_L^{CC} and κ_R^{CC} from the decay of the top quark to a bottom quark and a W boson, one needs to measure the polarization of the W boson which can be determined by the angular distribution of the lepton (say, e^+ in the rest frame of W^+) in the decay mode $t \rightarrow bW^+(\rightarrow e^+\nu)$. However, reconstructing the rest frame of the W -boson (in order to measure its polarization) could be a non-trivial matter due to the missing longitudinal momentum (P_z) (with a two-fold ambiguity) of the neutrino (ν) from W decay. Fortunately, as shown in Eq. (68), one can determine the polarization of the W -boson without reconstructing its rest frame by using the Lorentz-invariant observable m_{be} , the invariant mass of b and e from t decay.

The polar angle $\theta_{e^+}^*$ distribution of the e^+ in the rest frame of the W^+ boson whose z-axis is defined to be the moving direction of the W^+ boson in the rest frame of the top quark can be written in terms of m_{be} through the following derivation:

$$\begin{aligned} \cos \theta_{e^+}^* &= \frac{E_e E_b - p_e \cdot p_b}{|\vec{\mathbf{p}}_e| |\vec{\mathbf{p}}_b|} \\ &\simeq 1 - \frac{p_e \cdot p_b}{E_e E_b} = 1 - \frac{2m_{be}^2}{m_t^2 - M_W^2}. \end{aligned} \quad (68)$$

The energies E_e and E_b are evaluated in the rest frame of the W^+ boson from the top quark decay and are given by

$$\begin{aligned} E_e &= \frac{M_W^2 + m_e^2 - m_\nu^2}{2M_W}, & |\vec{\mathbf{p}}_e| &= \sqrt{E_e^2 - m_e^2}, \\ E_b &= \frac{m_t^2 - M_W^2 - m_b^2}{2M_W}, & |\vec{\mathbf{p}}_b| &= \sqrt{E_b^2 - m_b^2}. \end{aligned} \quad (69)$$

where we have not ignored the negligible masses m_e and m_ν , of e^+ and ν_e , for the sake of bookkeeping.

In Eq. (68), the first line comes from exact definition, whereas the second line comes from applying Eq. (69) in the limit $m_b = 0$. However, in practice two problems

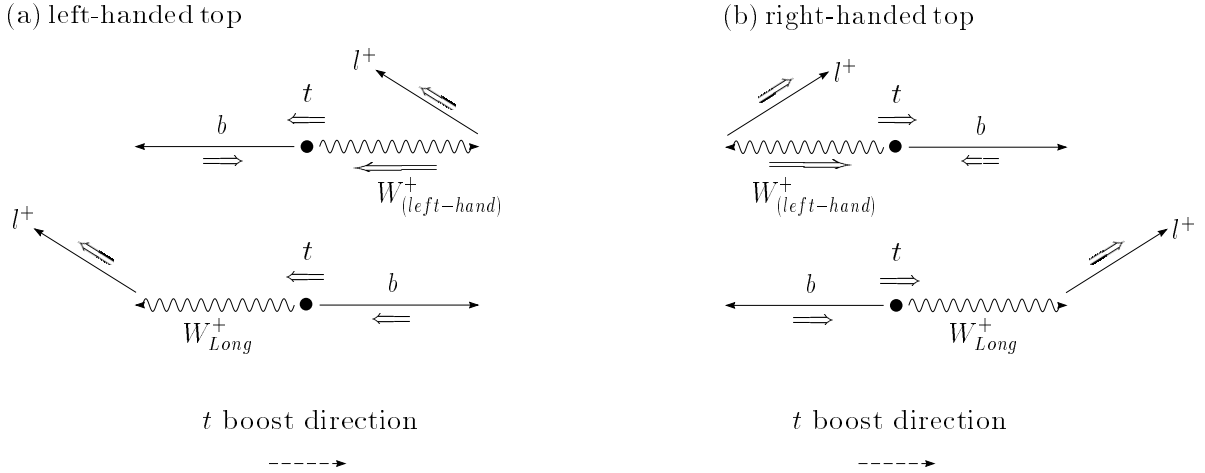


Figure 7: For a left-handed t - b - W vertex.

arise due to experimental limitations. First, the measured momenta of the bottom quark and the charged lepton will be smeared by detector effects, and second; it is difficult to do the identification of the right b to reconstruct t . There are three possible strategies to improve the efficiency of identifying the correct b . One is to demand a large invariant mass of the $t\bar{t}$ system so that t is boosted and its decay products are collimated. Namely, the right b will be moving closer to the lepton from t decay. This can be easily enforced by demanding leptons with a larger transverse momentum. Another strategy is to identify the soft (non-isolated) lepton from the \bar{b} decay (with a branching ratio $\text{Br}(\bar{b} \rightarrow \mu^+ X) \sim 10\%$). The third one is to statistically determine the electric charge of the b -jet (or \bar{b} -jet) to be $1/3$ (or $-1/3$).¹⁴ How precisely can the invariant mass $m_{b\ell}$ be measured is a question yet to be answered.

For a massless b (which is a good approximation for $m_b \ll m_t$), the W boson from top quark decay can only be either longitudinally or left-handed polarized for a purely left-handed charged current ($\kappa_R^{CC} = 0$). For a purely right-handed charged current ($\kappa_L^{CC} = -1$) the W boson can only be either longitudinally or right-handed polarized. (Note that the handedness of the W boson is reversed for a massless \bar{b} from \bar{t} decays.) This is the consequence of helicity conservation, as diagrammatically shown in Figs. 7 and 8 for a polarized top quark. In these figures we show the preferred moving direction of the lepton coming from a polarized W -boson decay in the rest frame of a polarized top quark, for both cases of a left-handed and a right-handed t - b - W vertex. As indicated in these figures, the invariant mass $m_{b\ell}$ depends on the polarization of the W -boson from the decay of a polarized top quark. Also, $m_{b\ell}$ is preferentially larger for a purely right-handed t - b - W vertex than for a purely left-handed one. This is clearly shown in Figure 9, in which the peak of the $m_{b\ell}$ distribution is shifted to the right and the distribution falls off sharply at the upper mass limit for a purely

¹⁴ This is the kind of analysis performed at LEP to separate a quark jet from a gluon jet.

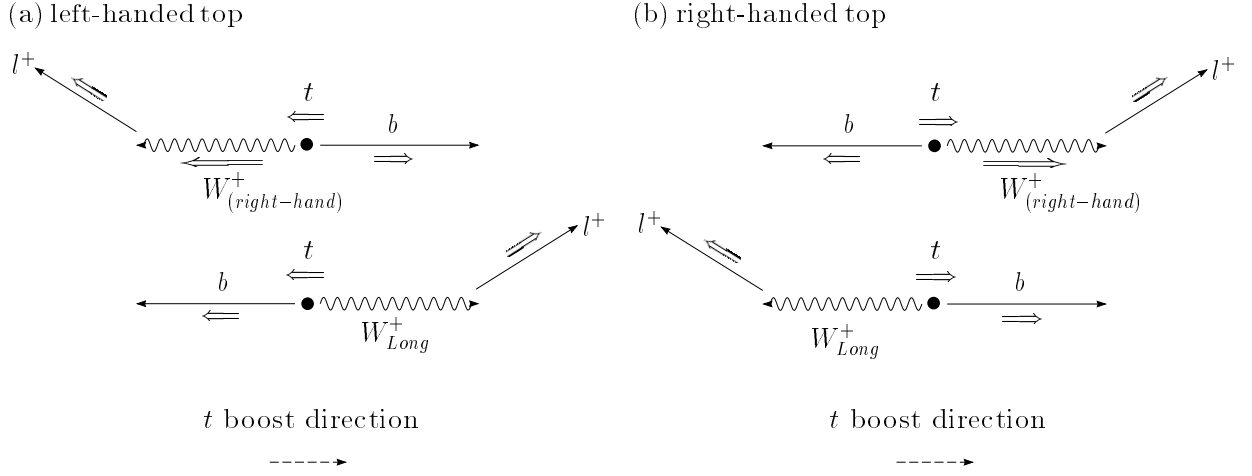


Figure 8: For a right-handed t - b - W vertex.

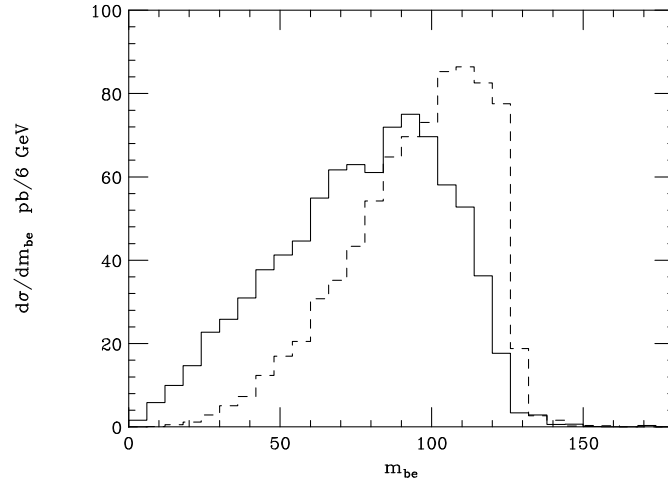


Figure 9: m_{be} distribution for SM top quark (solid) and for a purely right-handed t - b - W coupling (dash).

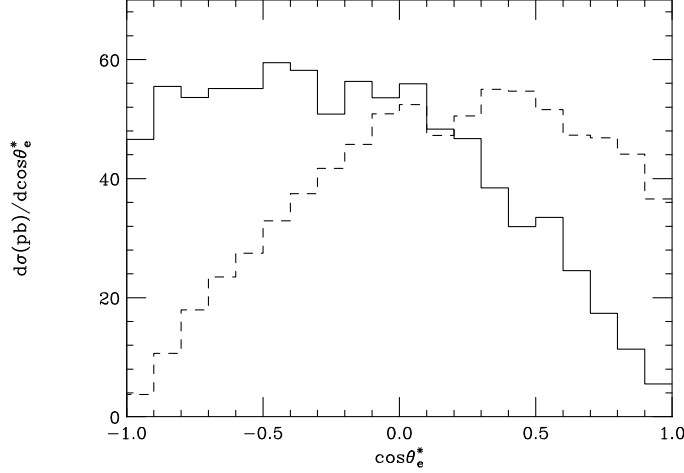


Figure 10: $\cos\theta_\ell^*$ distribution for SM top quark (solid) and for a purely right-handed t - b - W coupling (dash).

right-handed t - b - W vertex. Their difference is shown, in terms of $\cos\theta_\ell^*$, in Figure 10. However, in both cases the fraction (f_{Long}) of longitudinal W 's from top quark decay is enhanced by $m_t^2/2M_W^2$ as compared to the fraction of transversely polarized W 's [51], namely,

$$f_{\text{Long}} = \frac{\frac{m_t^2}{2M_W^2}}{1 + \frac{m_t^2}{2M_W^2}}. \quad (70)$$

Therefore, for a heavier top quark, it is more difficult to untangle the κ_L^{CC} and κ_R^{CC} contributions.¹⁵

As noted above, studying the decay of the top quark can tell us something about the relative size of the couplings $1 + \kappa_L^{CC}$ and κ_R^{CC} . To determine the values of κ_L^{CC} and κ_R^{CC} , one has to provide additional information such as the decay width of $t \rightarrow bW^+$ (which is about the total width of the top quark in the SM).¹⁶ If we *assume* the decay width of $t \rightarrow bW^+$ is the same as the SM prediction (i.e., about 1.5 GeV for a 175 GeV top quark), then the value of $(\kappa_L^{CC})^2 + (\kappa_R^{CC})^2$ is fixed. Thus, combining with

¹⁵On the other hand, because of the very same reason, the mass of a heavy top quark can be accurately measured from f_{Long} irrespective of the nature of the t - b - W couplings (either left-handed or right-handed).

¹⁶The information [cf. Eq. (33)] on κ_R^{CC} derived from the rare-decay process $b \rightarrow s\gamma$ could also be useful.

the information obtained from the previous analysis one can decisively determine κ_L^{CC} and κ_R^{CC} . The important question to ask then is how to measure the decay width of $t \rightarrow bW^+$, denoted as $\Gamma(t \rightarrow bW^+)$.

4.1.2 Measuring the decay width of $t \rightarrow bW^+$

As shown in Ref. [52], the intrinsic width of the top quark cannot be measured at hadron colliders from reconstructing the invariant mass of the jets from the decay of the top quark produced from the usual QCD processes ($q\bar{q}, gg \rightarrow t\bar{t}$) because of the poor resolution of the jet energy as measured by the detector. For a 175 GeV SM top quark, its intrinsic width is about 1.5 GeV, however the measured width from the invariant mass distribution of the top quark is unlikely to be much better than 10 GeV [50]. Is there a way to measure the top quark width $\Gamma(t \rightarrow bW^+)$ to within a factor of 2 or better, at hadron colliders? The answer is yes. It can be measured from single-top events.

The width $\Gamma(t \rightarrow bW^+)$ can be measured by counting the production rate of top quark from the W - b fusion process which is *equivalent* to the W -gluon fusion process by properly treating the bottom quark and the W boson as partons inside the hadron. In the following we shall discuss how to correctly treat the b -quark as a parton inside the proton to properly resum all the large logs to all orders in α_s . First, let us illustrate how to treat the W -boson as a parton inside the proton. Consider the $q'b \rightarrow qt$ process. It can be viewed as the production of an on-shell W -boson (i.e., effective- W approximation) which then rescatters with the b -quark to produce the top quark. This factorization is similar to that in the deep-inelastic scattering processes. The analytic expression for the flux ($f_\lambda(x)$) of the incoming W_λ -boson ($\lambda = 0, +, -$ for longitudinal, right-handed, or left-handed polarization) to rescatter with the b -quark can be found in Ref. [53]. The constituent cross section of $ub \rightarrow dt$ is given by

$$\hat{\sigma}(ub \rightarrow dt) = \sum_{\lambda=0,+,-} f_\lambda \left(x = \frac{m_t^2}{\hat{s}} \right) \left[\frac{16\pi^2 m_t^3}{\hat{s}(m_t^2 - M_W^2)^2} \right] \Gamma(t \rightarrow bW_\lambda^+),$$

where M_W is the mass of W^+ -boson and $\sqrt{\hat{s}}$ is the invariant mass of the hard part process. Note that in order to derive the above result one has to assume that the dynamics of the hard part scattering, i.e., $bW^+(k_\mu) \rightarrow t$, does not change dramatically from an off-shell ($k^2 < 0$) to an on-shell ($k^2 = M_W^2$) W -boson. Hence, the above equality is only valid under the effective- W approximation even though the kinematic factors are correctly included. Since the scattering rate of $Wb \rightarrow t$ is proportional to the decay rate of $t \rightarrow Wb$, the production rate of single-top event from the W -gluon fusion process measures the partial decay width of the top quark $\Gamma(t \rightarrow bW^+)$.

Furthermore, the branching ratio of $t \rightarrow Wb$ can be measured¹⁷ from the ratio of the numbers of double- b -tagged versus single- b -tagged $t\bar{t}$ events and the ratio of $(2\ell + jets)$ and $(1\ell + jets)$ rates in $t\bar{t}$ events for $t \rightarrow bW^+(\rightarrow \ell^+\nu)$ [50]. Combining this model-independent measurement of the branching ratio $\text{Br}(t \rightarrow bW)$ with the measurement of the partial decay width $\Gamma(t \rightarrow bW^+)$ from the single-top production rate, one can determine the total decay width $\Gamma_t = \Gamma(t \rightarrow bW)/\text{Br}(t \rightarrow bW)$ of the top quark, or equivalently, the lifetime $(1/\Gamma_t)$ of the top quark. At the Run-II of the Tevatron we expect that the lifetime of the top quark will be known to about 20% \sim 30%. Here, we have taken the values that the branching ratio $\text{Br}(t \rightarrow bW^+)$ can be measured to about 10% [50] and the cross section for W -gluon fusion process is known to about 15% \sim 20% (discussed in the next section).

Before closing this section, we comment on the importance of measuring the single-top production rate from the W -gluon fusion process. In the SM, the only nonvanishing coupling at the tree level is $\kappa_L^{CC} = 1$. These κ 's would have different values if new physics exists. Nevertheless, the conclusion that the production rate of the W -gluon fusion event is proportional to the decay width of $t \rightarrow Wb$ holds irrespective of the specific forms of the anomalous couplings (even including higher order operators). Hence, measuring the single-top event rate from the W -gluon fusion process is an *inclusive* method for detecting effects of new physics which might produce large modifications to the interactions of the top quark. Strictly speaking, from the production rate of single-top events, one measures the sum (weighted by parton densities) of all the possible partial decay widths, such as $\Gamma(t \rightarrow bW^+) + \Gamma(t \rightarrow sW^+) + \Gamma(t \rightarrow dW^+) + \dots$, therefore, this measurement is actually measuring the width of $\Gamma(t \rightarrow XW^+)$ where X can be more than one particle state as long as it originates from the partons inside the proton (or anti-proton). If new physics strongly enhances the flavor-changing-neutral-current t - c - Z , then the single-top production rate would also be enhanced from the Z - c fusion process $qc \rightarrow qt$.

4.1.3 The total production rate of W -gluon process

The calculation on the production rate of W -gluon fusion process involves a very important but not yet well-developed technique for handling the kinematics of a *heavy* b parton inside a hadron. Thus, the kinematics of the top quark produced from this process can not be accurately calculated. However, the total event rate of the single-top quark production via this process can be estimated using the method proposed in Ref. [55]. The total rate for W -gluon fusion process involves the $\mathcal{O}(\alpha^2)$ ($2 \rightarrow 2$) process $q'b \rightarrow qt$ plus the $\mathcal{O}(\alpha^2\alpha_s)$ ($2 \rightarrow 3$) process $q'g(W^+g) \rightarrow qt\bar{b}$ (where the gluon splits to $b\bar{b}$) minus the *splitting* piece $g \rightarrow b\bar{b} \otimes q'b \rightarrow qt$ in which $b\bar{b}$ are nearly collinear. These processes are shown diagrammatically in Figure 11.

¹⁷CDF group has reported a measurement of this branching ratio in [54].

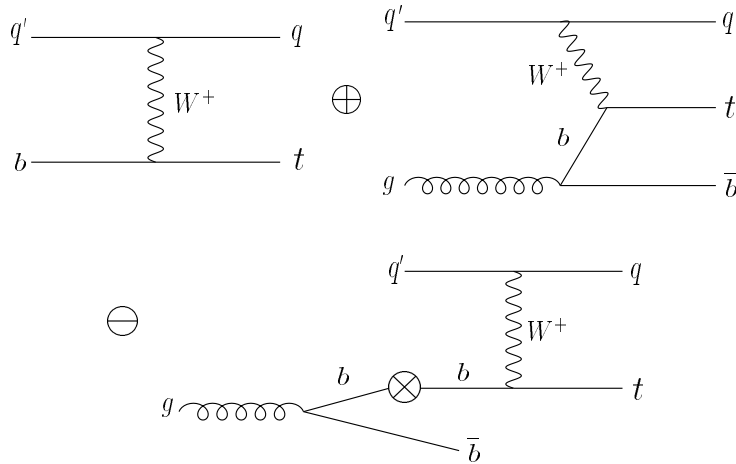


Figure 11: Feynman diagrams illustrating the subtraction procedure for calculating the total rate for W -gluon fusion: $q'b \rightarrow qt \oplus q'g(W^+g) \rightarrow qt\bar{b} \ominus (g \rightarrow b\bar{b} \otimes q'b \rightarrow qt)$.

The splitting piece is subtracted to avoid double counting the regime in which the b propagator in the $(2 \rightarrow 3)$ process closes to on-shell. This procedure is to resum the large logarithm $\alpha_s \ln(m_t^2/m_b^2)$ in the W -gluon fusion process to all orders in α_s and include part of the higher order $\mathcal{O}(\alpha^2\alpha_s)$ corrections to its production rate. (m_b is the mass of the bottom quark.) We note that to obtain the complete $\mathcal{O}(\alpha^2\alpha_s)$ corrections beyond just the leading log contributions one should also include virtual corrections to the $(2 \rightarrow 2)$ process, but we shall ignore these non-leading contributions in this work.¹⁸ Using the prescription described above we find that when using the $\overline{\text{MS}}$ parton distribution function (PDF) CTEQ2L [57] the total rate of the W -gluon fusion process is about 25% smaller than the $(2 \rightarrow 2)$ event rate either at the Tevatron or at the LHC.

To estimate the uncertainty in the production rate due to the choice of the scale Q in evaluating the strong coupling constant α_s and the parton distributions, we show in Figure 12 the scale dependence of the W -gluon fusion rate for a SM top quark. As shown in the figure, although the individual rate from either $(2 \rightarrow 2)$, $(2 \rightarrow 3)$, or the splitting piece is relatively sensitive to the choice of the scale, the total rate as defined by $(2 \rightarrow 2) + (2 \rightarrow 3) - (\text{splitting piece})$ only varies by about 30% for $M_W/2 < Q < 2m_t$ at the Tevatron. (At the LHC, it varies by about 10%). This uncertainty reduces to about 10% (at the Tevatron) for $m_t/2 < Q < 2m_t$.¹⁹ Based upon the results shown in Figure 12, we argue that $Q < M_W/2$ is probably not a good choice as the relevant scale for the production of the top quark from the W -gluon

¹⁸ In Ref. [56] it is shown that indeed these non-leading logs are not important.

¹⁹ This conclusion is in good agreement with a complete next-to-leading-order calculation (different from the above resummation procedure) performed in Ref. [56] in which the theoretical error on the total cross section at the Tevatron was estimated to be about 10% for Q ranging from $m_t/2$ to $2m_t$.

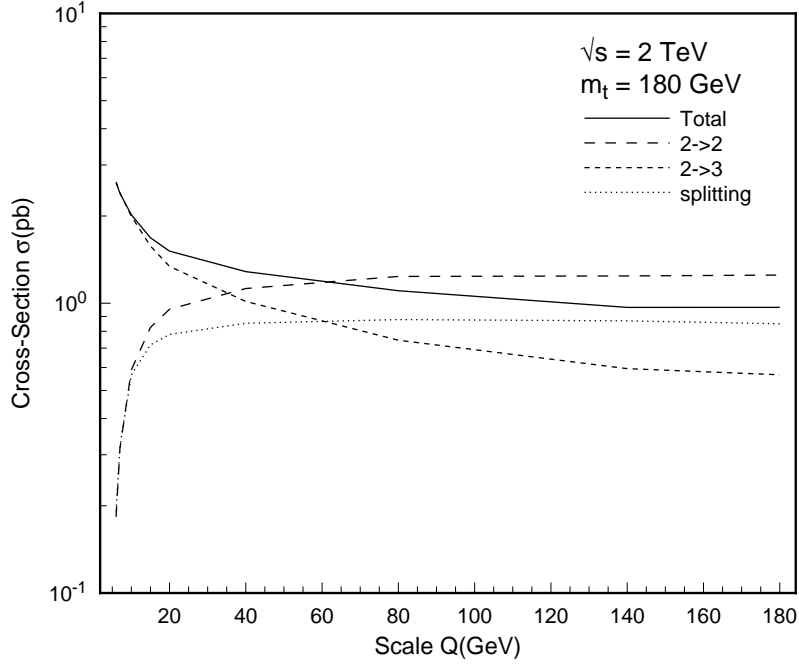


Figure 12: Rate of W -gluon fusion process versus scale Q for $m_t = 180$ GeV and $\sqrt{s} = 2$ TeV.

fusion process because the total rate rapidly increases by about a factor of 2 in the low Q regime. In view of the prescription adopted in calculating the total rate, the only relevant scales are the top quark mass m_t and the virtuality of the W -line in the scattering amplitudes. Since the typical transverse momentum of the quark (q) which comes from the initial quark (q') after emitting the W -line is about half of the W -boson mass, the typical virtuality of the W -line is about $M_W/2 \sim 40$ GeV. The scale $m_b \sim 5$ GeV is thus not an appropriate one to be used in calculating the W -gluon fusion rate when using our prescription. We note that in the $(2 \rightarrow 2)$ process the b quark distribution effectively contains sums to order $[\alpha_s \ln(Q/m_b)]^n$ from n -fold collinear gluon emission, whereas the subtraction term (namely, the splitting piece) contains only first order in $\alpha_s \ln(Q/m_b)$. Therefore, as $Q \rightarrow m_b$ the $(2 \rightarrow 2)$ contribution is almost cancelled by the splitting terms. Consequently, as shown in Figure 12, the total rate is about the same as the $(2 \rightarrow 3)$ rate for $Q \rightarrow m_b$. It is easy to see also that based upon the factorization of the QCD theory [55] the total rates calculated via this prescription will not be sensitive to the choice of $\overline{\text{MS}}$ PDF although each individual piece can have different results from different PDF's.

In conclusion, assuming $\kappa_R^{CC} = 0$, then κ_L^{CC} can be constrained to within $-0.08 < \kappa_L^{CC} < 0.03$ assuming a 20% uncertainty on the production rate of single-top quark from the W -gluon fusion process at the Tevatron [5]. This means that if we interpret

$(1 + \kappa_L^{CC})$ as the CKM matrix element $|V_{tb}|$, then $|V_{tb}|$ can be bounded as $|V_{tb}| > 0.9$.²⁰

4.1.4 Other single-top production rates

Another single-top quark production mechanism is the Drell-Yan type process $q'\bar{q} \rightarrow W^* \rightarrow t\bar{b}$ whose production rate can also provide information on κ_L^{CC} and κ_R^{CC} . Notice that the polarization of the top quark produced from this process is different from the one in W -gluon fusion events [46]. For instance, for a 175 GeV SM top quark produced at the Tevatron, W -gluon fusion produces almost 100% left handed top quarks, but the W^* process produces $\sim 50\%$ polarized top quarks (i.e., $\frac{1}{4}$ of top quarks are right handed and the rest are left handed). Hence, these production rates depend on κ_L^{CC} and κ_R^{CC} differently. Furthermore, since the kinematics of the top quark produced from these two processes are different [46], these two kinds of events can be separated at the Tevatron. In Ref. [47], a careful study was carried out of how to measure $|V_{tb}|$ from the production rate of W^* events. It was concluded that $|V_{tb}|$ can be measured to about 10% at the Tevatron if $\kappa_R^{CC} = 0$. It was shown in Ref. [59] that the production rate of W^* events up to the next-to-leading order QCD corrections is well under control (better than 10%). Hence, this process should provide a good measurement of κ_L^{CC} and κ_R^{CC} .²¹

We note that because the production cross sections of the single-top events from the W -gluon fusion and the W^* processes depend differently on κ_L^{CC} and κ_R^{CC} , they all have to be measured and combined with the measurement of the decay kinematics of the top quark to definitely constrain the anomalous couplings κ_L^{CC} and κ_R^{CC} . At the LHC, the single-top production rate from $bg \rightarrow Wt$ process is about 7 times the W^* rate and should also be measured to probe the interaction of the top quark with the W -boson.

4.2 At the LC

The best place to probe the couplings κ_L^{NC} and κ_R^{NC} associated with the t - t - Z coupling is at the LC through $e^-e^+ \rightarrow \gamma, Z \rightarrow t\bar{t}$ process because at hadron colliders the $t\bar{t}$ production rate is dominated by QCD interactions ($q\bar{q}, gg \rightarrow t\bar{t}$). A detailed Monte Carlo study on the measurement of these couplings at the LC including detector effects and initial state radiation can be found in Ref. [60]. The bounds were obtained by studying the angular distribution and the polarization of the top quark produced

²⁰ This method is different from the one used in the recent CDF measurement of $|V_{tb}|$ by measuring $\text{Br}(t \rightarrow bW^+)$ and assuming 3 generations of quarks plus unitarity [58]. Our method does not require such assumption.

²¹ We note that the production rate of the W^* process is not directly proportional to the decay width of $t \rightarrow bW^+$, but the production rate of the W -gluon process is.

in e^-e^+ collisions. Assuming a 50 fb^{-1} luminosity at $\sqrt{s} = 500 \text{ GeV}$, we concluded that within a 90% confidence level, it should be possible to measure κ_L^{NC} to within about 8%, while κ_R^{NC} can be known to within about 18%. A 1 TeV machine can do better than a 500 GeV machine in determining κ_L^{NC} and κ_R^{NC} because the relative sizes of the $t_R(\bar{t})_R$ and $t_L(\bar{t})_L$ production rates become small and the polarization of the $t\bar{t}$ pair is purer. Namely, it is more likely to produce either a $t_L(\bar{t})_R$ or a $t_R(\bar{t})_L$ pair. A purer polarization of the $t\bar{t}$ pair makes κ_L^{NC} and κ_R^{NC} better determined. (The degree of top quark polarization can be further improved by polarizing the electron beam [61].) Furthermore, the top quark is boosted more in a 1 TeV machine, thereby allowing a better determination of its polar angle in the $t\bar{t}$ system (because it is easy to find the right b associated with the lepton to reconstruct the top quark moving direction).

Finally, we remark that at the LC κ_L^{CC} and κ_R^{CC} can be studied either from the decay of the top quark pair or from the single-top quark production process, W -photon fusion process $e^-e^+(W\gamma) \rightarrow tX$, or $e^-\gamma(W\gamma) \rightarrow \bar{t}X$, which is similar to the W -gluon fusion process in hadron collisions.

5 Dimension five anomalous couplings

So far we have discussed how to probe new physics effects that are expected to give some information about the symmetry breaking mechanism, as they can give rise to anomalous terms in the dimension 4 standard gauge couplings of the top quark with the electroweak bosons. Of course, this is not the only way in which these effects can become apparent in future experiments. A complete analysis should include possible anomalous effective interactions of higher dimension. In this section we will construct the complete set of independent operators of the first higher order operators with dimension 5, such that the complete effective Lagrangian relevant to this study will be:

$$\mathcal{L}_{eff} = \mathcal{L}^B + \mathcal{L}^{(4)} + \mathcal{L}^{(5)}, \quad (71)$$

where $\mathcal{L}^{(5)}$ denotes the dimension 5 operators [62].

Our next task is to find all the possible dimension five hermitian interactions that involve the top quark and the fields \mathcal{W}_μ^\pm , \mathcal{Z}_μ and \mathcal{A}_μ . Notice that the gauge transformations associated with these and the composite fermion fields (Eq. (28)) are dictated simply by the $U(1)_{em}$ group. We will follow a procedure similar to the one in Ref. [63], which consists of constructing all possible interactions that satisfy the required gauge invariance ($U(1)_{em}$ in this work), and that are not equivalent to each other. The criterion for equivalence is based on the equations of motion and on partial integration. As for the five dimensions in these operators, three will come from the fermion fields, and the other two will involve the gauge bosons. To make a

clear and systematic characterization, let us recognize the only three possibilities for these two dimensions:

- (1) Operators with two boson fields.
- (2) Operators with one boson field and one derivative.
- (3) Operators with two derivatives.

(1) **Two boson fields.** First of all, notice that the \mathcal{A}_μ field gauge transformation (Eq. (22)) will restrict the use of this field to covariant derivatives only. Therefore, except for the field strength term $\mathcal{A}_{\mu\nu}$ only the \mathcal{Z} and \mathcal{W} fields can appear multiplying the fermions in any type of operators. Also, the only possible Lorentz structures are given in terms of the $\sigma_{\mu\nu}$ and $g_{\mu\nu}$ tensors. We do not need to consider the tensor product of γ_μ 's since

$$\not{a} \not{b} = g_{\mu\nu} a_\mu b_\nu - i\sigma_{\mu\nu} a_\mu b_\nu . \quad (72)$$

Finally, we are left with only three possible combinations: (1.1) two \mathcal{Z}_μ 's, (1.2) two \mathcal{W}_μ 's, and (1.3) one of each.

(1.1) Since $\sigma_{\mu\nu}$ is antisymmetric, only the $g_{\mu\nu}$ part is non-zero:²²

$$O_{g\mathcal{Z}\mathcal{Z}} = \bar{t}_L t_R \mathcal{Z}_\mu \mathcal{Z}^\mu + h.c. \quad (73)$$

(1.2) Here, the antisymmetric part is non-zero too:

$$O_{g\mathcal{W}\mathcal{W}} = \bar{t}_L t_R \mathcal{W}_\mu^+ \mathcal{W}^{-\mu} + h.c. \quad (74)$$

$$O_{\sigma\mathcal{W}\mathcal{W}} = \bar{t}_L \sigma^{\mu\nu} t_R \mathcal{W}_\mu^+ \mathcal{W}_\nu^- + h.c. \quad (75)$$

(1.3) In this case we have two different quark fields, therefore we can distinguish two different combinations of chiralities:

$$O_{g\mathcal{W}\mathcal{Z}L(R)} = \bar{t}_{L(R)} b_{R(L)} \mathcal{W}_\mu^+ \mathcal{Z}^\mu + h.c. \quad (76)$$

$$O_{\sigma\mathcal{W}\mathcal{Z}L(R)} = \bar{t}_{L(R)} \sigma^{\mu\nu} b_{R(L)} \mathcal{W}_\mu^+ \mathcal{Z}_\nu + h.c. \quad (77)$$

(2) **One boson field and one derivative.** The obvious distinction arises: (2.1) the derivative acting on a fermion field, and (2.2) the derivative acting on the boson.

(2.1) The covariant derivative for the fermions is given by ²³ (see Eqs. (22) and (28))

$$\begin{aligned} D_\mu f &= (\partial_\mu + iQ_f s_w^2 \mathcal{A}_\mu) f , \\ \overline{D}_\mu f &= \bar{f} (\overleftarrow{\partial}_\mu - iQ_f s_w^2 \mathcal{A}_\mu). \end{aligned} \quad (78)$$

²² In the next section we will write explicitly the hermitian conjugate (*h.c.*) parts.

²³ To simplify notation we will use the same symbol D_μ for all covariant derivatives. Identifying which derivative we are referring to should be straightforward, e.g. D_μ in Eq. (78) is different from D_μ in Eq. (6).

Notice that the covariant derivative depends on the fermion charge Q_f , hence the covariant derivative for the top quark is not the same as for the bottom quark; partial integration could not relate two operators involving derivatives on different quarks. Furthermore, by looking at the equations of motion we can immediately see that operators of the form, for example, $\bar{f}\not{Z}\not{D}f$ or $\bar{f}^{(up)}\not{W}^+\not{D}f^{(down)}$, are equivalent to operators with two bosons, which have all been considered already. Following the latter statement and bearing in mind the identity of Eq. (72) we can see that only one Lorentz structure needs to be considered here, either one with $\sigma_{\mu\nu}$ or one with $g_{\mu\nu}$. Let us choose the latter.

$$O_{\mathcal{W}DbL(R)} = \mathcal{W}^{+\mu}\bar{t}_{L(R)}D_\mu b_{R(L)} + h.c. \quad (79)$$

$$O_{\mathcal{W}DtR(L)} = \mathcal{W}^{-\mu}\bar{b}_{L(R)}D_\mu t_{R(L)} + h.c. \quad (80)$$

$$O_{\mathcal{Z}Df} = \mathcal{Z}^\mu\bar{t}_L D_\mu t_R + h.c. \quad (81)$$

Of course, the \mathcal{A} field did not appear. Remember that its gauge transformation prevents us from using it on anything that is not a covariant derivative or a field strength $\mathcal{A}_{\mu\nu}$.

(2.2) Since \mathcal{W} transforms as a field with electric charge one, the covariant derivative is simply given by (see Eq. (10)):

$$\begin{aligned} D_\mu \mathcal{W}_\nu^+ &= (\partial_\mu + i s_w^2 \mathcal{A}_\mu) \mathcal{W}_\nu^+ \\ D_\mu^\dagger \mathcal{W}_\nu^- &= (\partial_\mu - i s_w^2 \mathcal{A}_\mu) \mathcal{W}_\nu^- \end{aligned} \quad (82)$$

Obviously, since the neutral \mathcal{Z} field is invariant under the G group transformations (see Eq. (21)), we could always add it to our covariant derivative:

$$D_\mu^{(\mathcal{Z})} \mathcal{W}_\nu^+ = (\partial_\mu + i s_w^2 \mathcal{A}_\mu + i a \mathcal{Z}_\mu) \mathcal{W}_\nu^+$$

where a stands for any complex constant. Actually, considering this second derivative would insure the generality of our analysis, since for example by setting $a = c_w^2$ and comparing with Eqs. (14) and (15) we would automatically include the field strength term ²⁴

$$\mathcal{W}_{\mu\nu}^\pm = \partial_\mu \mathcal{W}_\nu^\pm - \partial_\nu \mathcal{W}_\mu^\pm \pm i(\mathcal{W}_\mu^\pm \mathcal{W}_\nu^3 - \mathcal{W}_\nu^3 \mathcal{W}_\mu^\pm) = D_\mu^{(\mathcal{Z})} \mathcal{W}_\nu^\pm - D_\nu^{(\mathcal{Z})} \mathcal{W}_\mu^\pm. \quad (83)$$

However, this extra term in the covariant derivative would only be redundant. We can always decompose any given operator written in terms of $D_\mu^{(\mathcal{Z})}$ into the sum of the same operator in terms of the original D_μ plus another operator of the form $O_{g\mathcal{W}ZL(R)}$ or $O_{\sigma\mathcal{W}ZL(R)}$ [cf. Eqs. (76) and (77)]. Therefore, we only need to consider the covariant derivative (82) for the charged boson and still maintain the generality

²⁴From Eqs. (11) and (24), we write $\mathcal{W}_{\mu\nu}^\pm = \frac{1}{\sqrt{2}}(\mathcal{W}_{\mu\nu}^1 \mp i\mathcal{W}_{\mu\nu}^2)$.

of our characterization. For the neutral \mathcal{Z} boson we have the simplest situation, the covariant derivative is just the ordinary one,

$$D_\mu \mathcal{Z}_\nu = \partial_\mu \mathcal{Z}_\nu. \quad (84)$$

The case for the \mathcal{A} boson is nevertheless different. Being the field that makes possible the $U(1)_{\text{em}}$ covariance in the first place, it can not be given any covariant derivative itself. For \mathcal{A} , we have the field strength:

$$\mathcal{A}_{\mu\nu} = \partial_\mu \mathcal{A}_\nu - \partial_\nu \mathcal{A}_\mu,$$

Finally, we can now write the operators with the covariant derivative-on-boson terms. Unfortunately, no equations of motion can help us reduce the number of independent operators in this case, and we have to bring up both the $\sigma_{\mu\nu}$ and the $g_{\mu\nu}$ Lorentz structures.

$$O_{\sigma D\mathcal{Z}} = \bar{t}_L \sigma^{\mu\nu} t_R \partial_\mu \mathcal{Z}_\nu + h.c. \quad (85)$$

$$O_{g D\mathcal{Z}} = \bar{t}_L t_R \partial_\mu \mathcal{Z}^\mu + h.c. \quad (86)$$

$$O_{\sigma DWL(R)} = \bar{t}_{L(R)} \sigma^{\mu\nu} b_{R(L)} D_\mu \mathcal{W}_\nu^+ + h.c. \quad (87)$$

$$O_{g DWL(R)} = \bar{t}_{L(R)} b_{R(L)} D_\mu \mathcal{W}^{+\mu} + h.c. \quad (88)$$

$$O_{\mathcal{A}} = \bar{t}_L \sigma^{\mu\nu} t_R \mathcal{A}_{\mu\nu} + h.c. \quad (89)$$

(3) Operators with two derivatives.

As it turns out, all operators of this kind are equivalent to the ones already given in the previous cases. Here, we shall present the argument of why this is so. First of all, we only have two possibilities, (3.1) one derivative acting on each fermion field, and (3.2) both derivatives acting on the same fermion field.

(3.1) Just like in the case (2.1) above, we first notice that an operator of the form $\bar{f} \overleftarrow{D} \not{D} f$ can be decomposed into operators of the previous cases (1.1), (1.2) and (1.3) by means of the equations of motion. Therefore, we only have to consider one of two options, either $\overline{D_\mu f} \sigma^{\mu\nu} D_\nu f$, or $\overline{D_\mu f} g^{\mu\nu} D_\nu f$. Let us choose the latter. By means of partial integration we can see that the term $(\partial_\mu \bar{f}) \partial^\mu f$ yields the same action as the term $-\bar{f} \partial^\mu \partial_\mu f$, and we only need to consider the case in which the covariant derivatives act on the same f , which is just the type of operator to be considered next.

(3.2) By using the equations of motion twice we can relate the operator $\bar{f} \not{D} \not{D} f$ to operators of the type (1.1), (1.2) or (1.3). Either $\bar{f} \sigma^{\mu\nu} D_\mu D_\nu f$, or $\bar{f} D^\mu D_\mu f$ needs to be considered. This time we choose the former, which can be proved to be nothing but the operator $O_{\mathcal{A}}$ itself (Eq. (96)).

5.1 Hermiticity and CP invariance

The list of operators above is complete in the sense that it includes all non-equivalent dimension five interactions that satisfy gauge invariance. It is convenient now to analyze their CP properties. In order to make our study more systematic and clear we will re-write this list again, but this time we will display the added hermitian conjugate part in detail. By doing this the CP transformation characteristics will be most clearly presented too.

Let us divide the list of operators in two: those with only the top quark, and those involving both top and bottom quarks.

5.1.1 Interactions with top quarks only

Let's begin by considering the operator O_{gZZ} . We will include an arbitrary constant coefficient, denoted as a , which in principle could be complex:

$$\begin{aligned} O_{gZZ} &= a \bar{t}_L t_R \mathcal{Z}_\mu \mathcal{Z}^\mu + a^* \bar{t}_R t_L \mathcal{Z}_\mu \mathcal{Z}^\mu \\ &= \text{Re}(a) \bar{t} t \mathcal{Z}_\mu \mathcal{Z}^\mu + \text{Im}(a) i \bar{t} \gamma_5 t \mathcal{Z}_\mu \mathcal{Z}^\mu \end{aligned}$$

Our hermitian operator has naturally split into two independent parts: one that preserves parity (scalar), and one that does not (pseudoscalar). Also, the first part is CP even whereas the second one is odd. The natural separation of these two parts happens to be a common feature of all operators with only one type of fermion field. Nevertheless, not always will the parity conserving part also be the CP even one, as we shall soon see.

Below, the complete list of all 7 operators with only the top quark is given. In all cases the two independent terms are included; the first one is CP even, and the second one is CP odd.

$$O_{gZZ} = \frac{1}{\Lambda} \text{Re}(a_{zz1}) \bar{t} t \mathcal{Z}_\mu \mathcal{Z}^\mu + \frac{1}{\Lambda} \text{Im}(a_{zz1}) i \bar{t} \gamma_5 t \mathcal{Z}_\mu \mathcal{Z}^\mu \quad (90)$$

$$O_{gWW} = \frac{1}{\Lambda} \text{Re}(a_{ww1}) \bar{t} t \mathcal{W}_\mu^+ \mathcal{W}^{-\mu} + \frac{1}{\Lambda} \text{Im}(a_{ww1}) i \bar{t} \gamma_5 t \mathcal{W}_\mu^+ \mathcal{W}^{-\mu} \quad (91)$$

$$O_{\sigma WW} = \frac{1}{\Lambda} \text{Im}(a_{ww2}) i \bar{t} \sigma^{\mu\nu} t \mathcal{W}_\mu^+ \mathcal{W}_\nu^- + \frac{1}{\Lambda} \text{Re}(a_{ww2}) \bar{t} \sigma^{\mu\nu} \gamma_5 t \mathcal{W}_\mu^+ \mathcal{W}_\nu^- \quad (92)$$

$$O_{ZDf} = \frac{1}{\Lambda} \text{Im}(a_{z3}) i \bar{t} D_\mu t \mathcal{Z}^\mu + \frac{1}{\Lambda} \text{Re}(a_{z3}) \bar{t} D_\mu \gamma_5 t \mathcal{Z}^\mu \quad (93)$$

$$O_{gDZ} = \frac{1}{\Lambda} \text{Im}(a_{z4}) i \bar{t} \gamma_5 t \partial_\mu \mathcal{Z}^\mu + \frac{1}{\Lambda} \text{Re}(a_{z4}) \bar{t} t \partial_\mu \mathcal{Z}^\mu \quad (94)$$

$$O_{\sigma DZ} = \frac{1}{\Lambda} \text{Re}(a_{z2}) \bar{t} \sigma^{\mu\nu} t \partial_\mu \mathcal{Z}_\nu + \frac{1}{\Lambda} \text{Im}(a_{z2}) i \bar{t} \sigma^{\mu\nu} \gamma_5 t \partial_\mu \mathcal{Z}_\nu \quad (95)$$

$$O_{\mathcal{A}} = \frac{1}{\Lambda} \text{Re}(a_{\mathcal{A}}) \bar{t} \sigma^{\mu\nu} t \mathcal{A}_{\mu\nu} + \frac{1}{\Lambda} \text{Im}(a_{\mathcal{A}}) i \bar{t} \sigma^{\mu\nu} \gamma_5 t \mathcal{A}_{\mu\nu} . \quad (96)$$

Notice that in the operator O_{gDZ} the parity violating part happens to be CP even. This is because under a CP transformation a scalar term $\bar{t}t$ remains intact, i.e. it does not change sign, whereas a pseudoscalar term $\bar{t}\gamma_5 t$ changes sign. The gauge bosons change sign too, and this is what makes the scalar part of the operator to change sign under CP. Compare with the operator O_{gZZ} , there we have two bosons; two changes of sign that counteract each other. Therefore, it is the scalar part that is CP even in O_{gZZ} . Furthermore, based on the naive dimensional analysis (NDA) the coefficients of these operators are of order $1/\Lambda$ [15]. Therefore, the normalized coefficients (the a 's) are expected to be of order 1.

5.1.2 Interactions with both top and bottom quarks

Below, we show the next list of 12 operators with both top and bottom quarks. Again, we include an arbitrary complex coefficient²⁵:

$$O_{gWZL(R)} = \frac{1}{\Lambda} a_{wz1L(R)} \bar{t}_{L(R)} b_{R(L)} \mathcal{W}_\mu^+ \mathcal{Z}^\mu + \frac{1}{\Lambda} a_{wz1L(R)}^* \bar{b}_{R(L)} t_{L(R)} \mathcal{W}_\mu^- \mathcal{Z}^\mu \quad (97)$$

$$O_{\sigma WZL(R)} = \frac{1}{\Lambda} a_{wz2L(R)} \bar{t}_{L(R)} \sigma^{\mu\nu} b_{R(L)} \mathcal{W}_\mu^+ \mathcal{Z}_\nu + \frac{1}{\Lambda} a_{wz2L(R)}^* \bar{b}_{R(L)} \sigma^{\mu\nu} t_{L(R)} \mathcal{W}_\mu^- \mathcal{Z}_\nu \quad (98)$$

$$O_{WD bL(R)} = \frac{1}{\Lambda} a_{bw3L(R)} \mathcal{W}^{+\mu} \bar{t}_{L(R)} D_\mu b_{R(L)} + \frac{1}{\Lambda} a_{bw3L(R)}^* \mathcal{W}^{-\mu} \overline{D_\mu b}_{R(L)} t_{L(R)} \quad (99)$$

$$O_{WD tR(L)} = \frac{1}{\Lambda} a_{w3R(L)} \mathcal{W}^{-\mu} \bar{b}_{L(R)} D_\mu t_{R(L)} + \frac{1}{\Lambda} a_{w3R(L)}^* \mathcal{W}^{+\mu} \overline{D_\mu t}_{R(L)} b_{L(R)} \quad (100)$$

$$O_{\sigma DWL(R)} = \frac{1}{\Lambda} a_{w2L(R)} \bar{t}_{L(R)} \sigma^{\mu\nu} b_{R(L)} D_\mu \mathcal{W}_\nu^+ + \frac{1}{\Lambda} a_{w2L(R)}^* \bar{b}_{R(L)} \sigma^{\mu\nu} t_{L(R)} D_\mu^\dagger \mathcal{W}_\nu^- \quad (101)$$

$$O_{gDWL(R)} = \frac{1}{\Lambda} a_{w4L(R)} \bar{t}_{L(R)} b_{R(L)} D_\mu \mathcal{W}^{+\mu} + \frac{1}{\Lambda} a_{w4L(R)}^* \bar{b}_{R(L)} t_{L(R)} D_\mu^\dagger \mathcal{W}^{-\mu} \quad (102)$$

In this case, if a is real ($a = a^*$) then $O_{gWZL(R)}$ and $O_{\sigma DWL(R)}$ are both CP even, but $O_{\sigma WZL(R)}$, $O_{WD bL(R)}$, $O_{WD tR(L)}$ and $O_{gDWL(R)}$ are odd. Just the other way around if a is purely imaginary.

The dimension five lagrangian $\mathcal{L}^{(5)}$ is simply the sum of all these 19 operators (Eqs. (90) to (102)):

$$\mathcal{L}^{(5)} = \sum_{i=1,19} O_i. \quad (103)$$

To study the possible effects on the production rates of top quarks in high energy collisions, only the CP conserving parts which give imaginary vertices (like the SM) are relevant. The amplitude squared will depend linearly on the CP even terms, but only quadratically on the CP odd terms, because the *no-Higgs* SM ($\mathcal{L}^{(4)}$) interac-

²⁵ $\overline{D_\mu f}_{R(L)}$ stands for $(D_\mu f_{R(L)})^\dagger \gamma_0$; $\bar{f}_{R(L)}$ stands for $(f_{R(L)})^\dagger \gamma_0$.

tions²⁶ are CP even when ignoring the CP-violating phase in the Cabibbo-Kobayashi-Maskawa (CKM) mixing elements.

However, this does not mean that it is not possible to probe the CP violating phase in the operators. Later on in the next section we will show one observable that depends linearly on the CP odd coefficients. From now on, the appropriate CP even part (either real or imaginary) is assumed for each coefficient. To simplify notation we will use the same label; a_{zz1} will stand for $Re(a_{zz1})$, $a_{wz2L(R)}$ will stand for $Im(a_{wz2L(R)})$, and so on, the only exception will be a_A , whose real part is recognized as proportional to the magnetic moment of the top quark, and will be denoted by a_m . It is thus understood that all coefficients below are real numbers.

In conclusion, the dimension 5 Lagrangian consists of 19 independent operators which are listed from Eq. (90) to Eq. (102). Since the top quark is heavy (its mass is of the order of the weak scale), it is likely to interact strongly with the Goldstone bosons which are equivalent to the longitudinal weak gauge bosons in the high energy regime. (This is known as the Goldstone Equivalence Theorem [19].) Hence, we shall study in the rest of this paper how to probe these anomalous couplings from the production of top quarks via the $V_L V_L$ fusion process, where V_L stands for the longitudinally polarized W^\pm or Z bosons.

6 Probing the dimension 5 anomalous couplings at the colliders

Our next task is to study these operators through their potential contribution to high energy scattering processes like longitudinal vector boson ($V_L V_L$) fusions (see Figure 13), and study how they can affect the production rates of top quarks in both the LHC and the LC. For simplicity, in this study we shall take all the non-standard dimension four couplings to be zero. The general result including these terms are given in Appendix B.

Before giving our analytical results (summarized in Appendices B and C), we shall estimate the expected sizes of these tree level amplitudes according to their high energy behavior. A general power counting rule has been given that estimates the high energy behavior of any amplitude T [20] as:

$$T = c_T v^{D_T} \left(\frac{v}{\Lambda}\right)^{N_O} \left(\frac{E}{v}\right)^{D_{E0}} \left(\frac{E}{4\pi v}\right)^{D_{EL}} \left(\frac{M_W}{E}\right)^{e_v} H(\ln(E/\mu)) \quad (104)$$

$$D_{E0} = 2 + \sum_n \mathcal{V}_n (d_n + \frac{1}{2} f_n - 2), \quad D_{EL} = 2L,$$

²⁶Since in the unitary gauge $\mathcal{L}^{(4)}$ reproduces the SM without the physical Higgs boson, we will refer to it as the *no-Higgs* SM.

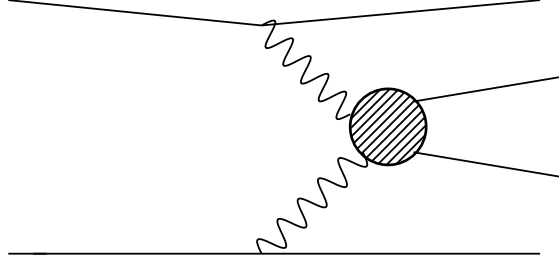


Figure 13: Production of $t\bar{t}$ ($t\bar{b}$ or $b\bar{t}$) from $W_L^+W_L^-$ or Z_LZ_L ($W_L^+Z_L$ or $W_L^-Z_L$) fusion processes.

where $D_T = 4 - e = 0$ (e is the number of external lines, 4 in our case), $N_{\mathcal{O}} = 0$ for all dimension 4 operators and $N_{\mathcal{O}} = 1$ for all dimension 5 operators based upon the naive dimensional analysis (NDA) [15],²⁷ $L = 0$ is the number of loops in the diagrams, $H(\ln(E/\mu)) = 1$ comes from the loop terms (none in our case), e_v accounts for any external v_μ -lines (none in our case of $V_L V_L \rightarrow t\bar{t}$, $t\bar{b}$),²⁸ \mathcal{V}_n is the number of vertices of type n that contain d_n derivatives and f_n fermionic lines. The dimensionless coefficient c_T contains possible powers of gauge couplings (g, g') and Yukawa couplings (y_f) from the vertices of the amplitude T , which can be directly counted.

One important remark about the above formula is that it cannot be directly applied to diagrams with external longitudinal V_L lines. As explained in Ref. [20], a significant part of the high energy behavior from diagrams with external V_L lines is cancelled when one adds all the relevant Feynman diagrams of the process; this is just a consequence of the gauge symmetry of the Lagrangian. To correctly apply Eq. (104), one has to make use of the Equivalence Theorem, and write down the relevant diagrams with the corresponding would-be Goldstone bosons. Then, the true high energy behavior will be given by the leading diagram. (If there is more than one leading diagram, there could be additional cancellations).

Let us analyze the high energy behavior of the $Z_L Z_L \rightarrow t\bar{t}$ process in the context of the dimension 4 couplings $\mathcal{L}^{(4)}$, as defined in Eq. 32. In Fig. 14 we show the corresponding Goldstone boson diagrams, i.e. $\phi^0 \phi^0 \rightarrow t\bar{t}$. The ϕ^0 - t - t vertex contains a derivative that comes from the expansion of the composite fields [cf. Eq. (19)], and the associated $(d_n + \frac{1}{2}f_n - 2)$ factor is $d_n + \frac{1}{2}f_n - 2 = 1 + \frac{1}{2}2 - 2 = 0$. This means $D_{E0} = 2$ for diagrams 14(a) and 14(b); both grow as E^2 at high energies. The four point vertex for diagram 14(c) can come from the mass term of the top quark or the

²⁷ NDA counts Σ as Λ^0 , D_μ as $\frac{1}{\Lambda}$, and fermion fields as $\frac{1}{v\sqrt{\Lambda}}$. Hence, \mathcal{W}^\pm , \mathcal{Z} and \mathcal{A} are also counted as $\frac{1}{\Lambda}$. After this counting, one should multiply the result by $v^2\Lambda^2$. Notice that up to the order of intent, the kinetic term of the gauge boson fields and the mass term of the fermion fields are two exceptions to the NDA, and are of order Λ^0 .

²⁸ v_μ is equal to $\epsilon_\mu^{(0)} - \frac{k_\mu}{M_V}$, where k_μ is the momentum of the gauge boson with mass M_V and $\epsilon_\mu^{(0)}$ is its longitudinal polarization vector.

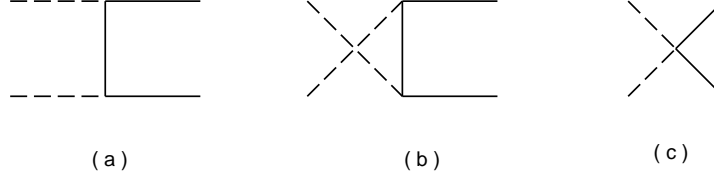


Figure 14: The corresponding Goldstone boson diagrams for $Z_L Z_L \rightarrow t\bar{t}$, i.e. $\phi^0 \phi^0 \rightarrow t\bar{t}$.

second order terms from the expansion of \mathcal{Z}_μ in the effective Lagrangian. The ϕ^0 - ϕ^0 - $t\bar{t}$ vertex that comes from the mass term $m_t \bar{t}t$ does not contain any derivatives, hence the high energy behavior from this term goes like E^1 . The vertex that comes from the second order expansion of a term like $\bar{t}\gamma^\mu t \mathcal{Z}_\mu$ contains one derivative, and the corresponding amplitude 14(c) grows as E^2 in the high energy region. The conclusion is that diagram 14(c) behaves like E^2 as well. Seeing that there is more than one leading diagram we can suspect that there may be additional cancellations. How can we then obtain the correct high energy behavior for the Goldstone boson scattering amplitudes?

To answer this question let us use an alternative non-linear parametrization that is equivalent to $\mathcal{L}_{SM}^{(4)}$ (Eq. (32) with the κ 's equal zero), in the sense that it produces the exact same matrix elements [14], but with the advantage that the couplings of the fermions with the Goldstone bosons do not contain derivatives. We can rewrite the sum of \mathcal{L}^B [cf. Eq. (23)] and $\mathcal{L}_{SM}^{(4)}$ as:

$$\begin{aligned}
\mathcal{L}_{SM} \equiv \mathcal{L}_{SM}^{(4)} + \mathcal{L}^B = & \quad \bar{\Psi}_L i\gamma^\mu D_\mu^L \Psi_L + \bar{\Psi}_R i\gamma^\mu D_\mu^R \Psi_R - \left(\bar{\Psi}_L \Sigma M \Psi_R + h.c. \right) \\
& - \frac{1}{4} W_{\mu\nu}^a W^{a\mu\nu} - \frac{1}{4} B_{\mu\nu} B^{\mu\nu} + \frac{v^2}{4} \text{Tr} \left(D_\mu \Sigma^\dagger D^\mu \Sigma \right) , \quad (105) \\
M = & \quad \begin{pmatrix} m_t & 0 \\ 0 & m_b \end{pmatrix} , \\
D_\mu^L = & \quad \partial_\mu - ig \frac{\tau^a}{2} W_\mu^a - ig' \frac{Y}{2} B_\mu , \\
D_\mu^R = & \quad \partial_\mu - ig' Q_f B_\mu .
\end{aligned}$$

Here, $Y = \frac{1}{3}$ is the hypercharge quantum number for the quark doublet, Q_f is the electric charge of the fermion, Ψ_L is the linearly realized left handed quark doublet, and Ψ_R is the right handed singlet for top or bottom quarks [cf. Eqs. (29) and (31)].

As we shall see shortly, in the context of this Lagrangian there is one (and only one) diagram with the leading high energy power. Hence, we do not expect any cancellations among diagrams and it is possible to correctly predict the high energy behavior of the scattering amplitude. Here is how it works: When we expand the Σ matrix field up to the second power [cf. Eq. (1)] in the fermion mass term of

Eq. (105), we will notice two things: (i) the first power term gives the vertex ϕ^3-t-t , and associates the coefficient $c_T = m_t/v$ to it; (ii) the second power term generates the four-point vertex [cf. Fig. 14(c)] with a coefficient $c_T = m_t/v^2$ associated to it. As it is well known, a $\bar{t}t = \bar{t}_R t_L + \bar{t}_L t_R$ term always involves a chirality flip, therefore we readily recognize that this four-point diagram will only participate when the chiralities of the top and anti-top are different. As $E \gg m_t$, different chiralities imply equal helicities for the fermion-antifermion pair. Hence, for the case of opposite helicities we only count the power dependance for diagrams 2(a) and 2(b), and take the highest one. For final state fermions of equal helicities we consider all three diagrams.

The results are the following: for diagrams 2(a) and 2(b) we have $D_{E0} = 2 + (-1) + (-1) = 0$, thus the amplitude $T_{\pm\mp}$ is of order m_t^2/v^2 (if there are no additional cancellations); which is the contribution given by the coefficients c_T from both vertices. On the other hand, diagram 2(c) has $D_{E0} = 2 - 1 = 1$; the equal helicities amplitude $T_{\pm\pm}$ will be driven by this dominant diagram, therefore $T_{\pm\pm} = m_t E/v^2$.

For the other processes; $W_L^+ W_L^- \rightarrow t\bar{t}$ and $W_L^+ Z_L \rightarrow t\bar{b}$, the analysis is the same, except that there is an extra s -channel diagram [cf. Figs. 16 and 17] whose high energy behavior is similar to the diagrams 14(a) and 14(b). Also, for the amplitude of $W_L^+ Z_L \rightarrow t\bar{b}$ no four-point diagram 14(c) is generated; this means that its high energy behavior can at most be of order m_t^2/v^2 as given by diagrams 14(a) and 14(b).

In conclusion, in order to estimate the high energy behavior of the $V_L V_L \rightarrow t\bar{t}, t\bar{b}$ process, one has to write down the relevant diagrams for $\phi\phi \rightarrow t\bar{t}, t\bar{b}$ and then apply the power counting formula given in Eq. (104). If more than one diagram have the same leading power in E then one can suspect possible additional cancellations. This is the case for the dimension 4 non-linear chiral Lagrangian $\mathcal{L}_{SM}^{(4)}$ (Eq. (32) with κ 's equal to zero), for which all three diagrams 14(a), (b) and (c) grow as E^2 at high energies. Another gauge invariant Lagrangian for $\mathcal{L}_{SM}^{(4)} + \mathcal{L}^B$ is given in Eq. (105) which gives the same matrix elements for any physical process, but does not have the problem of possible cancellations among the Goldstone boson diagrams. With this Lagrangian the power counting formula predicts a leading E^1 behavior for $\phi^0\phi^0 \rightarrow t\bar{t}$ or $\phi^+\phi^- \rightarrow t\bar{t}$ (which originates from the four-point couplings that contributing to the diagram 14(c)), but only E^0 power for $\phi^\pm\phi^0 \rightarrow t\bar{b}$ or $b\bar{t}$ (which does not have the diagram similar to 14(c)). This is verified in Appendix B.

Notice that, in general, if the dimension 4 anomalous couplings κ 's are not zero, then there is no reason to expect any cancellations among the Goldstone boson diagrams. As a matter of fact, the calculated leading contributions from these coefficients are of order E^2 and not E^1 [cf. Appendix B].²⁹

For the dimension 5 anomalous operators we do not suspect *a priori* any can-

²⁹This is related to the fact that non-zero anomalous κ terms break the linearly realized $SU(2)_L \times U(1)_Y$ gauge symmetry in the interaction part of Eq. (105). Notice that the κ terms respect this gauge symmetry only non-linearly.

cellations at high E among Goldstone boson diagrams, therefore we expect the parametrization used for our effective operators to reflect the correct high energy behavior. Actually, the chiral Lagrangian parametrization given by Eq. (71), which organizes the new physics effects in the momentum expansion, is the only framework that allows the existence of such dimension 5 gauge invariant operators. On the other hand, we know that as far as the *no-Higgs* SM contribution to these *anomalous* amplitudes is concerned, the correct high energy behavior is given by the equivalent parametrization of Eq. (105). We will therefore use the appropriate couplings from \mathcal{L}_{SM} and $\mathcal{L}^{(5)}$ in our next power counting analysis. Also, we are neglecting contributions of order $1/\Lambda^2$, which means that in diagrams 14(a) and 14(b) only one vertex is anomalous.

Given one dimension 5 operator, it either involves two boson fields (four-point operator), or one boson field and one derivative (three-point operator). Let us discuss four-point (4-pt) operators first.

There are three kinds of 4-pt operators: O_{ZZ} , O_{WW} and O_{WZ} . Each of them contributes to the $Z_L Z_L$, $W_L^+ W_L^-$ and $W_L^+ Z_L$ fusion processes separately. After expanding the composite boson fields \mathcal{Z} and \mathcal{W}^\pm [cf. Eqs. (19) and (20)], we find that the terms $\frac{4}{v^2} \partial_\mu \phi^3 \partial_\nu \phi^3$, $\frac{4}{v^2} \partial_\mu \phi^+ \partial_\nu \phi^-$ and $\frac{4}{v^2} \partial_\mu \phi^+ \partial_\nu \phi^3$ will contribute to a diagram of type 14(c) in each case. Therefore, in the power counting formula (104), $d_n = 2$, $c_T = 4a_O$ and $D_{E0} = 2 + (2 + 1 - 2) = 3$, which means that

$$T \sim 4a_O \frac{v}{\Lambda} \left(\frac{E}{v} \right)^3 \quad (106)$$

for all these 4-pt operators.

Let us discuss the case of 3-pt operators by considering one operator in particular: O_{ZDf} . This analysis will automatically apply to all the other six 3-pt; three with the neutral \mathcal{Z}_μ boson, O_{ZDf} , O_{gDZ} and $O_{\sigma DZ}$; and three with the charged \mathcal{W}_μ boson, O_{WDt} , O_{gDW} and $O_{\sigma DW}$. Using the expansions of the composite fields we obtain:

$$\begin{aligned} a_{z3} i \bar{t} \partial_\mu t \mathcal{Z}^\mu &= - \frac{g}{c_w} a_{z3} i \bar{\psi}_t \partial_\mu \psi_t Z^\mu + \frac{2i}{v} a_{z3} \left[\bar{\psi}_t \partial_\mu \psi_t \partial^\mu \phi^3 \right. \\ &\quad \left. - \bar{\psi}_t \gamma_5 \partial_\mu \psi_t \phi^3 \partial^\mu \phi^3 - \bar{\psi}_{tR} \partial_\mu \psi_{bL} \phi^+ \partial^\mu \phi^3 + \bar{\psi}_t \partial_\mu \psi_t (\phi^- \partial^\mu \phi^+ - \phi^+ \partial^\mu \phi^-) \right] + \dots \end{aligned} \quad (107)$$

Where ψ_t (ψ_b) denotes the usual linearly realized top (bottom) quark field. There are more terms in Eq. (107) that participate in the Goldstone boson diagrams of interest, but the ones shown are sufficient for our discussion. Notice that the first two terms on the right hand side of Eq. (107) contribute to 3-pt vertices, the first one is for the coupling of the top quark with the usual vector boson field (the only non-zero term in the unitary gauge); the second one represents the vertex of O_{ZDf} that enters in diagrams 14(a) and 14(b) for $\phi^3 \phi^3 \rightarrow t \bar{t}$, or in a *u-channel* diagram like 14(b) for $\phi^+ \phi^3 \rightarrow t \bar{b}$. The rest of the expansion contains vertices with two or more boson fields. In Eq. (107), we also show some of the 4-pt vertices generated by

O_{ZDf} , which dominate the contribution of this operator to the $V_L V_L$ fusion processes in the high energy regime. The last term, $\bar{\psi}_t \partial_\mu \psi_t (\phi^- \partial^\mu \phi^+ - \phi^+ \partial^\mu \phi^-)$, comes from the second order term in the expansion of \mathcal{Z}_μ [cf. Eq. (19)], and is responsible for the high energy behavior of the *s-channel* diagram for $W_L^+ W_L^- \rightarrow t\bar{t}$ [cf. Fig. 16]. We can infer that the other two 3-pt operators with the \mathcal{Z}_μ field can also contribute to all the $V_L V_L$ fusion processes. However, because of the relation $\epsilon_\mu p^\mu = 0$ for the on-shell external boson lines, the contributions of O_{gDZ} and $O_{\sigma DZ}$ vanish for $Z_L Z_L \rightarrow t\bar{t}$ and $W_L Z_L \rightarrow t\bar{b}$.

Notice that the expansion for \mathcal{W}_μ^\pm in Eq. (20) does not contain any term with ϕ^3 alone; hence, no operator with the field \mathcal{W}_μ^\pm can participate in the process $Z_L Z_L \rightarrow t\bar{t}$ at tree level. Except for this, the analysis on O_{ZDf} applies equally to the operators with \mathcal{W}_μ^\pm . However, the contributions of O_{gDW} and $O_{\sigma DW}$ on the process $W_L^+ W_L^- \rightarrow t\bar{t}$ vanish because of the relation $\epsilon_\mu p^\mu = 0$ for the on-shell external boson lines.

The analysis on the high energy behavior of the contributions from O_{ZDf} to the scattering process $Z_L Z_L \rightarrow t\bar{t}$ is similar to the previous one for the *no-Higgs* SM, in which we observed a distinction between the $T_{\pm\mp}$ and $T_{\pm\pm}$ amplitudes. The anomalous vertices generated by this operator contain two derivatives, thus $(d_n + \frac{1}{2}f_n - 2) = 1$. Then, $D_{E0} = 2 + 1 + (-1) = 2$ for the first two diagrams 14(a) and 14(b), and $T_{\pm\mp}$ is of expected to be of order

$$T_{\pm\mp} \sim 2a_O \frac{m_t}{v} \frac{v}{\Lambda} \left(\frac{E}{v}\right)^2.$$

On the other hand, diagram 14(c) comes from the first 4-pt term in Eq. (107). Thus, we have $(d_n + \frac{1}{2}f_n - 2) = 1$, $D_{E0} = 2 + 1 = 3$, and the predicted value for $T_{\pm\pm}$ is

$$T_{\pm\pm} \sim 2a_O \frac{v}{\Lambda} \left(\frac{E}{v}\right)^3.$$

Comparing with the estimate for 4-pt operators [cf. Eq. (106)] we can observe that the only difference is in the coefficient c_T associated to them; for the three-point operator (107) $c_T = 2a_O$, and for a four-point operator is twice as much.³⁰

Other possible contributions that vanish have to do with the fact that sometimes an amplitude can be zero from the product of two different helicities of spinors. For instance, by performing the calculation of the amplitudes in the CM frame we can easily verify that the spinor product $\bar{u}[\lambda = \pm 1]v[\lambda = \mp 1]$ vanishes for all $t\bar{t}$, $t\bar{b}$ and $b\bar{t}$ processes.³¹ This means that contributions from operators of the *scalar*-type, like $O_{gWZL(R)}$, O_{gZZ} , O_{gWW} , O_{ZDf} , and $O_{WDtR(L)}$ will vanish for $T_{\pm\mp}$ amplitudes in the *s-channel* and the four-point diagrams.

Furthermore, the relation $\epsilon_\mu p^\mu = 0$ applies to all the external on-shell boson lines; this makes the contribution of operators with derivative on boson, such as O_{gDZ} (our

³⁰ This difference in c_T may be related to the fact that four-point operators tend to give a bigger contribution to the helicity amplitudes [cf. Eqs. (117) and (118), for example].

³¹ $u[\lambda = +1]$ denotes the spinor of a quark with right handed helicity.

third case) and $O_{gDWL(R)}$, to vanish in the t - and u -channel diagrams. In principle, one would think that the exception could be the s -channel diagram. Actually, this is the case for the operator $O_{gDWL(R)}$ which contributes significantly to the single top production process $W_L^+ Z_L \rightarrow t\bar{b}$ via the s -channel diagram [cf. Table 3]. However, for the O_{gDZ} operator even this diagram vanishes; as can be easily verified by noting that the Lorentz contraction between the boson propagator $-g_{\mu\nu} + k_\mu k_\nu / M_Z^2$ and the tri-boson coupling is identically zero in the process $W_L^+ W_L^- \rightarrow t\bar{t}$. Therefore, for the O_{gDZ} operator all the possible diagrams vanish.

In Tables 1, 2, and 3 we show the leading contributions (in powers of the CM energy E) of all the operators for each different process; those cells with a dash mean that no anomalous vertex generated by that operator intervenes in the given process, and those cells with a zero mean that the anomalous vertex intervenes in the process but the amplitude vanishes for any of the reasons explained above.

Process	$\mathcal{L}_{SM}^{(4)}$	O_{gZZ} $a_{zz1} \times$	O_{gWW} $a_{ww1} \times$	$O_{\sigma WW}$ $a_{ww2} \times$	$O_{gWZL(R)}$ $a_{wz1L(R)} \times$	$O_{\sigma WZL(R)}$ $a_{wz2L(R)} \times$
$Z_L Z_L \rightarrow t\bar{t}$	$m_t E / v^2$	$E^3 / v^2 \Lambda$	—	—	—	—
$W_L^+ W_L^- \rightarrow t\bar{t}$	$m_t E / v^2$	—	$E^3 / v^2 \Lambda$	$E^3 / v^2 \Lambda$	—	—
$W_L^+ Z_L \rightarrow t\bar{b}$	m_t^2 / v^2	—	—	—	$E^3 / v^2 \Lambda$	$E^3 / v^2 \Lambda$

Table 1: The leading high energy terms for the 4-point operators.

Process	$\mathcal{L}_{SM}^{(4)}$	O_{ZDf} $a_{z3} \times$	O_{WDtR} $a_{w3R} \times$	O_{WDtL} $a_{w3L} \times$
$Z_L Z_L \rightarrow t\bar{t}$	$m_t E / v^2$	$E^3 / v^2 \Lambda$	—	—
$W_L^+ W_L^- \rightarrow t\bar{t}$	$m_t E / v^2$	$E^3 / v^2 \Lambda$	$E^3 / v^2 \Lambda$	$m_b E^2 / v^2 \Lambda \rightarrow 0$
$W_L^+ Z_L \rightarrow t\bar{b}$	m_t^2 / v^2	$E^3 / v^2 \Lambda$	$E^3 / v^2 \Lambda$	$E^3 / v^2 \Lambda$

Table 2: The leading high energy terms for the operators with derivative-on-fermion.

In conclusion, based on the NDA [15] and the power counting rule [20], we have found that the leading high energy behavior in the $V_L V_L \rightarrow t\bar{t}$ or $t\bar{b}$ scattering amplitudes from the *no-Higgs* SM operators ($\mathcal{L}_{SM}^{(4)}$) can only grow as $\frac{m_t E}{v^2}$ (for T_{++} or T_{--} ; E is the CM energy of the top quark system), whereas the contribution from the dimension 5 operators ($\mathcal{L}^{(5)}$) can grow as $\frac{E^3}{v^2 \Lambda}$ in the high energy regime. Let us compare the above results with those of the $V_L V_L \rightarrow V_L V_L$ scattering processes. For these $V_L V_L \rightarrow V_L V_L$ amplitudes the leading behavior at the lowest order gives $\frac{E^2}{v^2}$, and the

Process	$\mathcal{L}_{SM}^{(4)}$	O_{gDZ} $a_{z4} \times$	$O_{gDWL(R)}$ $a_{w4} \times$	$O_{\sigma DZ}$ $a_{z2} \times$	$O_{\sigma DWL(R)}$ $a_{w2} \times$	O_A $a_m \times$
$Z_L Z_L \rightarrow t\bar{t}$	$m_t E/v^2$	0	—	0	—	—
$W_L^+ W_L^- \rightarrow t\bar{t}$	$m_t E/v^2$	0	0	$E^3/v^2 \Lambda$	0	$E^3/v^2 \Lambda$
$W_L^+ Z_L \rightarrow t\bar{b}$	m_t^2/v^2	0	$E^3/v^2 \Lambda$	0	$E^3/v^2 \Lambda$	—

Table 3: The leading high energy terms for the operators with derivative-on-boson.

contribution from the next-to-leading order (NLO) bosonic operators gives $\frac{E^2}{\Lambda^2} \frac{E^2}{v^2}$ [20]. This indicates that the NLO contribution is down by a factor of $\frac{E^2}{\Lambda^2}$ in $V_L V_L \rightarrow V_L V_L$. On the other hand, the NLO fermionic contribution in $V_L V_L \rightarrow t\bar{t}$ or $t\bar{b}$ is only down by a factor $\frac{E^2}{m_t \Lambda}$ which compared to $\frac{E^2}{\Lambda^2}$ turns out to be bigger by a factor of $\frac{\Lambda}{m_t} \sim 4\sqrt{2}\pi$ for $\Lambda \sim 4\pi v$.³² Hence, we expect that the NLO contributions in the $V_L V_L \rightarrow t\bar{t}$ or $t\bar{b}$ processes can be better measured (by about a factor of 10) than the $V_L V_L \rightarrow V_L V_L$ counterparts for some class of electroweak symmetry breaking models in which the NDA gives reasonable estimates of the coefficients.

As will be shown later, the coefficients of the NLO fermionic operators in $\mathcal{L}^{(5)}$ can be determined via top quark production to an order of 10^{-2} or 10^{-1} . In contrast, the coefficients of the NLO bosonic operators are usually determined to about an order of 10^{-1} or 1 [19, 64] via $V_L V_L \rightarrow V_L V_L$ processes. Therefore, we conclude that the top quark production via longitudinal gauge boson fusion $V_L V_L \rightarrow t\bar{t}, t\bar{b}$, or $b\bar{t}$ at high energy may be a better probe, for some classes of symmetry breaking mechanisms, than the scattering of longitudinal gauge bosons, i.e. $V_L V_L \rightarrow V_L V_L$.

Our next step is to study the production rates of $t\bar{t}$ pairs and single- t or single- \bar{t} events at future colliders like LHC and LC. We will also estimate how accurate these NLO fermionic operators can be measured via the $V_L V_L \rightarrow t\bar{t}$ or $t\bar{b}$ processes.

6.1 Underlying custodial symmetry

To reduce the number of independent parameters in this study, we shall make the same assumption of an underlying custodial symmetric theory that gets broken in such a way that only the couplings that involve the top quark get modified; as was done for the case of $\mathcal{L}^{(4)}$ (see Eq. (64) and the discussion there). The analysis for the operators with derivatives is exactly the same.³³ The custodial symmetric dimension

³² For an energy E of about $\Lambda/4$ or more this factor $\frac{E^2}{m_t \Lambda} = \frac{M^{(5)}}{M^{(4)}}$ is actually greater than one. $M^{(4)}$ and $M^{(5)}$ are the LO and NLO amplitudes, respectively.

³³ For the purpose of this discussion we can replace D_μ by ∂_μ .

5 Lagrangian has the same $SU(2)$ structure³⁴ as $\mathcal{L}^{(custodial)}$ in Eq. (61):

$$\kappa \overline{F_L} g^{\mu\nu} \partial_\mu \mathcal{W}_\nu^a \tau^a F_R + h.c. = \kappa \overline{F_L} g^{\mu\nu} \begin{pmatrix} \partial_\mu \mathcal{W}_\nu^3 & \sqrt{2} \partial_\mu \mathcal{W}_\nu^+ \\ \sqrt{2} \partial_\mu \mathcal{W}_\nu^- & -\partial_\mu \mathcal{W}_\nu^3 \end{pmatrix} F_R + h.c. . \quad (108)$$

By adding the two possible breaking terms to this operator,³⁵ we obtain the effective dimension 5 Lagrangian as:

$$\begin{aligned} \mathcal{L}^{(5deriv)} &= \kappa \overline{F_L} g^{\mu\nu} \partial_\mu \mathcal{W}_\nu^a \tau^a F_R + \kappa_1 \overline{F_L} g^{\mu\nu} \tau^3 \partial_\mu \mathcal{W}_\nu^a \tau^a F_R + \kappa_2 \overline{F_L} g^{\mu\nu} \partial_\mu \mathcal{W}_\nu^a \tau^a \tau^3 F_R \\ &+ h.c. \\ &= \overline{F_L} g^{\mu\nu} \begin{pmatrix} (\kappa + \kappa_1 + \kappa_2) \partial_\mu \mathcal{W}_\nu^3 & \sqrt{2}(\kappa + \kappa_1 - \kappa_2) \partial_\mu \mathcal{W}_\nu^+ \\ \sqrt{2}(\kappa - \kappa_1 + \kappa_2) \partial_\mu \mathcal{W}_\nu^- & (-\kappa + \kappa_1 + \kappa_2) \partial_\mu \mathcal{W}_\nu^3 \end{pmatrix} F_R + h.c. , \end{aligned} \quad (109)$$

where, in order to obtain a vanishing b - b - Z coupling, we require

$$\kappa = \kappa_1 + \kappa_2 . \quad (110)$$

Also, to simplify the discussion we assume $\kappa_1 = \kappa_2$, and the conclusion is that in order to keep the couplings b - b - Z unaltered we have to impose the condition

$$a_{z(2,3,4)} = \sqrt{2} a_{w(2,3,4)L(R)} \quad (111)$$

to all the operators with derivatives.

The case for 4-point operators (contact terms) is somewhat different. The custodial Lagrangian in this case is of the form:

$$\begin{aligned} \mathcal{L}^{(5custod)} &= \kappa_{1g}^{4pt.} \overline{F_L} g^{\mu\nu} \mathcal{W}_\mu^a \tau^a \mathcal{W}_\nu^b \tau^b F_R + \kappa_{1\sigma}^{4pt.} \overline{F_L} \sigma^{\mu\nu} \mathcal{W}_\mu^a \tau^a \mathcal{W}_\nu^b \tau^b F_R \\ &= \kappa_{1g}^{4pt.} \overline{F_L} \begin{pmatrix} \mathcal{W}_\mu^3 \mathcal{W}^{\mu 3} + 2\mathcal{W}_\mu^+ \mathcal{W}^{\mu -} & 0 \\ 0 & \mathcal{W}_\mu^3 \mathcal{W}^{\mu 3} + 2\mathcal{W}_\mu^+ \mathcal{W}^{\mu -} \end{pmatrix} F_R \\ &\quad + \kappa_{1\sigma}^{4pt.} \overline{F_L} \sigma^{\mu\nu} \begin{pmatrix} 2\mathcal{W}_\mu^+ \mathcal{W}_\nu^- & 0 \\ 0 & 2\mathcal{W}_\mu^+ \mathcal{W}_\nu^- \end{pmatrix} F_R , \end{aligned} \quad (112)$$

and for the breaking terms we can consider:

$$\begin{aligned} \mathcal{L}^{(5contact)} &= \sum_{c=g,\sigma} c^{\mu\nu} \left(\kappa_{2c}^{4pt.} \overline{F_R} \tau^3 \mathcal{W}_\mu^a \tau^a \mathcal{W}_\nu^b \tau^b F_L + \kappa_{2c}^{4pt.\dagger} \overline{F_L} \mathcal{W}_\mu^a \tau^a \mathcal{W}_\nu^b \tau^b \tau^3 F_R \right. \\ &\quad \left. + \kappa_{3c}^{4pt.} \overline{F} \mathcal{W}_\mu^a \tau^a \tau^3 \mathcal{W}_\nu^b \tau^b F \right) , \end{aligned} \quad (113)$$

where $\kappa_{2c}^{4pt.}$ is complex and $\kappa_{3c}^{4pt.}$ is real. As it turns out, in order to set the anomalous couplings of the bottom quark equal to zero, we have to choose $\kappa_{3c}^{4pt.} = 0$, and $\kappa_{2c}^{4pt.}$

³⁴Notice that the composite left and right handed doublets $F_{L,R}$ transform in the same way under global $SU(2)_R \times SU(2)_L$, $F_{L,R} \rightarrow F'_{L,R} = R F_{L,R}$ with R in $SU(2)_R$.

³⁵ Another term could be $\overline{F_L} g^{\mu\nu} \tau^3 \partial_\mu \mathcal{W}_\nu^a \tau^a \tau^3 F_R$, which contains two symmetry breaking factors τ^3 and will not be considered in this work.

real and half the size of $\kappa_{1c}^{4pt.}$ (i.e. $\kappa_{1c}^{4pt.} = 2\kappa_{2c}^{4pt.}$ for $c = g, \sigma$). The non-standard 4-point dimension 5 interactions will then have the structure

$$\begin{pmatrix} c^{\mu\nu}\mathcal{W}_\mu^3\mathcal{W}_\nu^3 + 2c^{\mu\nu}\mathcal{W}_\mu^+\mathcal{W}_\nu^- & 0 \\ 0 & 0 \end{pmatrix} \quad (114)$$

where $c^{\mu\nu}$ is either $g^{\mu\nu}$ or $\sigma^{\mu\nu}$. This structure suggests $2a_{zz1} = a_{ww1}$, and $a_{wz1L(R)} = a_{wz2L(R)} = 0$ for $c^{\mu\nu}$ equal to $g^{\mu\nu}$. For $c^{\mu\nu}$ equal to $\sigma^{\mu\nu}$, it suggests that a_{ww2} can be of any value.

In conclusion, by assuming the dimension 5 operators are the result of an underlying custodial symmetric theory that is broken in such a way that at tree level the Z - b - b coupling does not get modified from its SM values, we derive the following relations among the coefficients of these anomalous couplings. They are:

$$\begin{aligned} a_{z(2,3,4)} &= \sqrt{2}a_{w(2,3,4)L(R)} , \\ 2a_{zz1} &= a_{ww1} , \\ a_{wz1L(R)} &= a_{wz2L(R)} = 0 . \end{aligned} \quad (115)$$

After including the hypercharge interactions, we can see that the set of independent coefficients has reduced from a total of 19 down to 6 only. These coefficients are $a_{z(2,3,4)}$, a_{zz1} , a_{ww2} and a_m (for the operator O_A).

6.2 Production rates for $Z_L Z_L$, $W_L W_L$, and $W_L Z_L$ fusion processes

Below, we present the helicity amplitudes for each process. We shall only consider the leading contributions in powers of E , the CM energy of the $V_L V_L$ system, coming from the *no-Higgs* SM (i.e. $\mathcal{L}_{SM}^{(4)}$), and the dimension 5 operators. We assume an approximate SU(2) custodial symmetry, as discussed in the previous sections, so that only 6 independent coefficients are relevant to our discussion. The amplitudes for the most general case are presented in Appendix B.

6.2.1 $Z_L Z_L \rightarrow t\bar{t}$

Fig. 15 shows the diagrams associated to this process. The total amplitude T is the sum of the $\mathcal{L}_{SM}^{(4)}$ contribution (denoted by zz), and the $\mathcal{L}^{(5)}$ contribution (denoted by azz). In diagrams with two vertices, only one anomalous vertex is considered at a time, i.e. we neglect contributions suppressed by $1/\Lambda^2$. We denote the helicity amplitudes by the helicities of the outgoing fermions: the first (second) symbol (+

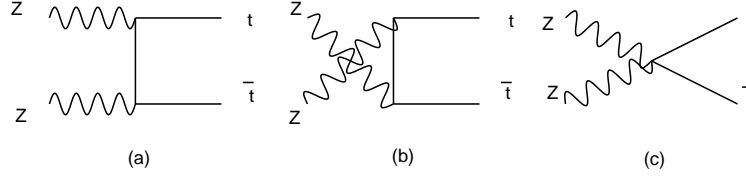


Figure 15: Diagrams for the $ZZ \rightarrow t\bar{t}$ process.

or $-$) refers to the fermion on top (bottom) part of the diagram. A right handed fermion is labelled by $'+'$, and a left handed fermion by $'-'$. For instance,

$$T_{zz++} = zz_{++} + azz_{++} , \quad (116)$$

where zz_{++} is the $\mathcal{L}_{SM}^{(4)}$ contribution, and azz_{++} is the *anomalous* contribution to the helicity amplitude $T(Z_L Z_L \rightarrow t_{Right-handed} \bar{t}_{Right-handed})$. The same notation is used for the other two processes.

The leading contributions to the $Z_L Z_L \rightarrow t\bar{t}$ helicity amplitudes are:

$$\begin{aligned} T_{zz++} &= -T_{zz--} = \frac{m_t E}{v^2} - \frac{2E^3 X}{v^2 \Lambda} , \\ T_{zz+-} &= T_{zz-+} = \frac{2 m_t^2 c_\theta s_\theta}{\left(\frac{4c_\theta^2 m_t^2}{E^2} + s_\theta^2 \right) v^2} + 0 , \end{aligned} \quad (117)$$

where

$$X = 2a_{zz1} + \left(\frac{1}{2} - \frac{4}{3}s_w^2 \right) a_{z3} , \quad (118)$$

and $E = \sqrt{s}$ is the CM energy of the $V_L V_L$ system.

Comparing with the results for $W_L^+ W_L^-$ and $W_L^+ Z_L$ fusions, this is the amplitude that takes the simplest form with no angular dependance. Also, for this process the assumption of an underlying custodial symmetry does not make the anomalous contribution any different from the most general expression given in Appendix C. This means that new physics effects coming through this process can only modify the S-partial wave amplitude (at the leading order of E^3). Notice that at this point it is impossible to distinguish the effect of the coefficient a_{zz1} from the effect of the coefficient a_{z3} . However, in the next section we will show how to combine this information with the results of the other processes, and obtain bounds for each coefficient. The reason why $azz_{\pm\mp}$ appear as zero is explained in Appendix C.

6.2.2 $W_L^+ W_L^- \rightarrow t\bar{t}$

The amplitudes of this process are similar to the ones of the previous process except for the presence of two s -channel diagrams (see Fig. 16), whose off-shell γ

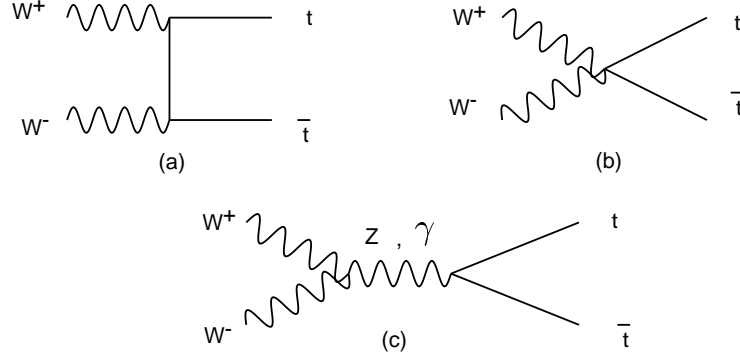


Figure 16: Diagrams for the $WW \rightarrow t\bar{t}$ process.

and Z propagators allow for the additional contribution from the magnetic moment of the top quark (a_m) and the operator with derivative on boson $O_{\sigma D Z}$ (a_{z2}). Since these two operators are not of the *scalar*-type, we have a non-zero contribution to the $T_{\pm\mp}$ amplitudes. Throughout this paper, the angle of scattering θ in all processes is defined to be the one subtended between the incoming gauge boson that appears on the top-left part of the Feynman diagram (W^+ in this case) and the momentum of the outgoing fermion appearing on the top-right part of the same diagram (t in this case); all in the CM frame of the $V_L V_L$ pair.

The leading contributions to the various helicity amplitudes for this process are:

$$\begin{aligned}
T_{ww++} &= -T_{ww--} = \frac{m_t E}{v^2} - \frac{4 E^3 (X_1 + X_m c_\theta)}{v^2 \Lambda}, \\
T_{ww+-} &= \frac{2 m_t^2 s_\theta}{\left(\frac{2m_b^2}{E^2} + (1 - c_\theta) \left(1 - \frac{2m_t^2}{E^2}\right)\right) v^2} + \frac{8 E^2}{v^2} m_t s_\theta \frac{(X_m - \frac{1}{4} a_{z3})}{\Lambda}, \\
T_{ww-+} &= 0 + \frac{8 E^2}{v^2} m_t s_\theta \frac{X_m - \frac{1}{8} a_{z3}}{\Lambda},
\end{aligned} \tag{119}$$

where $s_\theta = \sin \theta$, $c_\theta = \cos \theta$, and

$$\begin{aligned}
X_1 &= a_{zz1} + \frac{1}{8} a_{z3}, \\
X_m &= a_m - \frac{1}{2} a_{z2} + \frac{1}{8} a_{z3} + \frac{1}{2} a_{ww2}.
\end{aligned} \tag{120}$$

Notice that the angular distribution of the leading contributions in the $T_{\pm\pm}$ amplitudes consists of the flat component (S-wave) and the $d_{0,0}^1 = \cos \theta$ component (P-wave). The $T_{\pm\mp}$ helicity amplitudes only contain the $d_{0,\pm 1}^1 = -\frac{\sin \theta}{\sqrt{2}}$ component. This is so because the initial state consists of longitudinal gauge bosons and has zero helicity. The final state is a fermion pair so that the helicity of this state can be -1 , 0 , or $+1$. Therefore, in high energy scatterings, the anomalous dimension 5 operators only modify (at the leading orders E^3 and E^2) the

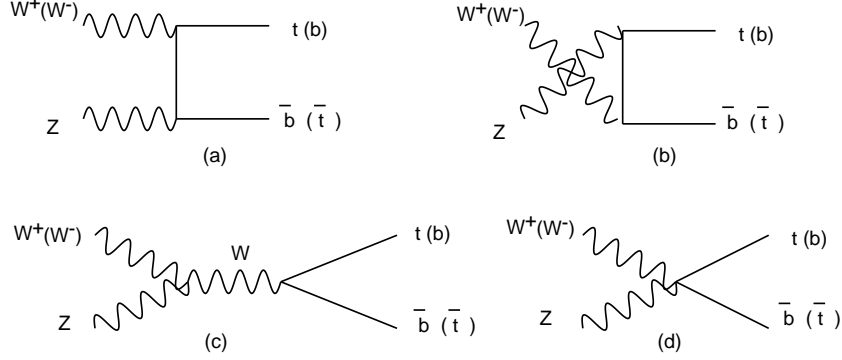


Figure 17: Diagrams for the $WZ \rightarrow t\bar{b}$ process.

S- and P-partial waves of the scattering amplitudes. We also note that, as expected from the discussion in section 5, $aww_{\pm\pm}$ has an E^3 leading behavior, whereas $aww_{\pm\mp}$ goes like E^2 . Furthermore, the $\mathcal{L}_{SM}^{(4)}$ amplitudes are of order $m_t E/v^2$ for $ww_{\pm\pm}$, and m_t^2/v^2 for ww_{+-} . (ww_{-+} is proportional to m_b^2/v^2 and is taken as zero.) To calculate the event rate, we need to sum over four helicity amplitudes squared, and $|T_{\pm\pm,\pm\mp}|^2 = ww_{\pm\pm,\pm\mp}^2 + 2ww_{\pm\pm,\pm\mp}aww_{\pm\pm,\pm\mp} + O(1/\Lambda^2)$. Because $|ww_{\pm\mp}aww_{\pm\mp}| \sim \frac{m_t^2}{E^2} |ww_{\pm\pm}aww_{\pm\pm}|$, the amplitude squared $|T_{\pm\mp}|^2$ is only a few percent of the value of $|T_{\pm\pm}|^2$ for $E \sim 1$ TeV. Thus, $|T_{\pm\mp}|^2$ will not contribute largely to the total event rate, provided the coefficients of the dimension 5 operators are of order one.

6.2.3 $W_L^+ Z_L \rightarrow t\bar{b}$

Finally, we have the amplitudes for the single-top quark production process $W^+ Z \rightarrow t\bar{b}$ (which are just the same as for the conjugate process $W^- Z \rightarrow b\bar{t}$). Fig. 17 shows the diagrams that participate in this process.

The leading contributions to the various helicity amplitudes for this are:³⁶

$$\begin{aligned}
T_{wzt++} &= -\frac{\sqrt{2} m_t^3 (1 - c_\theta)}{E \left(1 - \frac{2m_t^2}{E^2}\right) \left(1 + c_\theta + \frac{2m_t^2}{E^2}\right) v^2} - \frac{\sqrt{2} E^3 (X_2 + c_\theta X_3)}{4v^2 \Lambda}, \\
T_{wzt--} &= 0 - \frac{\sqrt{2} E^3 \left((4s_w^2 a_{z4} + \frac{2}{3} s_w^2 - 1) + (a_{z3} - 4c_w^2 a_{z2}) c_\theta \right)}{4v^2 \Lambda}, \\
T_{wzt+-} &= 0 + \frac{\sqrt{2} E^2}{4v^2} m_t s_\theta \frac{(a_{z3} + 4c_w^2 a_{z2})}{\Lambda},
\end{aligned}$$

³⁶As shown in Eq. (115), for models with this approximate custodial symmetry, $a_{wz1L(R)} = a_{wz2L(R)} = 0$, so that the 4-point vertex diagram of Fig. 17(d) gives no contribution.

$$T_{wzt-+} = -\frac{\sqrt{2}m_t^2 s_\theta}{\left(1 - \frac{2m_t^2}{E^2}\right) \left(1 + c_\theta + \frac{2m_t^2}{E^2}\right) v^2} - \frac{3\sqrt{2}E^2}{4v^2} m_t s_\theta \frac{X_4}{\Lambda}, \quad (121)$$

where

$$\begin{aligned} X_2 &= \left(1 + \frac{2}{3}s_w^2\right)a_{z3} - 4s_w^2 a_{z4}, \\ X_3 &= a_{z3} + 4c_w^2 a_{z2}, \\ X_4 &= a_{z3} - \frac{4}{3}c_w^2 a_{z2}. \end{aligned} \quad (122)$$

The anomalous amplitudes $awzt_{--}$ and $awzt_{+-}$ can be ignored in our analysis. The reason is because the $\mathcal{L}^{(4)}$ amplitudes wzt_{--} and wzt_{+-} are zero, which means that, when we consider the total helicity amplitudes squared, they turn out to be of order $1/\Lambda^2$. This is why only $awzt_{++}$ and $awzt_{-+}$ are presented in terms of the parameters X_2 , X_3 and X_4 , each parameter associated to a different partial wave.

6.3 Top quark production rates from $V_L V_L$ fusions

As discussed above, the top quark productions from $V_L V_L$ fusion processes can be more sensitive to the electroweak symmetry breaking sector than the longitudinal gauge boson productions from $V_L V_L$ fusions. In this section we shall examine the possible increase (or decrease) of the top quark event rates, due to the anomalous dimension 5 couplings, at the future hadron collider LHC (a pp collider with $\sqrt{s} = 14$ TeV and 100 fb^{-1} of integrated luminosity) and the electron linear collider LC (an e^-e^+ collider with $\sqrt{s} = 1.5$ TeV and 200 fb^{-1} of integrated luminosity).

To simplify our discussion, we shall assume an approximate custodial symmetry and make use of the helicity amplitudes given in the previous section to compute the production rates for $t\bar{t}$ pairs and for single- t or \bar{t} quarks. We shall adopt the effective- W approximation method [42, 65], and use the CTEQ3L [66] parton distribution function with the factorization scale chosen to be the mass of the W -boson. For this study we do not intend to do a detailed Monte Carlo simulation for the detection of the top quark; therefore, we shall only impose a minimal set of cuts on the produced t or b . The rapidity of t or b produced from the $V_L V_L$ fusion process is required to be within 2 (i.e. $|y^{t,b}| \leq 2$) and the transverse momentum of t or b is required to be at least 20 GeV. To validate the effective- W approximation, we also require the invariant mass M_{VV} to be larger than 500 GeV.

Since we are working in the high energy regime $E \gg v$, the approximation made when we expand the $V_L V_L \rightarrow t\bar{t}$ or $t\bar{b}$ scattering amplitudes in powers of E and keep the leading terms only, becomes a very good one. As noted in the previous section, in all the $T_{\pm\pm}$ amplitudes, the dimension 5 operators will only modify the constant term (S-wave) and the $\cos\theta$ (P-wave: $d_{0,0}^1$) dependence in the angular distributions of the

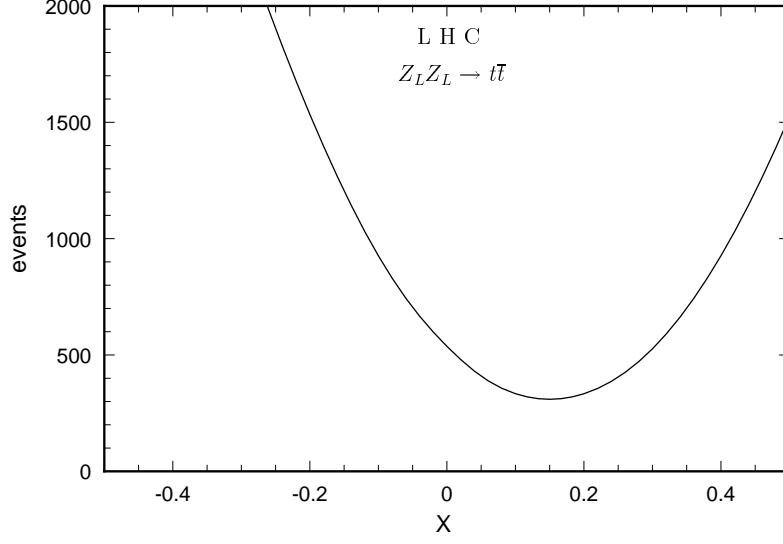


Figure 18: Number of events at the LHC for $Z_L Z_L$ fusion. The variable X is defined in Eq. (118).

leading E^3 contributions, whereas all the $T_{\pm\mp}$ amplitudes have a $\sin\theta$ (P-wave: $d_{0,\pm 1}^1$) dependence in their leading E^2 contributions. Each of the effective coefficients, X , X_1 , X_m , X_2 , X_3 and X_4 , parametrizes the contribution to one of the partial waves.³⁷ Since contributions to different partial waves do not interfere with each other, we can make a consistent analysis by taking only one coefficient non-zero at a time.

The predicted top quark event rates as a function of these coefficients are given in Figs. 18, 19 and 20 for the LHC, and in Figs. 21, 22 and 23 for the LC. In these plots, neither the branching ratio nor the detection efficiency have been included.

For $X = 0$, the LHC results show that there are in total about 1500 $t\bar{t}$ pair and single- t or \bar{t} events predicted by the *no-Higgs* SM. The $W_L^+ W_L^-$ fusion rate is about a factor of 2 larger than the $Z_L Z_L$ fusion rate, and about an order of magnitude larger than the $W_L^+ Z_L$ fusion rate. The $W_L^- Z_L$ rate, which is not shown here, is about a factor of 3 smaller than the $W_L^+ Z_L$ rate due to smaller parton luminosities at a pp collider. It will be challenging to actually detect any signal from these channels at the LHC due to the considerable amount of background in this hadron-hadron collision. What we can learn from Fig. 19 is that, with a production of about 900 events and the large slope of the $W_L^+ W_L^- \rightarrow t\bar{t}$ curve, this process might be able to probe the anomalous coupling (X_1).

For the LC, because of the small coupling of Z - e - e , the event rate for $Z_L Z_L \rightarrow t\bar{t}$ is small. For the *no-Higgs* SM, the top quark event rate at LC is about half of that at the LHC and yields a total of about 550 events ($t\bar{t}$ pairs and single- t or \bar{t}). Again,

³⁷In $W_L^+ W_L^- \rightarrow t\bar{t}$, X_m contributes to both P-partial waves.

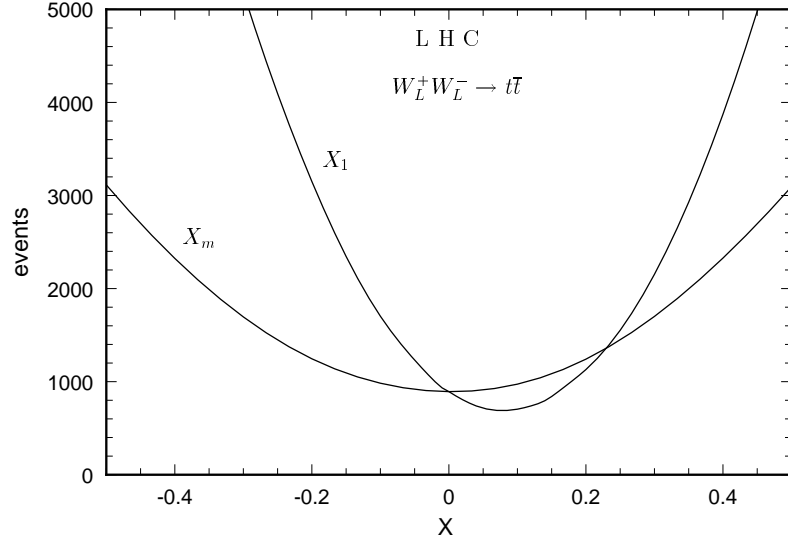


Figure 19: Number of events at the LHC for $W_L^+ W_L^-$ fusion. The variable X stands for the effective coefficients X_1 and X_m defined in Eq. (120).

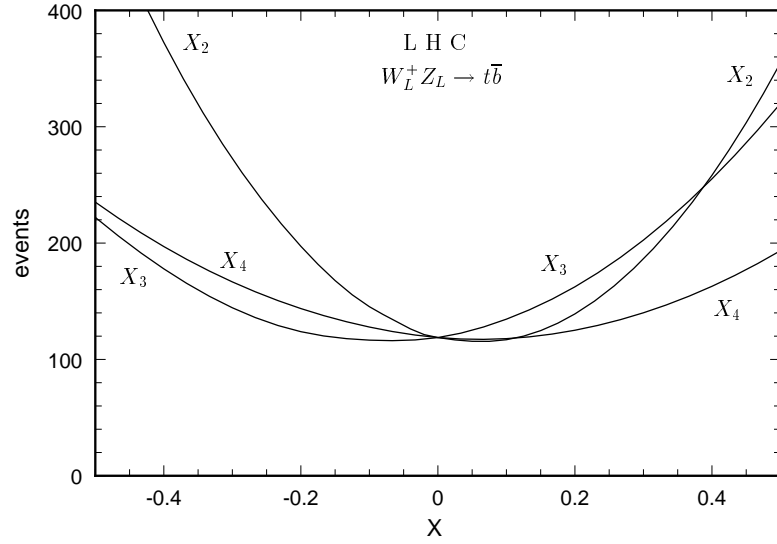


Figure 20: Number of events at the LHC for $W_L^+ Z_L$ fusion. The variable X stands for the effective coefficients X_2 , X_3 and X_4 defined in Eq. (122).

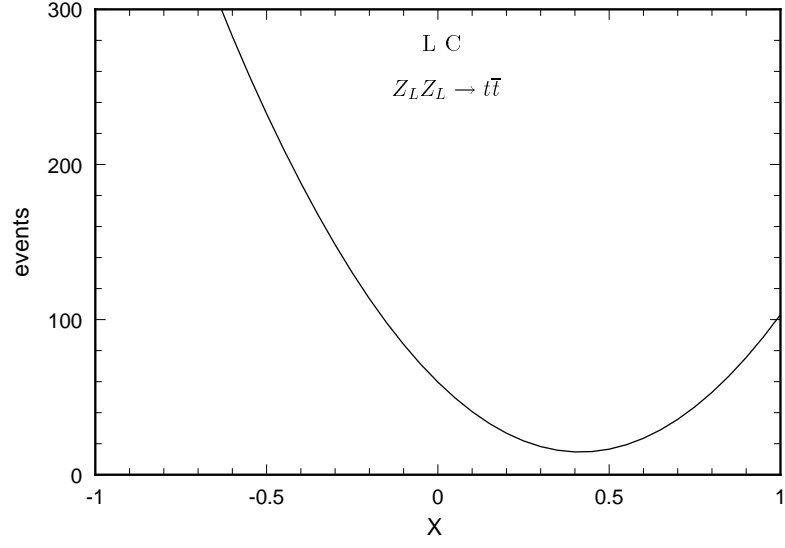


Figure 21: Number of events at the LC for $Z_L Z_L$ fusion. The variable X is defined in Eq. (118).

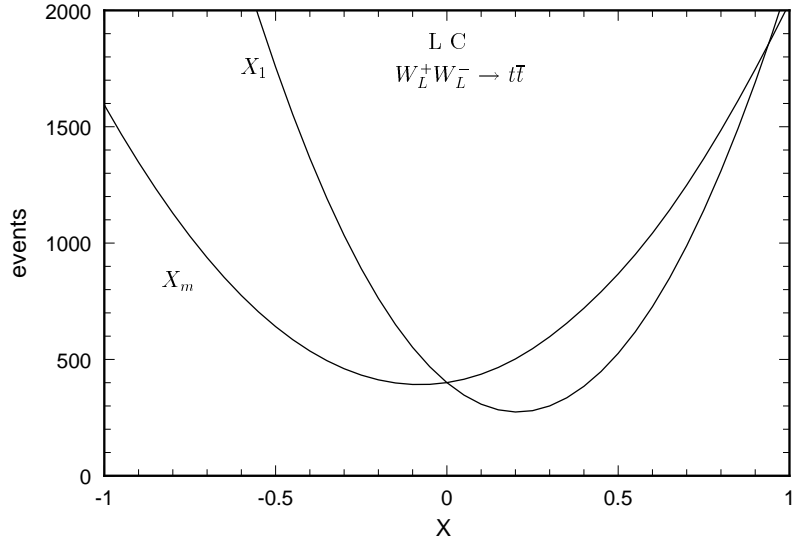


Figure 22: Number of events at the LC for $W_L^+ W_L^-$ fusion. The variable X stands for the effective coefficients X_1 and X_m defined in Eq. (120).

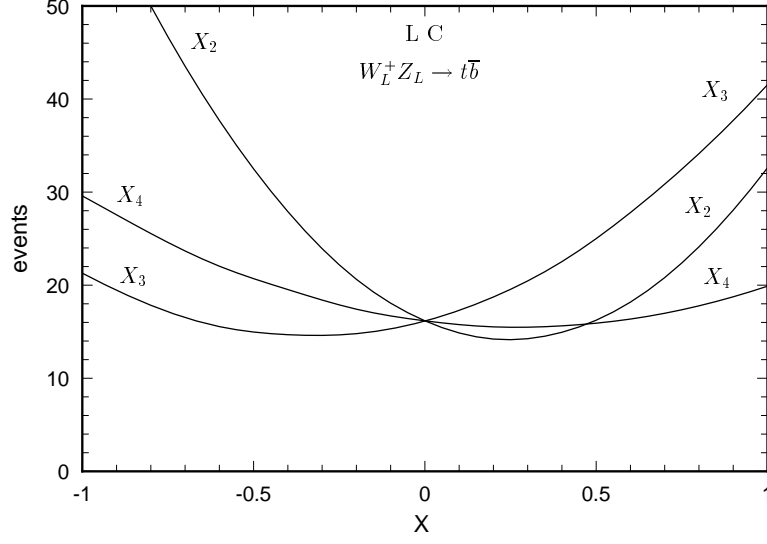


Figure 23: Number of events at the LC for $W_L^+ Z_L$ fusion. The variable X stands for the effective coefficients X_2 , X_3 and X_4 defined in Eq. (122).

we find that the $W_L^+ W_L^- \rightarrow t\bar{t}$ rate is sensitive to the dimension 5 operators that correspond to X_1 , but the $Z_L Z_L \rightarrow t\bar{t}$ rate is much less sensitive.³⁸

The production rates shown in Figs. 21, 22 and 23 are for an unpolarized e^- beam at the LC. Because the coupling of the W boson to the electron is purely left handed, the parton luminosity of the W boson will double for a left-handed polarized e^- beam at the LC; hence, the $t\bar{t}$ rate from $W_L^+ W_L^-$ fusion will double too. However, this is not true for the parton luminosity of Z because in this case the Z - e - e coupling is nearly purely axial-vector ($1 - 4s_w^2 \approx 0$) and the production rate of $Z_L Z_L \rightarrow t\bar{t}$ does not strongly depend on whether the electron beam is polarized or not. As shown in these plots, if the anomalous dimension 5 operators can be of order 10^{-1} (as expected by the naive dimensional analysis) then their effect can in principle be identified in the measurement of either $Z_L Z_L$ or $W_L^+ W_L^-$ fusion rates at the LC.³⁹ A similar conclusion holds for the $W_L^\pm Z_L$ fusion process, but with less sensitivity.

From the six independent coefficients, $a_{z(2,3,4)}$, a_{zz1} , a_{ww2} and a_m , one stands out: a_{zz1} . The two most potentially significant parameters X and X_1 depend essentially on just this coefficient [cf. Eqs. (118) and (120)]. This suggests that a good test for the possible models of EWSB is to calculate their predictions for the sizes of the four point operators O_{gZZ} and O_{gWW} because these are more likely to produce a measurable signal at either the LC or the LHC. The second better test could be the magnetic moment a_m because this coefficient gives the largest contribution to X_m [cf.

³⁸ Needless to say, the $W_L^- Z_L$ rate is the same as the $W_L^+ Z_L$ rate at an unpolarized $e^+ e^-$ LC

³⁹ Specifically, for anomalous coefficients of order 10^{-1} there is a 2σ deviation from the *no-Higgs* SM event rates.

Eq. (120)], and Figs. 19 and 22 show that this parameter can be measured as well.

It is useful to ask for the bounds on the coefficients of the anomalous dimension 5 operators if the measured production rate at the LC is found to be in agreement with the *no-Higgs* SM predictions (i.e. with $X = 0$). In order to simplify this analysis for the parameter X_m , we have made the approximation $aww_{+-} \simeq \frac{8E^2}{v^2} m_t s_\theta \frac{X_m}{\Lambda}$; notice that the anomalous contribution aww_{+-} to the total amplitude squared is smaller by a factor of m_t^2/E^2 than the contribution from $aww_{\pm\pm}$ [cf. end of section 7.2].

At the 95% C.L. we summarize the bounds on the X 's in Table 4. Here, only the statistical error is included. In practice, after including the branching ratios of the relevant decay modes and the detection efficiency of the events, these bounds will become somewhat weaker, but we do not expect an order of magnitude difference. Also, these bounds shall be improved by carefully analyzing angular correlations when data is available.

Process	Bounds (e^+e^-)
$Z_L Z_L \rightarrow t\bar{t}$	$-0.07 < X < 0.08$
$W_L^+ W_L^- \rightarrow t\bar{t}$	$-0.03 < X_1 < 0.035$
$W_L^+ W_L^- \rightarrow t\bar{t}$	$-0.28 < X_m < 0.12$
$W_L^{+(-)} Z_L \rightarrow t\bar{b} (b\bar{t})$	$-0.32 < X_2 < 0.82$
$W_L^{+(-)} Z_L \rightarrow t\bar{b} (b\bar{t})$	$-1.2 < X_3 < 0.5$
$W_L^{+(-)} Z_L \rightarrow t\bar{b} (b\bar{t})$	$-0.8 < X_4 < 1.3$

Table 4: The range of parameters for which the total number of events at the LC deviates by less than 2σ from the *no-Higgs* SM prediction.

As shown in Table 4, these coefficients can be probed to about an order of 10^{-1} or even 10^{-2} . For this Table, we have only considered an unpolarized e^- beam for the LC. To obtain the bounds we have set all the anomalous coefficients to be zero except the one of interest. This procedure is justified by the fact that at the leading orders of E^3 and E^2 , different coefficients contribute to different partial waves. (The definitions of the combined coefficients X , X_1 , X_2 , X_3 and X_4 are given in the previous section.)

If the LC is operated at the e^-e^- mode with the same CM energy of the collider, then it cannot be used to probe the effects for $W_L^+ W_L^- \rightarrow t\bar{t}$, but it can improve the bounds on the combined coefficients X_4 , X_2 and X_3 , because the event rate will increase by a factor of 2 for $W_L^- Z_L \rightarrow b\bar{t}$ production.

By combining the limits on these parameters we can find the corresponding limits on the effective coefficients a_{zz1} , a_{z2} , a_{z3} , a_{z4} , and $(a_m + \frac{1}{2}a_{ww2})$. For example, if we consider the limits for X_3 and X_4 , we will find the limits for a_{z2} , a_{z3} . Then we can compare the bounds on a_{z3} and those on X_1 to derive the constraints on a_{zz1} . Also, the bounds on a_{z3} and on X_2 will give the constraints on a_{z4} . Finally, we use the

bounds on a_{z3} , a_{z2} and X_m to obtain constraints for $(a_m + \frac{1}{2}a_{ww2})$. Table 5 shows these results.

Bounds on X parameters	Bounds on anomalous coefficients
$-1.2 < X_3 < 0.5$	$-0.6 < a_{z2} < 0.32$
$-0.8 < X_4 < 1.3$	$-0.9 < a_{z3} < 1.1$
$-.03 < X_1 < .035$	$-0.17 < a_{zz1} < 0.15$
$-0.32 < X_2 < 0.82$	$-1.9 < a_{z4} < 1.7$
$-.28 < X_m < .12$	$-0.7 < a_m + \frac{1}{2}a_{ww2} < 0.4$

Table 5: The constraints on the anomalous coefficients obtained by the linear combination of the bounds on the X parameters.

Nevertheless, we can also follow the usual procedure of taking only one anomalous coefficient as non-zero at a time. Under this approach the bounds become more stringent:

$$\begin{aligned}
-0.03 &< a_{zz1} < 0.035, \\
-0.28 &< a_m < 0.12, \\
-0.24 &< a_{z3} < 0.28, \\
-0.4 &< a_{z2} < 0.2, \\
-0.82 &< a_{ww2} < 0.32, \\
-0.56 &< a_{z4} < 0.24.
\end{aligned} \tag{123}$$

Again, these bounds come from the consideration of a 2σ deviation from the *no-Higgs* SM event rates. For instance, at the LC, the *no-Higgs* SM predictions for the processes $Z_L Z_L \rightarrow t\bar{t}$ and $W_L^+ W_L^- \rightarrow t\bar{t}$ are 60 and 400, respectively [cf. Figs. 21 and 22]. This means that a number of events between 75 and 45 for the first process, and between 440 and 360 for the second one, is considered consistent with the *no-Higgs* SM prediction at the 95% C.L.. Fig. 21 shows an interesting situation for $Z_L Z_L \rightarrow t\bar{t}$, if the parameter X happened to be between 0.75 and 0.90 then we would obtain a number of events consistent with the *no-Higgs* SM. However, if this were the case, then X_1 would have to be at least of order 0.7 and we would observe a substantial deviation (of about 600) in the number of events produced from $W_L^+ W_L^- \rightarrow t\bar{t}$. This also happens the other way around, if X_1 is between 0.38 and 0.45, we would obtain a production rate consistent with the *no-Higgs* SM for $W_L^+ W_L^-$ fusion [cf. Fig. 22], but then X would be at least of order 0.3, and according to Fig. 21, we would observe only 18 $t\bar{t}$ pairs from $Z_L Z_L$ fusion, too far from the 60 ± 15 range of the *no-Higgs* SM prediction. Hence, all the production channels have to be measured to conclusively test the SM and probe new physics.

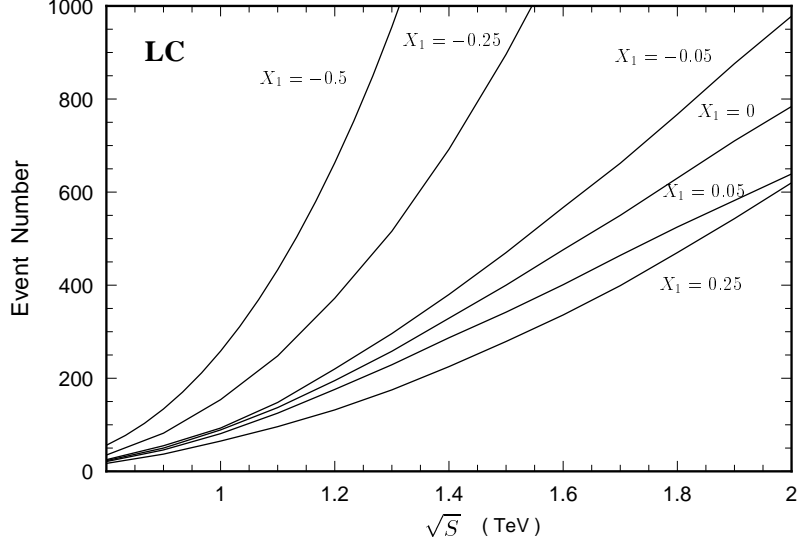


Figure 24: Number of $t\bar{t}$ events at the LC from $W_L^+W_L^-$ fusion for different values of the effective coefficient X_1 as a function of the CM energy.

The above results are for the LC with a 1.5 TeV CM energy. To study the possible new effects in the production rates of $W_L^+W_L^- \rightarrow t\bar{t}$ at the LC with different CM energies, we plot the production rates for various values of X_1 in Fig. 24. (Again, $X_1 = 0$ stands for the *no-Higgs* SM.) Notice that, if X_1 were as large as -0.5 , then a 1 TeV LC could well observe the anomalous rate via $W_L^+W_L^-$ fusion.⁴⁰ For $X_1 = 0.25$ the event rate at 1.5 TeV is down by about a factor of 2 from the SM event rate.⁴¹

6.4 CP violating effects due to dimension 5 interactions

The complete set of anomalous dimension 5 operators listed in $\mathcal{L}^{(5)}$ consists of operators with CP- conserving and non-conserving parts. In our study of the top quark production rates we have only considered the CP-even part of these operators; their contribution, like the one from the *no-Higgs* SM at tree level, is real. However, a CP-odd operator can contribute to the imaginary part of the helicity amplitudes, and it can only be probed by examining CP-odd observables.

To illustrate this point, let us consider the CP-odd part of the four-point scalar type operator $O_{g\mathcal{W}\mathcal{W}}$ and the electric dipole moment term of O_A [cf. Eqs. (91) and (96)]. After including contributions from the *no-Higgs* SM and from the above two CP-odd operators, the helicity amplitudes for the $W_L^+W_L^- \rightarrow t\bar{t}$ process in the $W_L^+W_L^-$

⁴⁰If X_1 is too big, partial wave unitarity can be violated at this order.

⁴¹For positive values of X_1 the rate tends to diminish below the SM rate. However, near 0.25, the rate begins to rise again, toward the SM rate.

CM frame are:

$$\begin{aligned}
T_{\pm\pm} &= \pm \frac{m_t E}{v^2} + i2 \frac{E^3 (\tilde{a}_{ww1} + 2a_d c_\theta)}{v^2 \Lambda}, \\
T_{+-} &= \frac{2m_t^2 s_\theta}{\left(\frac{m_b^2}{2E^2} + (1 - c_\theta) \left(1 - \frac{m_t^2}{2E^2}\right)\right) v^2}, \\
T_{-+} &= 0,
\end{aligned} \tag{124}$$

where, by a_d and \tilde{a}_{ww1} , we refer to the imaginary part of the coefficients of O_A and $O_{g\mathcal{W}\mathcal{W}}$, respectively.

One of the CP-odd observables that can measure a_d and \tilde{a}_{ww1} is the transverse polarization (P_\perp) of the top quark, which is the degree of polarization of the top quark in the direction perpendicular to the plane of the $W_L^+ W_L^- \rightarrow t\bar{t}$ scattering process. It was shown in Ref. [51] that

$$P_\perp = \frac{2\text{Im} \left(T_{++}^* T_{-+} + T_{+-}^* T_{--} \right)}{|ww_{++}|^2 + |ww_{+-}|^2 + |ww_{-+}|^2 + |ww_{--}|^2}, \tag{125}$$

which, up to the order $\frac{1}{\Lambda}$, is

$$P_\perp \cong \frac{4s_\theta E}{\left(\frac{m_b^2}{2E^2} + (1 - c_\theta) \left(1 - \frac{m_t^2}{2E^2}\right)\right)} \frac{(\tilde{a}_{ww1} + 2a_d c_\theta)}{\Lambda}. \tag{126}$$

Again, $E = \sqrt{s}$ is the CM energy of the $W_L^+ W_L^-$ system; P_\perp , by definition, can only obtain values between -1 and 1 . For $E = 1.5$ TeV, $\Lambda = 3$ TeV, and $\theta = \frac{\pi}{2}$, or $\frac{\pi}{3}$, we obtain $P_\perp = 4\tilde{a}_{ww1}$, or $4\sqrt{3}(\tilde{a}_{ww1} + a_d)$, respectively. Since $|P_\perp|$ is at most 1 , this requires $|\tilde{a}_{ww1}| < \frac{1}{4}$ or $|\tilde{a}_{ww1} + a_d| < \frac{1}{4\sqrt{3}}$.

At a 1.5 TeV e^+e^- collider, the *no-Higgs* SM predicts about 100 $t\bar{t}$ pairs, with an invariant mass between 800 GeV and 1100 GeV, via the $W_L^+ W_L^-$ fusion process. Let us assume that $a_d = 0$, and that P_\perp can be measured to about $\frac{1}{\sqrt{100}} = 10\%$, then an agreement between data and the *no-Higgs* SM prediction ($P_\perp = 0$ at tree level) would imply $|\tilde{a}_{ww1}| \leq 0.04$.

7 Conclusions

Because top quark is heavy ($m_t \sim v/\sqrt{2}$), it is likely that the interaction of the top quark can deviate largely from the SM predictions if the electroweak symmetry breaking and the generation of fermion masses are closely related. In this study, we have applied the electroweak chiral Lagrangian to probe new physics beyond the SM by studying the couplings of the top quark to gauge bosons. We have restricted

ourselves to only consider the interactions of the top and bottom quarks and not the flavor changing neutral current vertices like t - c - Z . Furthermore, seeing the heaviness of the top quark as a possible indication that any new physics effects associated to the symmetry breaking (and mass generating) sector will manifest themselves preferably on this particle, we have considered only the couplings that involve the top quark as showing possible deviations from the standard values. (The vertex b - b - Z is considered unmodified.) We introduced 4 effective coefficients: two that represent the non-standard couplings associated to the left and right handed charged currents κ_L^{CC} and κ_R^{CC} , and two more for the anomalous left and right handed neutral currents κ_L^{NC} and κ_R^{NC} . Then, we used the precision LEP data to set bounds on the couplings κ_L^{NC} , κ_R^{NC} , and κ_L^{CC} , and we also discussed how the SLC measurement of A_{LR} can modify these constraints. The right handed charged current coupling κ_R^{CC} is constrained by means of the CLEO measurement on $b \rightarrow s\gamma$: $-0.037 < \kappa_R^{CC} < 0.0015$ [26, 27].

Last, we showed how to improve our knowledge about the top quark nonstandard couplings at current and future colliders such as at the Tevatron, the LHC, and the LC.

Because of the non-renormalizability of the electroweak chiral Lagrangian one can only estimate the size of these nonstandard couplings by studying the contributions to LEP/SLC observables at the order of $m_t^2 \ln \Lambda^2$, where $\Lambda = 4\pi v \sim 3$ TeV is the cutoff scale of the effective Lagrangian. Nevertheless, this does not mean we can not extract useful information. For instance, by assuming that the b - b - Z vertex is not modified, we found that $-0.35 \leq \kappa_L^{NC} \leq 0.35$ ($-0.30 \leq \kappa_L^{NC} \leq 0.35$) by using the LEP/SLC data at the 95% C.L. for a 160 (180) GeV top quark. Although κ_R^{NC} and κ_L^{CC} are allowed to be in the full range of ± 1 , the precision LEP/SLC data do impose some correlations among κ_L^{NC} , κ_R^{NC} , and κ_L^{CC} . (κ_R^{CC} does not contribute to the LEP/SLC observables of interest in the limit of $m_b = 0$.) For instance, if $\kappa_L^{CC} \sim 0$ then $\kappa_R^{NC} \sim \kappa_L^{NC}$ with $-0.09 \leq \kappa_L^{NC} \leq 0.15$.

Because of the experimental fact $\rho \approx 1$, reflecting the existence of an approximate custodial symmetry, κ_L^{NC} and κ_L^{CC} are related so that $\kappa_L^{NC} = 2\kappa_L^{CC}$. Then, the remaining two free parameters $\kappa_L = \kappa_L^{NC}$ and $\kappa_R = \kappa_R^{NC}$ get to be strongly correlated as well: $\kappa_L \sim 2\kappa_R$, with $-0.08 \leq \kappa_L^{NC} \leq 0.13$.

We noted that the relations among the κ 's can be used to test different models of electroweak symmetry-breaking. For instance, a heavy SM Higgs boson ($m_H \gg m_t$) will modify the couplings t - t - Z and t - b - W of a heavy top quark at the scale m_t such that $\kappa_L^{NC} = 2\kappa_L^{CC}$, $\kappa_L^{NC} = -\kappa_R^{NC}$, and $\kappa_R^{CC} = 0$. Another example is the effective model discussed in Ref. [2] where, $\kappa_R^{CC} = \kappa_L^{CC} = 0$, in which the low energy precision data impose the relation $\kappa_L \sim \kappa_R$. On the other hand, the simple commuting extended technicolor model presented in Ref. [4] predicts that the nonstandard top quark couplings are of the same order as the nonstandard bottom quark couplings, and are thus small.

Undoubtedly, direct detection of the top quark at the Tevatron, the LHC, and the

LC is crucial to measuring the couplings of t - b - W and t - t - Z . At hadron colliders, κ_L^{CC} and κ_R^{CC} can be measured by studying the polarization of the W boson from top quark decay in $t\bar{t}$ events, and from the production rate of the single top quark event via W -gluon fusion, W^* or Wt processes. The LC is the best machine to measure κ_L^{NC} and κ_R^{NC} which can be measured from studying the angular distribution and the polarization of the top quark produced in e^-e^+ collision.

If a strong dynamics of the electroweak symmetry breaking mechanism can largely modify the dimension 4 anomalous couplings, it is natural to ask whether the same dynamics can also give large dimension 5 anomalous couplings. In the framework of the electroweak chiral Lagrangian, we have found that there are 19 independent dimension five operators associated with the top quark and the bottom quark system. The high energy behavior, two powers in E above the *no-Higgs* SM, for the $V_L V_L \rightarrow t\bar{t}$, $t\bar{b}$, (or $b\bar{t}$) processes, gives them a good possibility to manifest themselves through the production of $t\bar{t}$ pairs or single- t or \bar{t} events at the LHC and LC in high energy collisions. Since in the high energy regime a longitudinal gauge boson is equivalent to the corresponding would-be Goldstone boson (cf. Goldstone Equivalence Theorem [19]), the production of top quarks via $V_L V_L$ fusions can probe the part of the electroweak symmetry breaking sector which modifies the top quark interactions. To simplify our discussion on the accuracy for the measurement of these anomalous couplings at future colliders, we have taken the dimension 4 anomalous couplings to be zero for this part of the study. Also we have considered a special class of new physics effects in which an underlying custodial $SU(2)$ symmetry is assumed that gets broken in such a way as to keep the vertices of the bottom quark unaltered (as was done for the dimension 4 case). This approximate custodial symmetry then relates some of the coefficients of the anomalous operators. Then we study the contributions of these couplings to the production rates of the top quark. We find that for the leading contributions at high energies, only the S- and P-partial wave amplitudes are modified by these anomalous couplings if the magnitudes of the coefficients of the anomalous dimension 5 operators are allowed to be as large as 1 (as suggested by the naive dimensional analysis [15]), then we will be able to make an unmistakable identification of their effects to the production rates of top quarks via the longitudinal weak boson fusions. However, if the measurement of the top quark production rate is found to agree with the SM prediction, then one can bound these coefficients to be at most of order 10^{-2} or 10^{-1} . This is about a factor $\frac{\Lambda}{m_t} \simeq \frac{3\text{TeV}}{175\text{GeV}} \sim O(10)$ more stringent than in the case of the study of NLO bosonic operators via the $V_L V_L \rightarrow V_L V_L$ scattering processes [19, 20, 64]. Hence, for those models of electroweak symmetry breaking for which the naive dimensional analysis gives the correct size for the coefficients of dimension 5 effective operators, the top quark production via $V_L V_L$ fusions can be a more sensitive probe of EWSB than the longitudinal gauge boson pair production via $V_L V_L$ fusions which is commonly studied. For completeness, we also briefly discuss how to study the CP-odd operators by measuring the CP-odd observables. In this

paper we study their effects on the transverse (relative to the plane of $W_L^+ W_L^- \rightarrow t\bar{t}$ scattering) polarization of the top quark.

In conclusion, the production of top quarks via $V_L V_L$ fusions at the LHC and the LC should be carefully studied when data is available because it can be sensitive to the electroweak symmetry breaking mechanism, even more than the commonly studied $V_L V_L \rightarrow V_L V_L$ processes in some models of strong dynamics.

Acknowledgments

C.P.Y. would like to thank Professors Yu-Ping Kuang and Qing Wang, and all those involved in organizing this Workshop for their warm hospitality. We thank Hong-Jian He, G. L. Kane, E. Malkawi and T. Tait for helpful discussions. F. Larios was supported in part by the Organization of American States, and by the Sistema Nacional de Investigadores. C.P.Y. was supported in part by the NSF grants PHY-9309902 and PHY-9507683.

A Equations of Motion

From the electroweak chiral Lagrangian $\mathcal{L}^{(4)}$ of Eq. (32), we can use the Euler-Lagrange equations to obtain the equations of motion for the top quark. They are:

$$\begin{aligned}
i\gamma^\mu(\partial_\mu + i\frac{2}{3}s_w^2\mathcal{A}_\mu)t_L - \frac{1}{2}(1 - \frac{4}{3}s_w^2 + \kappa_L^{NC})\gamma^\mu\mathcal{Z}_\mu t_L - \frac{1}{\sqrt{2}}(1 + \kappa_L^{CC})\gamma^\mu\mathcal{W}_\mu^+ b_L - m_t t_R &= 0, \\
i\gamma^\mu(\partial_\mu + i\frac{2}{3}s_w^2\mathcal{A}_\mu)t_R - \frac{1}{2}(-\frac{4}{3}s_w^2 + \kappa_R^{NC})\gamma^\mu\mathcal{Z}_\mu t_R - \frac{1}{\sqrt{2}}\kappa_R^{CC}\gamma^\mu\mathcal{W}_\mu^+ b_R - m_t t_L &= 0, \\
i\gamma^\mu(\partial_\mu - i\frac{1}{3}s_w^2\mathcal{A}_\mu)b_L - (-\frac{1}{2} + \frac{1}{3}s_w^2)\gamma^\mu\mathcal{Z}_\mu b_L - \frac{1}{\sqrt{2}}(1 + \kappa_L^{CC\dagger})\gamma^\mu\mathcal{W}_\mu^- t_L - m_b b_R &= 0, \\
i\gamma^\mu(\partial_\mu - i\frac{1}{3}s_w^2\mathcal{A}_\mu)b_R - \frac{1}{3}s_w^2\gamma^\mu\mathcal{Z}_\mu b_R - \frac{1}{\sqrt{2}}\kappa_R^{CC\dagger}\gamma^\mu\mathcal{W}_\mu^- t_R - m_b b_L &= 0.
\end{aligned}$$

B $\mathcal{L}^{(4)}$ helicity amplitudes

Below, we show the leading contributions in powers of E (the CM energy of the $V_L V_L$ system) of the helicity amplitudes for the processes $V_L V_L \rightarrow t\bar{t}$, $t\bar{b}$ and $b\bar{t}$, in the limit $E \gg m_t \gg m_b$, and for the *no-Higgs* SM (i.e. $\mathcal{L}_{SM}^{(4)}$).⁴² In general, any contribution that is not proportional to E^3 or $m_t E^2$ (the highest leading factors) is neglected throughout this paper.

⁴²These amplitudes agree with those given in Ref. [67].

B.1 $Z_L Z_L \rightarrow t\bar{t}$ and $W_L^+ W_L^- \rightarrow t\bar{t}$

The helicity amplitudes for $t\bar{t}$ production are given as follows. The first two letters, zz or ww , refer to the $Z_L Z_L \rightarrow t\bar{t}$ or $W_L^+ W_L^- \rightarrow t\bar{t}$ scattering processes, respectively. The first and second adjacent symbols (+ or -), refer to the helicities of the final top and anti-top quarks, respectively. Throughout this paper, the scattering angle θ is defined as the one subtended between the momentum of the incoming gauge boson that appears on the top-left part of the Feynman diagram [cf. Figs. 15, 16 and 17] and the momentum of the outgoing fermion appearing on the top-right part of the same diagram; all in the CM frame of the $V_L V_L$ pair. We denote its sine and cosine functions as s_θ and c_θ , respectively.

$$\begin{aligned}
zz_{++} &= -zz_{--} = \frac{m_t E}{v^2} , \\
zz_{+-} &= zz_{-+} = \frac{2 m_t^2 c_\theta s_\theta}{\left(\frac{4c_\theta^2 m_t^2}{E^2} + s_\theta^2\right) v^2} , \\
ww_{++} &= -ww_{--} = zz_{++} , \\
ww_{+-} &= \frac{2 m_t^2 s_\theta}{\left(\frac{2m_b^2}{E^2} + (1 - c_\theta) \left(1 - \frac{2m_t^2}{E^2}\right)\right) v^2} , \\
ww_{-+} &= \frac{2 m_b^2 s_\theta}{\left(\frac{2m_b^2}{E^2} + (1 - c_\theta) \left(1 - \frac{2m_t^2}{E^2}\right)\right) v^2} .
\end{aligned} \tag{B.1}$$

For ww_{+-} we have kept the term proportional to the b -mass in the denominator of the fermion-propagator to avoid infinities at $\theta = 0$ in the numerical computations.

For completeness, we include the leading contributions that may come from the κ coefficients in $\mathcal{L}^{(4)}$ [cf. Eq. (32)]:

$$\begin{aligned}
zz_{++}^\kappa &= -zz_{--}^\kappa = \frac{m_t E}{v^2} \left[(\kappa_L^{NC} - \kappa_R^{NC} + 1)^2 - 1 \right] , \\
zz_{+-}^\kappa &= zz_{-+}^\kappa = \frac{2 m_t^2 c_\theta s_\theta}{\left(\frac{4c_\theta^2 m_t^2}{E^2} + s_\theta^2\right) v^2} \left[(\kappa_L^{NC} - \kappa_R^{NC} + 1)^2 - 1 \right] , \\
ww_{++}^\kappa &= \frac{m_t E}{v^2} \left[(1 + c_\theta) (2\kappa_L^{CC} + (\kappa_L^{CC})^2 + (\kappa_R^{CC})^2) - c_\theta (\kappa_L^{NC} + \kappa_R^{NC}) \right] , \\
ww_{--}^\kappa &= -ww_{++}^\kappa , \\
ww_{+-}^\kappa &= \frac{E^2 s_\theta}{v^2} \left[\kappa_R^{NC} - (\kappa_R^{CC})^2 \right] , \\
ww_{-+}^\kappa &= \frac{E^2 s_\theta}{v^2} \left[\kappa_L^{NC} - \kappa_L^{CC} (2 + \kappa_L^{CC}) \right] .
\end{aligned} \tag{B.2}$$

B.2 $W_L^+ Z_L \rightarrow t\bar{b}$ and $W_L^- Z_L \rightarrow b\bar{t}$

The following helicity amplitudes for single top or anti-top production were not given in Ref. [67]. We have taken the limit $E \gg m_t \gg m_b$. The first three letters, wzt or wzb , refer to the $W_L^+ Z_L \rightarrow t\bar{b}$ or $W_L^- Z_L \rightarrow b\bar{t}$ scattering process, respectively.

$$\begin{aligned}
wzt_{++} &= -\frac{\sqrt{2} m_t^3 (1 - c_\theta)}{E \left(1 - \frac{2m_t^2}{E^2}\right) \left(1 + c_\theta + \frac{2m_t^2}{E^2}\right) v^2} , \\
wzt_{--} &= 0 , \\
wzt_{+-} &= 0 , \\
wzt_{-+} &= -\frac{\sqrt{2} m_t^2 s_\theta}{\left(1 - \frac{2m_t^2}{E^2}\right) \left(1 + c_\theta + \frac{2m_t^2}{E^2}\right) v^2} , \\
wzb_{++} &= -wzt_{--}(c_\theta \rightarrow -c_\theta) = 0 , \\
wzb_{--} &= -wzt_{++}(c_\theta \rightarrow -c_\theta) = \frac{\sqrt{2} m_t^3 (1 + c_\theta)}{E \left(1 - \frac{2m_t^2}{E^2}\right) \left(1 - c_\theta + \frac{2m_t^2}{E^2}\right) v^2} , \\
wzb_{-+} &= -wzt_{-+}(c_\theta \rightarrow -c_\theta) = \frac{\sqrt{2} m_t^2 s_\theta}{\left(1 - \frac{2m_t^2}{E^2}\right) \left(1 - c_\theta + \frac{2m_t^2}{E^2}\right) v^2} , \\
wzb_{+-} &= -wzt_{+-}(c_\theta \rightarrow -c_\theta) = 0 . \tag{B.3}
\end{aligned}$$

Including the contributions from the κ coefficients in $\mathcal{L}^{(4)}$, we obtain:

$$\begin{aligned}
wzt_{++}^\kappa &= \frac{E m_t}{v^2 \sqrt{2}} (1 + \kappa_L^{CC}) \left[(1 - c_\theta) \kappa_L^{NC} - 2 \kappa_R^{NC} \right] , \\
wzt_{--}^\kappa &= \frac{E m_t}{v^2 \sqrt{2}} \kappa_R^{CC} \left[2 \kappa_L^{NC} + (1 - c_\theta) (2 - \kappa_R^{NC}) \right] , \\
wzt_{+-}^\kappa &= \frac{E^2 s_\theta}{v^2 \sqrt{2}} \kappa_R^{CC} (\kappa_R^{NC} - 2) , \\
wzt_{-+}^\kappa &= \frac{E^2 s_\theta}{v^2 \sqrt{2}} \kappa_L^{NC} (1 + \kappa_L^{CC}) . \tag{B.4}
\end{aligned}$$

C $\mathcal{L}^{(5)}$ helicity amplitudes

Below, we show the anomalous coupling contributions to the helicity amplitudes for the $V_L V_L \rightarrow t\bar{t}$, $t\bar{b}$ or $b\bar{t}$ scattering processes. The first letter, a , stands for *anomalous*. All the 19 anomalous operators listed in section 4 have been considered.

C.1 $Z_L Z_L \rightarrow t\bar{t}$

There are four operators relevant to this process. The four-point operator O_{gZZ} , with coefficient a_{zz1} , contributes only through the diagram of Fig. 15(c). The other three,

$O_{\sigma DZ}$, O_{ZDf} and O_{gDZ} , with coefficients a_{z2} , a_{z3} and a_{z4} , respectively, contribute through diagrams 15(a) and 15(b). However, since external on-shell Z bosons satisfy the condition $p_\mu \epsilon^\mu = 0$, the contribution from the derivative-on-boson operators $O_{\sigma DZ}$ and O_{gDZ} vanishes. The only non-zero contributions come from O_{gZZ} and O_{ZDf} . The anomalous contributions to the helicity amplitudes are:

$$\begin{aligned} azz_{++} &= \frac{-E^3 \left(4a_{zz1} + \left(1 - \frac{8}{3}s_w^2 \right) a_{z3} \right)}{v^2 \Lambda}, \\ azz_{--} &= -azz_{++}, \\ azz_{+-} &= az_{-+} = 0, \end{aligned} \tag{C.1}$$

The amplitudes with opposite sign helicities azz_{+-} and azz_{-+} appear as zero. This is so because the contribution from the four-point operator O_{gZZ} is proportional to the spinor product $\bar{u}[\lambda = \pm 1]v[\lambda = \mp 1]$, which is zero in the CM frame of the $t\bar{t}$ pair. Furthermore, for the operator with derivative-on-fermion, O_{ZDf} , the leading energy power for $azz_{\pm\mp}$ is E^0 and we do not include it in the above results.

C.2 $W_L^+ W_L^- \rightarrow t\bar{t}$

The relevant operators are: the four-point operators O_{gWW} and $O_{\sigma WW}$ with coefficients a_{ww1} and a_{ww2} , respectively; derivative-on-boson operators $O_{\sigma DZ}$, O_{gDZ} , $O_{\sigma DWL(R)}$, $O_{gDWL(R)}$ and O_A , with coefficients a_{z2} , a_{z4} , $a_{w2L(R)}$, $a_{w4L(R)}$ and a_m , respectively; derivative-on-fermion operators O_{ZDf} , $O_{WDtR(L)}$ and $O_{WDbL(R)}$, with coefficients a_{z3} , $a_{w3R(L)}$ and $a_{bw3L(R)}$, respectively.

However, some operators give null contributions. For instance, $a_{w2L(R)}$ and $a_{w4L(R)}$ enter in the t -channel diagram of Fig. 16(a), but the condition $\epsilon_\mu p^\mu = 0$ for the on-shell W^+ and W^- bosons makes their contribution to vanish. Similarly, the contribution from O_{gWW} is proportional to the spinor product $\bar{u}[\lambda = \pm 1]v[\lambda = \mp 1]$, which is zero in the $t\bar{t}$ CM frame; also, the contribution from O_{gDZ} , which enters in the s -channel diagram 16(c), vanishes when the Lorentz contraction in the product of the tri-boson coupling, the bosonic propagator and the anomalous coupling is done. There is no effect from operators that depend on b_R , such as O_{gDWL} , O_{WDtL} and O_{WDbL} , because the bottom quark is purely left handed in diagram 16(a) in the limit $m_b \rightarrow 0$. Also, the contributions from the operators $O_{WDtR(L)}$ (with coefficient $a_{w3R(L)}$) and $O_{WDbL(R)}$ (with coefficient $a_{bw3L(R)}$) are identical. Hence, the helicity amplitudes are:

$$\begin{aligned} aww_{++} &= -\frac{2E^3}{v^2 \Lambda} (a_{ww1} + a_{ww2} c_\theta) - \\ &\quad \frac{E^3}{v^2 \Lambda} \left(\frac{a_{w3R} + a_{bw3R}}{\sqrt{2}} + c_\theta \left(-\frac{a_{w3R} + a_{bw3R}}{\sqrt{2}} - 2a_{z2} + a_{z3} + 4a_m \right) \right), \\ aww_{--} &= -aww_{++}, \end{aligned}$$

$$\begin{aligned}
aww_{+-} &= \frac{2 E^2 m_t s_\theta}{v^2 \Lambda} \left(2 a_{ww2} - \frac{a_{w3R} + a_{bw3R}}{\sqrt{2}} - 2 a_{z2} + 4 a_m \right), \\
aww_{-+} &= \frac{2 E^2 m_t s_\theta}{v^2 \Lambda} (2 a_{ww2} - 2 a_{z2} + 4 a_m).
\end{aligned} \tag{C.2}$$

C.3 $W_L^+ Z_L \rightarrow t \bar{b}$

There are two kinds of operators that contribute to this process. The first ones (operators with top and bottom quarks) distinguish chirality; the second ones (operators with top quarks only) do not. The ones that distinguish chirality are: the four-point operators $O_{gWZL(R)}$ and $O_{\sigma WZL(R)}$, with coefficients $a_{wz1L(R)}$ and $a_{wz2L(R)}$, respectively; derivative-on-boson operators $O_{\sigma DWL(R)}$ and $O_{gDWL(R)}$, with coefficients $a_{w2L(R)}$ and $a_{w4L(R)}$, respectively; derivative-on-fermion operators $O_{WDtR(L)}$ and $O_{WDbL(R)}$, with coefficients $a_{w3R(L)}$ and $a_{bw3L(R)}$, respectively. The second ones, that do not distinguish chirality, are: derivative-on-boson operators $O_{\sigma DZ}$ and O_{gDZ} , with coefficients a_{z2} and a_{z4} , respectively; derivative-on-fermion operator O_{ZDf} , with coefficient a_{z3} .

A particular feature, common to all the operators that distinguish chirality, takes place: If the helicity of the particle is *opposite* to the chirality in the coupling, then the contribution will be proportional to the mass of that particle. For instance, the leading term for the contribution of O_{WDtR} to $awzt_{++}$ is proportional to E^3 , but the leading term for $awzt_{--}$ is proportional to $m_t m_b E^1$. (The left handed helicity of the anti-bottom is *opposite* to its left handed chiral component.)

The three relevant operators that do not distinguish chirality participate only through the *u-channel* diagram of Fig. 17(b), and only O_{ZDf} gives non-zero contribution. The other two, with derivative on boson, have their contribution vanished from the condition $\epsilon_\mu p^\mu = 0$ of the on-shell Z boson. On the other hand, the contribution of O_{ZDf} to those amplitudes with a left handed helicity anti-bottom is zero in the limit $m_b \rightarrow 0$ because the bottom becomes purely left handed in this diagram. Hence,

$$\begin{aligned}
awzt_{++} &= \frac{E^3}{2v^2 \Lambda} \left(a_{w3R} + a_{bw3R} \left(1 + \frac{2}{3} s_w^2 + c_\theta \right) - \right. \\
&\quad \left. 4 a_{wz1R} - 4 a_{wz2R} c_\theta - \sqrt{2} a_{z3} (1 + c_\theta) - 4 c_w^2 a_{w2R} c_\theta + 4 s_w^2 a_{w4R} \right), \\
awzt_{+-} &= \frac{E^2 m_t s_\theta}{2v^2 \Lambda} \left(4 a_{wz2L} + a_{w3L} + a_{bw3L} + 4 c_w^2 a_{w2L} \right), \\
awzt_{-+} &= \frac{E^2 m_t s_\theta}{2v^2 \Lambda} \left(4 a_{wz2R} - a_{w3R} + a_{bw3R} - \sqrt{2} a_{z3} + 4 c_w^2 a_{w2R} \right), \\
awzt_{--} &= \frac{E^3}{2v^2 \Lambda} \left(4 a_{wz1L} + 4 a_{wz2L} c_\theta + 4 c_w^2 a_{w2L} c_\theta + \right. \\
&\quad \left. a_{w3L} + a_{bw3L} \left(1 - \frac{2}{3} s_w^2 - c_\theta \right) - 4 s_w^2 a_{w4L} \right),
\end{aligned} \tag{C.3}$$

C.4 $W_L^- Z_L \rightarrow b\bar{t}$

This process is similar to $W_L^+ Z_L \rightarrow t\bar{b}$, as discussed above. The same kind of operators contribute here, and the same reasons of why some contributions are negligible or zero apply.

$$\begin{aligned}
awzb_{++} &= -awzt_{--} (c_\theta \rightarrow -c_\theta) \\
&= \frac{E^3}{2v^2\Lambda} \left(-4a_{wz1L} + 4a_{wz2L}c_\theta + 4c_w^2 a_{w2L}c_\theta - \right. \\
&\quad \left. a_{w3L} + a_{bw3L} \left(1 - \frac{2}{3}s_w^2 + c_\theta \right) + 4s_w^2 a_{w4L} \right) , \\
awzb_{--} &= -awzt_{++} (c_\theta \rightarrow -c_\theta) \\
&= \frac{E^3}{2v^2\Lambda} \left(4a_{wz1R} + \sqrt{2}a_{z3} (1 - c_\theta) - \right. \\
&\quad \left. 4a_{wz2R}c_\theta - 4c_w^2 a_{w2R}c_\theta - a_{w3R} + a_{bw3R} \left(1 + \frac{2}{3}s_w^2 - c_\theta \right) - 4s_w^2 a_{w4R} \right) , \\
awzb_{+-} &= -awzt_{+-} , \\
awzb_{-+} &= -awzt_{-+} .
\end{aligned} \tag{C.4}$$

References

- [1] F. Abe *et al.*, Phys. Rev. Lett. **73**, 225 (1994);
S. Abachi *et al.*, Phys. Rev. Lett. **72**, 2138 (1994);
CDF Collaboration, Phys. Rev. Lett. **74**, 2626 (1995);
D0 Collaboration, Phys. Rev. Lett. **74**, 2632 (1995);
L. Roberts, to appear in the Proceedings of the 28th International Conference on High Energy Physics, Warsaw, Poland, 1996.
- [2] R.D. Peccei, S. Peris and X. Zhang, Nucl. Phys. **B349**, 305 (1991);
T. Han, R.D. Peccei and X. Zhang, Nucl. Phys. **B454**, 527 (1995);
E. Malkawi and T. Tait, Phys. Rev. **D54**, 5758 (1996).
- [3] R.S. Chivukula, E.H. Simmons, and J. Terning, Phys. Lett. **B331**, 383 (1994).
- [4] R.S. Chivukula, E. Gates, E.H. Simmons and J. Terning, Phys. Lett. **B311**, 157 (1993).
- [5] E. Malkawi and C.-P. Yuan, Phys. Rev. **D50**, 4462 (1994).
- [6] G.L. Kane, in Proceedings of the Workshop on High Energy Phenomenology, Mexico City, July 1-10, 1991.
- [7] For a review see,
H.E. Haber, Lectures given at Theoretical Advanced Study Institute (TASI-90), Boulder, CO, Jun 3-29, 1990.

- [8] K. Lane, Lectures given at the Theoretical Advanced Study Institute (TASI 93) in Elementary Particle Physics: The Building Blocks of Creation - From Microfermis to Megaparsecs, Boulder, CO, 6 Jun - 2 Jul 1993; and the references therein.
- [9] Y. Nambu, In Proceedings of the 1988 International Workshop on New Trends in Strong Coupling gauge Theories, Nagoya, Japan, eds. by M. Bando, T. Muta and K. Yamawaki (World Scientific, Singapore, 1989);
W.A. Bardeen, C.T. Hill and M. Lindner, Phys. Rev. **D41**, 1647 (1990);
R. Bönisch and A. Leike, DESY-93-111, hep-ph/9308346 (unpublished);
B. A. Kniehl and A. Sirlin, Phys. Rev. **D51**, 3803 (1995).
- [10] M. Chanowitz and M.K. Gillard, Phys. Lett. **B142**, 85 (1984);
J. Bagger et al., Phys. Rev. **D49**, 1246 (1994).
- [11] H. Georgi, Annu. Rev. Nucl. Part. Sci. **43** (1993) 209.
- [12] R. Martinez, M.A. Perez and J.J. Toscano, Phys. Lett. **B340**, 91 (1994);
M.A. Perez, J.J. Toscano and J. Wudka, Phys. Rev. **D52**, 494 (1995).
- [13] C.-P. Yuan, published in Proceedings of Workshops on Particles and Fields and Phenomenology of Fundamental Interactions, Puebla, Mexico, Nov. 1995.
- [14] S. Coleman, J. Wess and B. Zumino, Phys. Rev. **D177**, 2239 (1969);
C.G. Callan, S. Coleman, J. Wess and B. Zumino, Phys. Rev. **D177**, 2247 (1969);
S. Weinberg, Physica **96A**, 327 (1979).
- [15] H. Georgi, *Weak Interactions and Modern Particle Theory* (The Benjamin/Cummings Publishing Company, 1984);
A. Manohar and H. Georgi, Nucl. Phys. **B234**, 189 (1984).
- [16] J.M. Cornwall, D.N. Levin, and G. Tiktopoulos, Phys. Rev. **D10**, 1145 (1974);
C.E. Vayonakis, Lett. Nuovo. Cimento **17**, 383 (1976);
B.W. Lee, C. Quigg, and H. Thacker, Phys. Rev. **D16**, 1519 (1977);
M.S. Chanowitz and M.K. Gaillard, Nucl. Phys. **B261**, 379 (1985);
G.J. Gounaris, R. Kögerler, and H. Neufeld, Phys. Rev. **D34**, 3257 (1986);
H. Veltman, *ibid*, **D41** 2294 (1990);
W.B. Kilgore, Phys. Lett. **B294**, 257 (1992).
- [17] Y.-P. Yao and C.-P. Yuan, Phys. Rev. **D38**, 2237 (1988);
J. Bagger and C. Schmidt, Phys. Rev. **D41**, 264 (1990).
- [18] H.-J. He, Y.-P. Kuang, and X. Li, Phys. Rev. Lett. **69**, 2619 (1992);
Phys. Rev. **D49**, 4842 (1994); Phys. Lett. **B329**, 278 (1994);
H.-J. He and W.B. Kilgore, hep-ph/9609326 (Phys. Rev. **D**, in press).

- [19] H.-J. He, Y.-P. Kuang, and C.-P. Yuan, Phys. Rev. **D51**, 6463 (1995);
hep-ph/9503359, Published in Proceedings of the International Symposium *Beyond The Standard Model IV*, Eds. J.F. Gunion, T. Han, J. Ohnemus, December 13-18, 1994, Tahoe, California, USA.
- [20] H.-J. He, Y.-P. Kuang and C.-P. Yuan, Phys. Lett. **B382**, 149 (1996); and hep-ph/9611316, to appear in Phys. Rev. **D**, (1997); and MSUHEP-51201, Published in Proc. of International Workshop on *Physics and Experiments with Linear Colliders*, September 8-12, 1995, Iwate, Japan.
- [21] E. Malkawi and C.-P. Yuan, Phys. Rev. **D52** (1995) 472.
- [22] M. Chanowitz, M. Golden, and H. Georgi, Phys. Rev. **D36**, 1490 (1987).
- [23] F. Feruglio, Int. J. Mod. Phys. **A8**, 4937 (1993); and the references therein.
- [24] T. Appelquist and C. Bernard, Phys. Rev. **D22**, 200 (1980);
A.C. Longhitano, Nucl. Phys. **B188**, 118 (1981);
T. Appelquist and G.-H. Wu, Phys. Rev. **D48**, 3235 (1993); **D51**, 240 (1995);
and references therein.
- [25] R.D. Peccei and X. Zhang, Nucl. Phys. **B337**, 269 (1990).
- [26] K. Fujikawa and A. Yamada, Phys. Rev. **D49**, 5890 (1994).
- [27] M. Alam *et al.*, CLEO collaboration, Phys. Rev. Lett. **74**, 2885 (1995).
- [28] R. Barbieri, in Proceedings for the Symposium on Particle Physics at the Fermi scale, Beijing, May 27 –June 4, 1993.
- [29] G. Altarelli, R. Barbieri, and F. Caravaglios, Nucl. Phys. **B405**, 3 (1993).
- [30] G. Altarelli and R. Barbieri, Phys. Lett. **B253**, 161 (1990);
G. Altarelli, R. Barbieri and S. Jadach, Nucl. Phys. **B369**, 3 (1992).
- [31] G. Altarelli, Lectures presented at the Hellenic School on Elementary Particle Physics, Corfu, Greece, Sep 3-11, 1995 and Rencontres du Vietnam, Ho Chi Minh City, Vietnam, Oct 21-24, 1995; CERN-TH/96-05.
- [32] G. Altarelli, R. Barbieri, and F. Caravaglios, Phys. Lett. **B349**, 145 (1995);
W. J. Marciano and A. Sirlin, Phys. Rev. **D22**, 2695 (1980).
- [33] C.P. Burgess and D. London, Phys. Rev. **D48**, 4337 (1993).
- [34] M.B. Einhorn, in Proceedings for the Symposium on Unified symmetry in the small and in the large, Coral Gables 1993.

- [35] H. Georgi, Nucl. Phys. **B361**, 339 (1991).
- [36] G. Altarelli, CERN-TH/96-295, hep-ph/9611239; and the references therein.
- [37] E. Malkawi, Ph.D. thesis, Michigan State University, August 1996; and the references therein.
- [38] J.F. Donoghue, E. Golowich and B.R. Holstein, *Dynamics of the Standard Model* Cambridge monographs on particle physics, nuclear physics and cosmology. Cambridge University Press (1992).
- [39] M. Veltman, Nucl. Phys. **B123**, 89 (1977).
- [40] P. Langacker, *Precision Tests of the Standard Electroweak Model*, ed. by P. Langacker (World Scientific, 1994).
- [41] The SLD Collaboration, K. Abe et al., Phys. Rev. Lett. **73**, 25 (1994).
- [42] S. Dawson, Nucl. Phys. **B249**, 42 (1985).
- [43] S. Dawson and S. Willenbrock, Nucl. Phys. **B284**, 449 (1987);
S. Willenbrock and D.A. Dicus, Phys. Rev. **D34**, 155 (1986);
F. Anselmo, B. van Eijk and G. Bordes, Phys. Rev. **D45**, 2312 (1992);
T. Moers, R. Priem, D. Rein and H. Reithler, in Proceedings of the Large Hadron Collider Workshop, preprint CERN 90-10, 1990;
R.K. Ellis and S. Parke, Phys. Rev. **D46**, 3785 (1992).
- [44] C.-P. Yuan, Phys. Rev. **D41**, 42 (1990);
D. Carlson and C.-P. Yuan, Phys. Lett. **B306** (1993) 386.
- [45] S. Cortese and R. Petronzio, Phys. Lett. **B253**, 494 (1991).
- [46] D.O. Carlson, Ph.D. thesis, Michigan State University, MSUHEP-050727, August 1995; and the references therein.
- [47] T. Stelzer and S. Willenbrock, Phys. Lett. **B374**, 169 (1996).
- [48] G.A. Ladinsky and C.-P. Yuan, Phys. Rev. **D43**, 789 (1991).
- [49] C.-P. Yuan, et al., Report of the subgroup on the Top Quark, Proceedings of Workshop on Physics at Current Accelerators and Supercolliders, edited by J. Hewett, A. White and D. Zeppenfeld, 1993, pp 495–505; and the references therein.
- [50] D. Amidei and R. Brock Eds., Future Electro Weak Physics at the Fermilab Tevatron, Report of the TeV_2000 study group. Fermilab-Pub-96/082 (1996).

- [51] G. L. Kane, G. A. Ladinsky and C.-P. Yuan, Phys. Rev. **D45**, 124 (1992).
- [52] S. Mrenna and C.-P. Yuan, Phys. Rev. **D46**, 1007 (1992).
- [53] P.W. Johnson, F.I. Olness and W.-K. Tung, Phys. Rev. **D36**, 291 (1987); and the references therein.
- [54] The CDF Collaboration and J. Incandela, “CDF Top Quark Production and Mass”, FERMILAB-CONF-95/237-E, July 1995.
- [55] J. C. Collins and W.-K. Tung, Nucl. Phys. **B278** (1986) 934;
F. Olness and W.-K. Tung, Nucl. Phys. **B308** (1988) 813;
M. Aivazis, F. Olness and W.-K. Tung, Phys. Rev. Lett. **65** (1990) 2339; Phys. Rev. **D50**, 3085 (1994);
M. Aivazis, J.C. Collins, F. Olness and W.-K. Tung, Phys. Rev. **D50**, 3102 (1994).
- [56] G. Bordes and B. van Eijk, Nucl. Phys. **B435**, 23 (1995).
- [57] J. Botts, J. Huston, H. Lai, J. Morfin, J. Owens, J. Qiu, W.-K. Tung, H. Weerts, Michigan State University preprint MSUTH-93/17.
- [58] A. Castro, The CDF Collaboration, FERMILAB-CONF-96/319-E. Published in Proceedings 28th International Conference on High Energy Physics (ICHEP’96), Warsaw, Poland, July 25-31, 1996.
- [59] M. Smith and S. Willenbrock, Phys. Rev. **D54**, 6696 (1996).
- [60] G.A. Ladinsky and C.-P. Yuan, Phys. Rev. **D49**, 4415 (1994).
- [61] T. Barklow and C.R. Schmidt, SCIPP 94/22, Aug 1994.
- [62] F. Larios and C.-P. Yuan, MSUHEP-60620, hep-ph/9606397, to appear on Phys. Rev. **D** (1997).
- [63] W. Buchmüller and D. Wyler, Nucl. Phys. B **268**, 621 (1986).
- [64] J. Bagger, V. Barger, K. Cheung, J. Gunion, T. Han, G. A. Ladinsky, R. Rosenfeld, C.-P. Yuan, Phys. Rev. **D49**, 1 (1994); **D52** (1995) 3878;
V. Barger, J. F. Beacom, K. Cheung, T. Han, Phys. Rev. **D50**, 6704 (1993).
- [65] R. N. Cahn and S. Dawson, Phys. Lett. **B136**, 196 (1984), Phys. Lett. **B138**, 464(E) (1984);
M. S. Chanowitz and M. K. Gaillard, Phys. Lett. **B142**, 85 (1984);
G. L. Kane, W. W. Repko and W. R. Rolnick, Phys. Lett. **B148**, 367 (1984);
J. Lindfors, Z. Phys. **C28**, 427 (1985);

- W. B. Rolnick, Nucl. Phys. **B274**, 171 (1986);
P. W. Johnson, F. I. Olness and W.-K. Tung, Phys. Rev. **D36**, 291 (1987);
Z. Kunszt and D. E. Soper, Nucl. Phys. **B296**, 253 (1988);
A. Abbasabadi, W. W. Repko, D. A. Dicus and R. Vega, Phys. Rev. **D38**, 2770 (1988);
S. Dawson, Phys. Lett. **B217**, 347 (1989);
S. Cortese and R. Petronzio, Phys. Lett. **B276**, 203 (1992);
I. Kuss and H. Spiesberger, Phys. Rev. **D53**, 6078 (1996).
- [66] H.L. Lai, J. Botts, J. Huston, J.G. Morfin, J.F. Owens, J.W. Qiu, W.-K. Tung, H. Weerts, Phys. Rev. **D51** (1995) 4763.
- [67] M.S. Chanowitz, M.A. Furman and I. Hinchliffe, Nucl. Phys. **B153**, 402 (1979).